AN INVESTIGATION OF INSTANTANEOUS HEAT TRANSFER
DURING COMPRESSION AND EXPANSION
IN RECIPROCATING GAS HANDLING EQUIPMENT

by

HENRY B. FAULKNER

A.B., Harvard College
(1963)

S.M., Massachusetts Institute of Technology
(1970)

SUBMITTED TO THE DEPARTMENT OF
MECHANICAL ENGINEERING IN PARTIAL
FULFILLMENT OF THE
REQUIREMENTS FOR THE
DEGREE OF

DOCTOR OF PHILOSOPHY

in

MECHANICAL ENGINEERING

at the

MASSACHUSETTS INSTITUTE OF TECHNOLOGY

May 1983

© Massachusetts Institute of Technology 1983

Signature of Author___
Department of Mechanical Engineering
May 6, 1983

Certified by_____
Joseph L. Smith
Thesis Supervisor

Accepted by_____
Warren M. Rohsenow
Chairman, Departmental Graduate Committee

AN INVESTIGATION OF INSTANTANEOUS HEAT TRANSFER
DURING COMPRESSION AND EXPANSION
IN RECIPROCATING GAS HANDLING EQUIPMENT

by

HENRY B. FAULKNER

Submitted to the Department of Mechanical Engineering
on May 6, 1983 in partial fulfillment of the
requirements for the Degree of Doctor of Philosophy in
Mechanical Engineering

ABSTRACT

In reciprocating gas handling machinery, there is both a net or average heat transfer over many cycles between the gas and the environment, and an instantaneous heat flux back and forth between the gas and the cylinder wall within each cycle. The latter phenomenon occurs both in open cylinder processes and in closed cylinder processes, where it results in what is sometimes referred to as "gas spring loss". This thesis addresses the instantaneous heat transfer as it occurs in a closed cylinder without combustion. In order to evaluate the effect of the heat transfer on the thermodynamic cycle of the gas taken as a whole, the heat transfer is spatially averaged over the boundary of the gas space.

The T-S diagram, based on the mixed mean temperature and entropy of the gas, is shown to be an excellent indicator of instantaneous heat transfer process at the wall. The T-S diagram can be derived from measurements of pressure and volume for a fixed mass of gas, without any knowledge of the temperature distribution in the gas. The instantaneous heat flux at the wall is not in phase with the temperature difference between the bulk gas and the wall, so the classical correlation of these two quantities is not appropriate for this problem.

Several series of experiments with a closed cylinder are reported. Work lost per cycle and the shape of the T-S diagram are correlated with an average Reynolds number for the cycle for four gases, two volume ratios and three cylinder liner materials. The distinguishing properties of the gas are the specific heat ratio and the molecular weight. Work lost per cycle reaches a maximum at intermediate Reynolds number and increases with gas specific heat ratio and cycle volume ratio.

Thesis Supervisor: Joseph L. Smith
          Title: Professor of Mechanical Engineering

ACKNOWLEDGEMENTS

TABLE OF CONTENTS

LIST OF TABLES

LIST OF FIGURES

LIST OF SYMBOLS

A	area through which heat transfer occurs
a	a system constant in entropy generation model
amp	amplification factor
$a_0 \ldots a_4$	linear regression coefficients
b	cylinder bore
C	thermal capacitance of gas
$C_1 \ldots C_3$	arbitrary constants in differential equation solution
C_{de}	a system constant in entropy generation model
c	distance from cylinder head to piston at top dead center
c	specific heat per unit mass of solid wall
c_p	specific heat per unit mass of gas at constant pressure
c_v	specific heat per unit mass of gas at constant volume
f_c	function in differential equation solution
f_s	function in differential equation solution
h	surface coefficient of heat transfer
k	thermal conductivity
ℓ	characteristic length
ℓ_a	average length between piston and cylinder head
L	non-dimensional energy loss per cycle
$\bar{L}$	non-dimensional energy loss per cycle in entropy generation model

L/r	ratio of connecting rod length to crankshaft radius
M	molecular weight of gas
m	mass of gas in cylinder
m	mass position coordinate in entropy generation model
N	crankshaft rotational speed or frequency
Pr	Prandtl number of gas
p	pressure
P_{atm}	atmospheric pressure
P_{mc}	mean pressure in compression
P_{signal}	voltage of signal from pressure instrumentation
Q	quantity of heat transferred
q	heat transfer rate or heat flux
q_g	heat flux between two regions in gas
q_s	heat source rate
R	gas constant
R	thermal resistance
Re	average Reynolds number of cycle
r_c	ratio of thermal capacitances
r_p	pressure ratio of cycle
r_R	ratio of thermal resistances
r_s	ratio of magnitudes of heat sources
r_{ta}	approximate temperature ratio of cycle
r_v	volume ratio of cycle
S	entropy

S_{gen}	entropy generated per cycle in all of gas
$\dot{S}_{gen}$	entropy generation rate
s	stroke of piston
s	entropy per unit mass in entropy generation model
$\dot{s}_{gen}$	entropy generation rate per unit mass
$s_{gen/cycle}$	entropy generated per unit mass per cycle at position m
sens	pressure transducer sensitivity
T	temperature
T_{mean}	assumed mean temperature of the gas
t	time
U	internal energy
u	time variable scaled by pressure
V	volume
V_D	displacement volume
v	characteristic velocity
v	specific volume in entropy generation model
W	quantity of work transferred
W_c	work input in the compression process
W_e	work output in the expansion process
x	distance from wall in entropy generation model
$x_1 \cdots x_4$	harmonic functions in crank angle approximation
y	perpendicular distance from cylinder wall
z	dummy variable for defining functions

α	constant in differential equation solution
γ	ratio of specific heats of gas
ζ	damping ratio
ζ	function in differential equation solution
θ	temperature difference from wall
θ	crank angle, starting at top dead center
μ	average viscosity of gas
ξ	non-dimensional position variable in entropy generation model
ρ	density
σ	non-dimensional measure of the attenuation of the entropy wave with distance from the wall
τ	thermal time constant
ϕ	function in differential equation solution
ω	average angular velocity of crankshaft
ω_n	natural frequency

Subscripts

bdc	pertaining to bottom dead center position of crankshaft
ctr	pertaining to an arbitrarily selected central state of gas
g	at a local point in gas
mm	mixed mean
nu	pertaining to gas at non-uniform temperature
0	at reference state
tdc	pertaining to top dead center position of crankshaft
u	pertaining to gas at uniform temperature

w   at the boundary between the gas and the cylinder wall

Superscript

*   non-dimensional

CHAPTER 1

INTRODUCTION

1.1 Background

A large portion of the devices which exchange energy between a rotating shaft and a working gas use reciprocating machinery. In the thermodynamic models used to approximate the behavior of these devices, the processes occurring within a cylinder are often assumed to be adiabatic. At each instant there is in general some heat transfer taking place between the gas and the cylinder wall. In many cases it is desireable to have some knowledge of the magnitude and timing of this heat transfer to increase the accuracy of performance calculations.

The thermodynamic process of the gas taken as a whole is influenced by the heat flux integrated over the entire boundary of the gas space. Hence we are concerned with this integrated flux, that is the instantaneous spatially averaged heat transfer at the wall. When this instantaneous heat transfer is integrated around the cycle, we obtain the net or time averaged heat transfer between the gas and the wall, which is also the heat transfer between the gas and the environment. In general, knowledge of the net heat transfer is not very useful in trying to assess the instantaneous heat transfer.

The processes in the cylinder can be divided into two categories, with heat transfer occurring in both. Intake and exhaust are high flow rate processes occurring at constant pressure in an open cylinder. On

the other hand, compression and expansion are low flow rate processes with rapidly varying pressure in a closed cylinder. This thesis is concerned with the instantaneous spatially averaged heat transfer in compression and expansion only, i.e. in a closed cylinder without combustion.

In some devices the working volume is always closed, although it may consist of more than a simply shaped clearance volume over a piston in a cylinder. These are devices without valves, such as gas springs, pulse tube refrigerators and Stirling cycle machines. Although the pressure may not be uniform through the working volume, at each point in space the pressure undergoes a smooth oscillation in time, unlike the pressure variation in devices with valves. Therefore in these devices the instantaneous heat transfer occurs in compression or expansion throughout the cycle and is called the cyclic heat transfer. Usually the cyclic heat transfer in these devices is large enough to make it very desireable to include this effect in performance calculations.

An understanding of the instantaneous heat transfer pattern in a closed cylinder could also be useful in predicting the performance of a variety of other devices. Examples are those which have a rapid pressure variation in a closed space during part of their cycle, such as reciprocating compressors, expanders and internal combustion engines, and those which have a one shot process in a closed space, such as combustion bombs. For instance, in reciprocating internal combustion engines, heat transfer in compression lowers the temperature and pressure slightly at the start of combustion. The effect on the thermal efficiency of the cycle is small and is difficult to separate from the effect of piston ring leakage. How-

ever, if we need to know the states of the cycle with some precision, as in the prediction of detonation or pollutant emissions, it may be necessary to take the heat transfer in compression into account.

1.2 Literature

There is a large body of literature dealing with heat transfer between the wall and the gas in reciprocating machines. Much of this literature is concerned with the overall energy balance or overheating of components and hence deals with the net or time average heat flux over many cycles. Most of the remaining literature focuses on the instantaneous heat flux at specific points on the cylinder wall. It is generally accepted that it is very difficult to obtain the heat transfer, spatially averaged over the boundary of the gas space, from known local heat fluxes at certain points on the boundary. We turn therefore to the small body of literature dealing directly with instantaneous spatially averaged heat transfer. The discussion includes only publications in which the results of proposed models or correlations are compared with experimental data.

There are two widely quoted papers, by Annand [1] and Woschni [2], which discuss instantaneous spatially averaged heat transfer in reciprocating internal combustion engines. Both authors proposed correlations based on the assumption that the form of the Nusselt, Reynolds and Prandtl number relationship is the same as that found for turbulent flow in pipes or over flat plates. This is the classical formulation of the heat transfer problem, whose limitations are discussed in Chapter 2. Annand used only local instantaneous heat flux data as the basis for his correlation,

but it has often been used to estimate instantaneous spatially averaged heat transfer. Woschni used time averaged experimental data as the basis for his correlation, with the distribution around the cycle based on estimated average gas velocities. Thus neither of these correlations is based on instantaneous spatially averaged heat flux data. The only practical way to obtain such data for closed cylinder processes seems to be to make careful simultaneous measurements of pressure and volume. A possible reason for the absence of such data in reciprocating internal combustion engine literature is the difficulty of separating the effects of heat transfer from the effects of piston seal leakage.

Wendland [3] studied heat transfer in a closed piston and cylinder device. He focused on heat transfer to the cylinder head, which was inferred from measurements of instantaneous local heat flux at several points. Although he measured pressure and crank angle through the cycle, he did not use this data to calculate the work lost in the cycle or T-S data as is done in this work, probably because there was significant piston seal leakage. Therefore his results are not directly comparable to the results of this work. He did, however, make several important general observations which are referred to in this work where they are pertinent.

Vincent et al. [4] reported measurements of the energy loss in a cycle in a closed cylinder for two average pressure levels, two gases, and two volume ratios. The questions of piston seal leakage and friction were not addressed and there was not enough information given to make direct comparisons with the work reported here. However their results seem to be in general agreement with the results reported here.

1.3 Problem Description

We wish to consider a mass of gas undergoing a periodic variation in pressure. The amplitude of the pressure swing is of the same order as the average pressure. The gas is confined by, and in thermal contact with, solid walls. The periodic pressure variation produces a periodic temperature variation in the gas, which in turns leads to periodic heat transfer between the gas and the walls. The heat capacity of the walls is several orders of magnitude larger than the heat capacity of the gas. Hence the spatially averaged wall temperature does not vary significantly with time and will be close to the mean temperature of the gas. Since there is a small net heat transfer from the gas to the wall, the wall temperature will be slightly below the average temperature of the gas. When the gas temperature is sufficiently far from its mean there is a temperature gradient and heat conduction in the gas.

The pressure variation is produced by the motion of a piston, which directly causes gas motion. In addition, the motion of the corner between the piston and the fixed cylinder side wall produces alternate scraping and laying down of the boundary layer on the cylinder side wall and jet flow in and out of the clearance space between the piston and the wall. Over many cycles a pattern of turbulent motion is produced in the gas, leading to convective enhancement of the heat transfer process. The area, and spatially averaged temperature, of the wall varies in time with the motion of the piston.

Clearly the complete process is quite complex, making it nearly impossible to study the simultaneous variation in time and space of all

the important quantities. We have therefore taken a macroscopic viewpoint
in this work. We have measured properties which apply to the gas as a
whole, the pressure and the volume, and from these calculated the work and
heat transfers to the gas as a whole.

A dimensional analysis was done to identify logical dimensionless
groups of the macroscopic independent variables. Geometrical similarity
was assumed, including constant volume ratio, although the volume ratio
was treated as a variable in the experiments. Also material properties
of the cylinder walls were considered constant, although they were varied
in the experiments. The groups identified were the ratio of specific
heats of the gas, the Prandtl number of the gas, the average Mach number
and the average Reynolds number of the cycle. The Prandtl numbers of the
gases used in the experiments did not differ significantly, so the varia-
tion of Prandtl number is not considered in this work. With the possible
exception of flow in the side clearance space between the piston and the
cylinder, the Mach numbers are very low throughout the cycle, and so the
variation of Mach number is ignored also. The remaining dimensionless
independent variables are then the specific heat ratio of the gas and the
average Reynolds number of the cycle. The average Reynolds number is
based on the average density of the gas, average piston speed, the bore
of the cylinder and the average viscosity of the gas.

It was necessary to identify some measure of the instantaneous
spatially averaged heat transfer as a dependent variable. The heat transfer
is irreversible, causing some net work to be absorbed in the cycle, which
is equal to the net heat rejected in the cycle. This net work is seen as

the area enclosed by the p-V diagram of the cycle. This net work was chosen as the dependent variable and it was made non-dimensional by dividing by the work required for the compression part of the cycle. In addition to this single number measure, it was desireable to have some indication of the pattern of the instantaneous spatially averaged heat transfer around the cycle. This indication was provided by the T-S diagram, which is discussed in detail in Chapter 2.

1.4 Objectives

The overall objective of this work is to increase the understanding of the heat transfer process in reciprocating machines. The ultimate goal is to enable the heat transfer to be predicted for accurate thermodynamic performance analysis.

The first immediate objective is to present and evaluate the T-S diagram as a tool for illustrating how the heat transfer process changes within the cycle of the machine. The second immediate objective is to see how the heat transfer measures we have selected, namely the non-dimensional loss and the shape of the T-S diagram, vary with the independent variables we have identified, namely the average Reynolds number of the cycle, the specific heat ratio of the gas, the volume ratio of the cycle, and the cylinder wall material.

CHAPTER 2

THE T-S DIAGRAM

We want to know the pattern over a cycle of the instantaneous, spatially averaged heat transfer between the cylinder walls and the gas. The gas temperature is varying with the cycle and the wall temperature can be considered constant for the purposes of this discussion, as discussed in Section 1.3. There are two ways of formulating this problem which we will now discuss and compare. The first method, the classical formulation involving the surface coefficient of heat transfer, is shown to be inappropriate for this problem. The second method, which involves calculating the mixed mean temperature and entropy and plotting the T-S diagram, is shown to be a very helpful tool.

2.1 Classical Formulation

The mechanism of heat transfer between the wall and the gas is conduction and Fourier's equation must apply,

$$q_w = - kA \frac{\partial T}{\partial y} \Big|_w \qquad (2.1)$$

However here, as in many other situations, the temperature distribution in the gas is difficult to determine. But we can simplify the analysis if we can assume that the temperature of the fluid varies monotonically with distance from the wall, and that the shape of the variation is the same for the same geometry, Prandtl number of the fluid, and Reynolds

number of the flow. Then the temperature profile perpendicular to the wall is scaled by the difference between the wall temperature and some characteristic temperature of the fluid, usually the mixed mean temperature for internal flow problems. We can write,

$$\frac{\partial T}{\partial y}\bigg|_W = f(geometry, Re, Pr)(T_W - T_{mm}) \qquad (2.2)$$

For convenience we define a surface coefficient of heat transfer,

$$h = -k \, f(geometry, Re, Pr) = \frac{-k}{T_W - T_{mm}} \frac{\partial T}{\partial y}\bigg|_W \qquad (2.3)$$

and then the rate of heat transfer becomes,

$$q_W = hA(T_W - T_{mm}) \qquad (2.4)$$

The function $h = f(Re, Pr)$ is usually determined experimentally for a given set of geometrically similar problems.

It is doubtful whether the assumptions given above are appropriate for a closed piston and cylinder device in operation. The reason is that within the thermal boundary layer of the gas there is heat capacity and there is distributed heat generation due to work input, as observed by Wendland [3]. This is likely to produce a non-monotonic temperature profile in some parts of the cycle. This subject is explored further in the development of models in Appendix E. It is also doubtful whether the

classical formulation can reasonably be extended from a local viewpoint to a spatial average over the inside surface of the cylinder and piston. Nevertheless this is the approach that has usually been used, as discussed in Section 1.2.

2.2 T-S Formulation

We now take a more macroscopic view and think of the gas in the cylinder as a closed thermodynamic system. We assume the gas is perfect and the mass is known. In this problem the Mach numbers are very low, so we can assume the pressure is uniform in space.

If for the moment we also assume the temperature is uniform in space, then the system is quasi-static and two independent properties are sufficient to determine the state of the system. The most convenient properties to measure are the pressure and volume. From them we can calculate the temperature and entropy using the perfect gas relations,

$$T = \frac{pV}{mR} \tag{2.5}$$

$$S - S_0 = m(c_v \ln \frac{p}{p_0} + c_p \ln \frac{V}{V_0}) \tag{2.6}$$

where p_0, V_0 and S_0 are the properties at some arbitrary reference state. If we measure pressure and volume around the cycle and we then calculate temperature and entropy around the cycle, we can calculate the instantaneous spatially averaged heat transfer at any point in the cycle,

$$q_w = T \frac{dS}{dt} \tag{2.7}$$

The difficulty with this argument is that the assumption that the temperature is uniform is not valid, and in fact the heat transfer results from the non-uniformity of temperature.

We now propose that the same method can be used to find the heat transfer even though the temperature is not uniform. Values for the temperature and entropy can still be calculated from the pressure and volume using Eqs. (2.5) and (2.6), as if the temperature were uniform. The resulting temperature is the mixed mean or mass average temperature. The resulting entropy we call the mixed mean entropy and is the entropy that the gas would have if it were at uniform temperature. It is not the actual entropy of the gas, which depends on how the temperature is distributed. We will now show that the mixed mean temperature and entropy determine the heat transfer at the wall,

$$q_W = T_{mm} \frac{dS_{mm}}{dt} \tag{2.8}$$

without any dependence on the temperature distribution.

To demonstrate that this is so, consider two equal masses of gas, one at uniform temperature and the other containing two regions having different temperatures which are uniform within each region. Let each mass start with the same pressure and volume and undergo a process in which there is work transfer and heat transfer (Fig. 2.1). We define the mixed mean temperature for the non-uniform mass as,

UNIFORM
TEMPERATURE

NON-UNIFORM
TEMPERATURE

dQ_w

T_u

m

dW_u

dQ_{nu}

T_1 T_2

m_1 m_2

dW_{nu}

$$V_u = V_{nu} = V$$

$$p_u = p_{nu} = p$$

$$m = m_1 + m_2$$
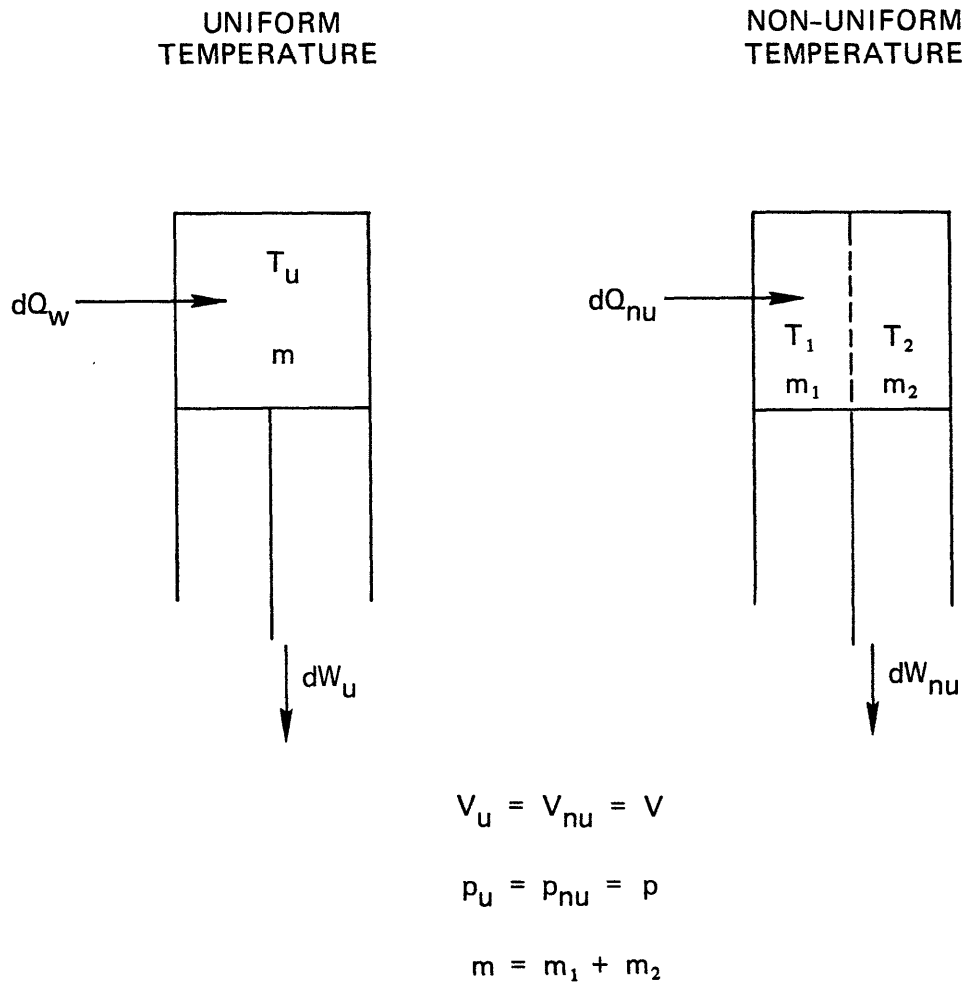
Fig. 2-1. Comparison of Processes in Two Equal Masses of Gas Having
Uniform and Non-Uniform Temperatures.

$$T_{mm} = \frac{m_1 T_1 + m_2 T_2}{m} \qquad (2.9)$$

and then the equation of state for the non-uniform mass is,

$$pV = pV_1 + pV_2 = m_1 RT_1 + m_2 RT_2 = mRT_{mm} \qquad (2.10)$$

and for the uniform mass,

$$pV = m R T_u \qquad (2.11)$$

Therefore, the temperatures are the same,

$$T_{mm} = T_u \qquad (2.12)$$

Now we consider an infinitesimal volume change dV. We require that the heat transfer to each mass during the volume change be such that the pressure change is the same in each mass. The change in the mixed mean temperature of the non-uniform mass is,

$$dT_{mm} = \frac{m_1 dT_1 + m_2 dT_2}{m} \qquad (2.13)$$

We can differentiate the equation of state for the non-uniform mass,

$$d(pV) = d(pV_1) + d(pV_2) = m_2 R dT_1 + m_2 R dT_2 = m R dT_{mm} \qquad (2.14)$$

and for the uniform mass,

$$d(p\mathbb{V}) = m R d T_u \qquad (2.15)$$

Therefore the temperature changes are the same,

$$dT_{mm} = d T_u \qquad (2.16)$$

Now looking at the changes in internal energy in each mass,

$$dU_{nu} = m_2 c_v dT_1 + m_2 c_v dT_2 = m c_v dT_{mm} = mc_v dT_u = dU_u \qquad (2.17)$$

Also the work transfers for each mass are the same,

$$dW_{nu} = pd\mathbb{V} = dW_u \qquad (2.18)$$

Now the first law of thermodynamics says that for any process,

$$dU = dQ - dW \qquad (2.19)$$

Since the changes in internal energy and the work transfers are the same for the two masses, the heat transfers must also be the same

$$dQ_{nu} = dQ_u \qquad (2.20)$$

We define the change in the mixed mean entropy for the non-uniform mass as,

$$dS_{mm} = c_v \frac{dp}{p} + c_p \frac{dV}{V} \qquad (2.21)$$

Clearly,

$$dS_{mm} = dS_u \qquad (2.22)$$

and then,

$$dQ_{mm} = dQ_u = T_u d S_u = T_{mm} d S_{mm} \qquad (2.23)$$

The time derivative of this equation is Eq. (2.8).

This argument can easily be extended from two regions of differing temperature to any arbitrary spatial distribution of temperature having the same mixed mean temperature. Thus it becomes unnecessary to have any knowledge of the temperature distribution in the gas in order to calculate the instantaneous spatially averaged heat transfer at the cylinder wall from instantaneous values of pressure and volume.

2.3 The T-S Diagram

Having calculated the temperature and entropy around the cycle we can plot the T-S diagram. The interpretation of the diagram will now be discussed with reference to an example cycle. This cycle was chosen from the experimentally measured cycles presented in Section 3.5. The p-V and T-S diagrams for this cycle are shown in Figs. 2.2 and 2.3. This
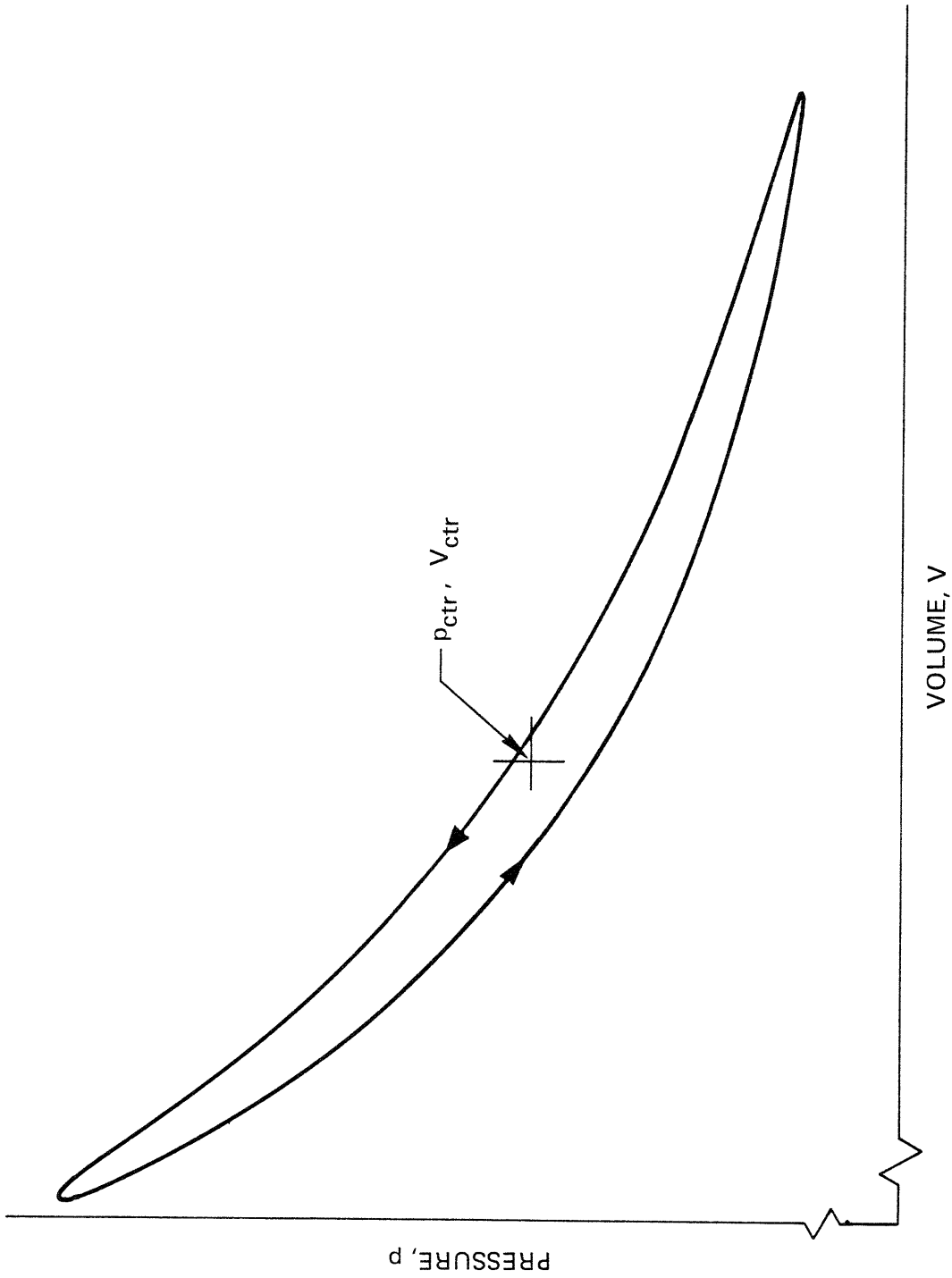
Fig. 2-2. Example Pressure Volume Diagram.
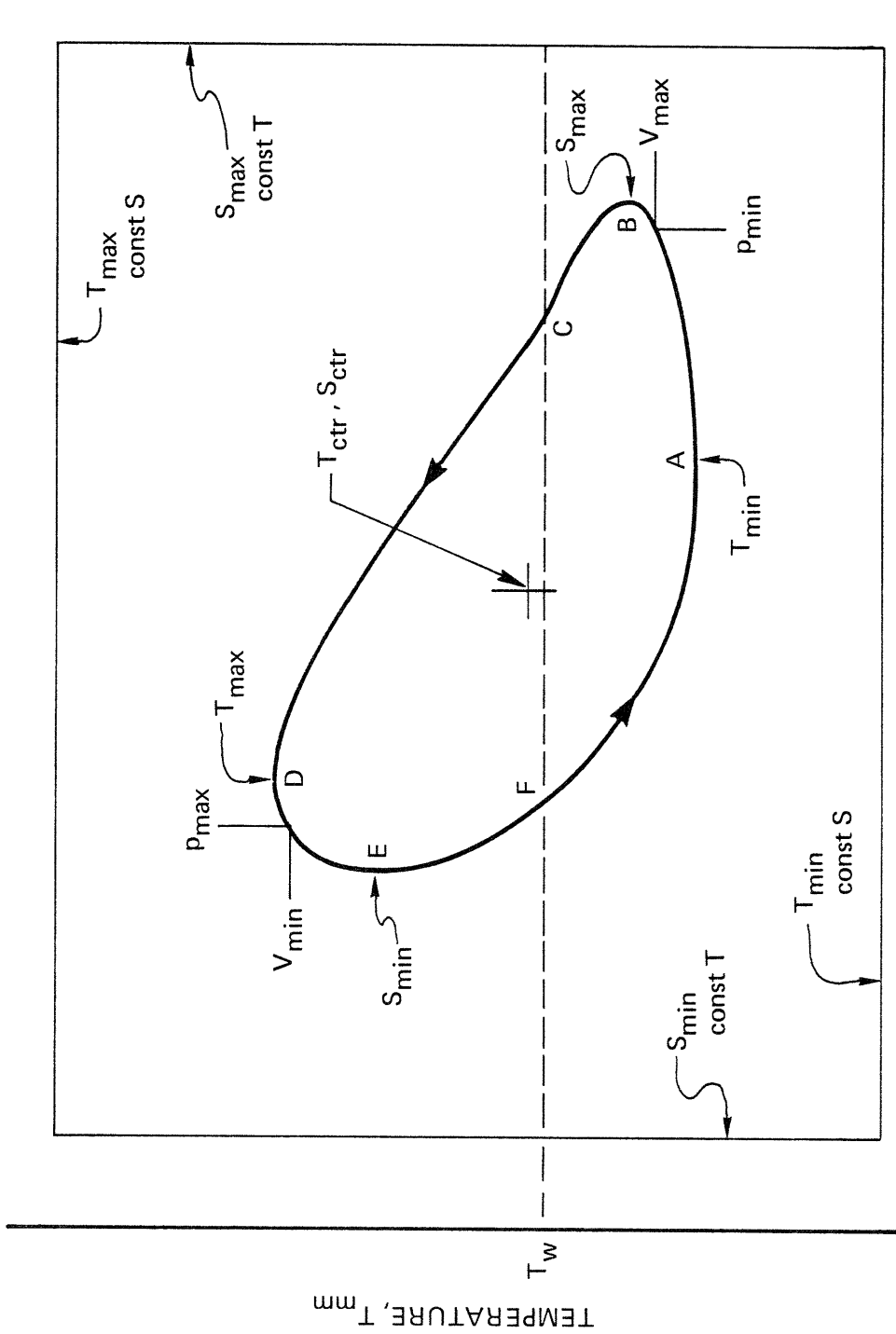
Fig. 2-3. Example Temperature-Entropy Diagram.

cycle was chosen because the T-S diagram has a shape which is intermediate in the range of shapes found in this work and because the points of interest on the diagram are easily distinguished.

The area under any segment of the T-S curve represents the heat transferred at the wall during that part of the cycle,

$$Q_w = \int T_{mm} \, dS_{mm} \qquad (2.24)$$

The diagram is thus a convenient way to show graphically the pattern of the instantaneous spatially averaged heat transfer around the cycle.

On the diagram an isentropic process is indicated by a vertical line, and an isothermal process is indicated by a horizontal line. Therefore the slope of the T-S curve indicates the strength of the heat transfer process during that part of the cycle, relative to the adiabatic and isothermal extremes. However the apparent slope can be strongly biased either way by the choice of horizontal and vertical scales, so it becomes important to choose these scales in an appropriate and consistent manner. The method used in this work is as follows. A state corresponding to a central point inside the p-V and T-S diagrams is arbitrarily selected. The volume is selected as the geometric mean volume,

$$V_{ctr} = \sqrt{V_{max} V_{min}} = \sqrt{r_v} \, V_{min} \qquad (2.25)$$

The pressure is taken to be the average of the pressures in compression and expansion corresponding to this volume. The maximum and minimum

temperatures corresponding to an isentropic process between the maximum and minimum volumes which passes through this central state are then found,

$$T_{max} \bigg|_{const\ S} = r_v^{\frac{\gamma-1}{2}} T_{ctr} \tag{2.26}$$

$$T_{min} \bigg|_{const\ S} = r_v^{-\frac{\gamma-1}{2}} T_{ctr} \tag{2.27}$$

where

$$T_{ctr} = \frac{P_{ctr} V_{ctr}}{mR} \tag{2.28}$$

And then the maximum and minimum entropies corresponding to an isothermal process between the maximum and minimum volumes which passes through this central state are found,

$$S_{max} \bigg|_{const\ T} = S_{ctr} + \frac{1}{2} mR \ln r_v \tag{2.29}$$

$$S_{min} \bigg|_{const\ T} = S_{ctr} - \frac{1}{2} mR \ln r_v \tag{2.30}$$

where

$$S_{ctr} - S_0 = m(c_v \ln \frac{P_{ctr}}{P_0} + c_p \ln \frac{V_{ctr}}{V_0}) \tag{2.31}$$

These temperature and entropy extremes may be thought of roughly as the extremes that the cycle could reach if it were completely isentropic or completely isothermal. In this work these extremes are shown as a box on the T-S diagram. When the diagram space is made slightly larger than the box, the scales of each diagram are adjusted to appropriate values for the cycle being shown.

It is desireable to have some idea of how the timing of the p-V cycle of Fig. 2.2 relates to the timing of the T-S cycle of Fig. 2.3. This can be indicated by marking the points on the T-S diagram corresponding to the maximum and minimum pressure and the maximum and minimum volume, as shown in Fig. 2.3.

As discussed in Section 1.3, the spatially averaged wall temperature can be assumed to be slightly lower than the average temperature of the cycle, which should be approximately the temperature of the central point. Therefore on Fig. 2.3 the estimated wall temperature is shown slightly below that of the central point.

Now we can begin to look at the phase relationship between q_w and $T_w - T_{mm}$. q_w passes through zero when the T-S curve is vertical. Referring to Fig. 2.3, we can see that these points, B and E, are distinctly different from those where $T_w - T_{mm}$ passes through zero, C and F. Therefore q_w and $T_w - T_{mm}$ are not in phase.

In order to describe the relationship between the heat transfer and the temperature distribution further we will now take a tour around the T-S diagram, beginning with point A. Corresponding to each lettered point

on the T-S diagram are profiles of instantaneous gas temperature versus distance from the wall, which are shown in Fig. 2.4. These profiles are not based on any kind of direct measurements, but instead are rough estimates of the gas temperature behavior based on the heat transfer shown in the T-S diagram. They therefore represent an average of the local profiles corresponding to each point on the cylinder wall.

At point A the gas is being heated relatively strongly by the wall and the temperature profile is straightforward. As we move toward point B the pressure reaches its minimum and begins to increase as the piston passes through bottom dead center. The increasing pressure raises the temperature in all of the gas, and the gas near the wall is also heated by the wall and therefore reaches the wall temperature, causing the heat transfer to pass through zero at point B. The increasing pressure continues to raise the gas temperature throughout and the gas near the wall now becomes warmer than the wall. There is then, between points B and C, heat transfer from the gas to the wall, even though the mixed mean temperature of the gas is below the wall temperature. At point C the mixed mean temperature of the gas passes through the wall temperature, while heat transfer to the wall continues. The temperature in the gas continues to rise until point D, where there is strong cooling of the gas by the wall and the temperature profile is again straightforward. As we move toward point E the pressure reaches its maximum and begins to decrease as the piston passes through top dead center. The decreasing pressure now lowers the temperature in all of the gas, and the gas near
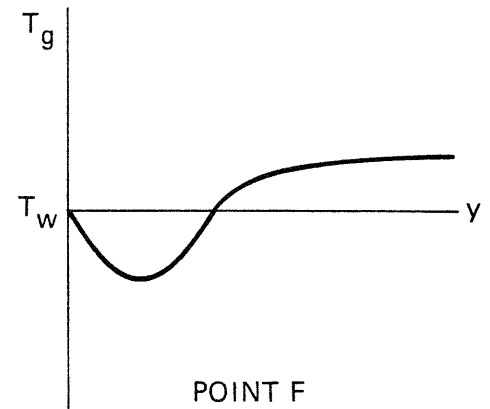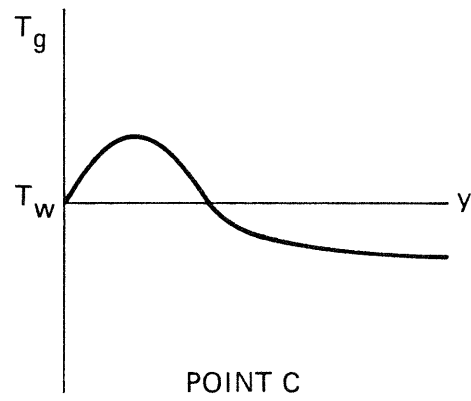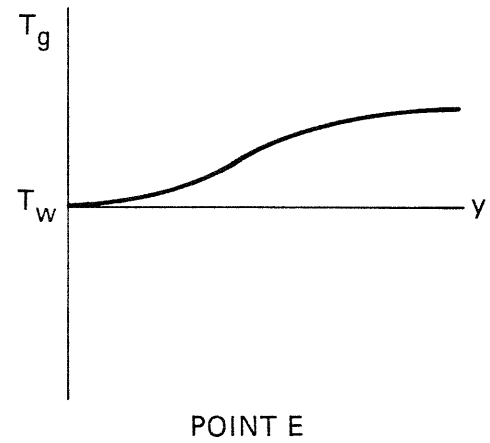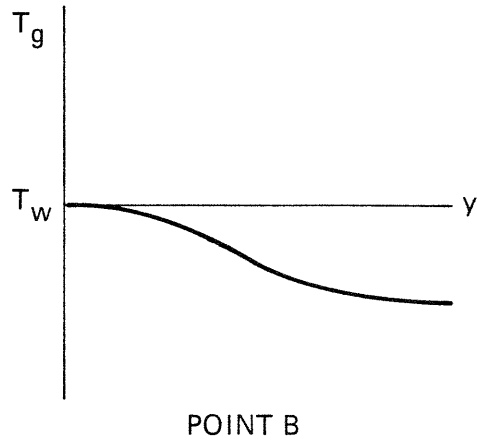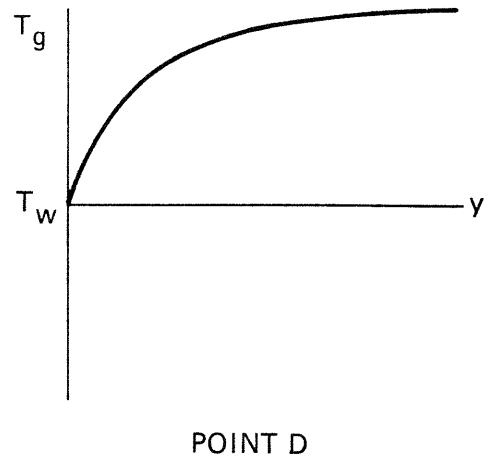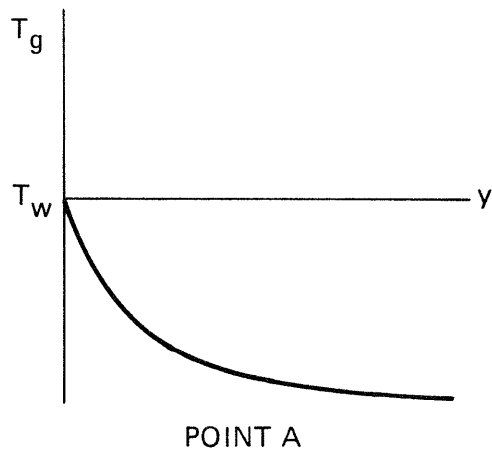
Fig. 2-4. Instantaneous Gas Temperature Profiles Corresponding to Points on T-S Diagram, Fig. 2-3.

the wall is also cooled by the wall and therefore reaches the wall
temperature, causing the heat transfer to pass again through zero at point
E. The decreasing pressure continues to lower the gas temperature through-
out and the gas near the wall becomes cooler than the wall. There is
then, between points E and F, heat transfer from the wall to the gas,
even though the mixed mean temperature of the gas is above the wall
temperature. At point F the mixed mean temperature of the gas passes
through the wall temperature again while heat transfer from the wall con-
tinues. The temperature in the gas continues to fall until point A,
which brings us through a complete cycle.

2.4 Comparison of Formulations

From the previous section it is clear that, when using the T-S
formulation, q_w and $T_w - T_{mm}$ are not in phase, and in
particular that q_w is not zero when $T_{mm} = T_w$. Referring to Eq.
(2.4), it is clear that the classical formulation requires that q_w
be zero when $T_{mm} = T_w$. Wendland [3] reached the same conclusions
by observing that the heat transfer coefficient in the classical formu-
lation took on negative, zero and infinite values at different points
in the cycle. Therefore no adjustment or variation of the heat transfer
coefficient or the area can bring the two methods into agreement. Since
the assumptions in the T-S formulation are much less questionable, it is
much more likely to be accurate. Therefore we must conclude that the
classical formulation is inappropriate for this problem.

The discussion in the previous section provides some insight into
why this should be so. The gas temperature must vary non-monotonically

with distance from the wall in order for the heat transfer to behave
as shown on the T-S diagram. In particular, when the heat transfer is
in the opposite direction to the gross temperature difference, T_w -
T_{mm} , the gas temperature profile must rise and fall, crossing through the
wall temperature some distance away from the wall. Thus a key assumption
of the classical formulation is violated. It is not surprising, there-
fore, that this formulation, which is so useful in a wide variety of
problems, is not useful here.

CHAPTER 3

EXPERIMENTS

3.1 Overview

Several series of experiments were performed with a closed cylinder apparatus to investigate how the instantaneous spatially averaged heat transfer varies with a number of parameters.

A single experiment was performed as follows. The cylinder space was filled with gas through a valve which was then closed. The piston was then moved up and down by a crank mechanism which was driven by an electric motor. The pressure inside the cylinder was measured continuously with a pressure transducer mounted in the cylinder head. The angular position of the crankshaft was simultaneously measured and from this the cylinder volume was later calculated. A single cycle of the pressure versus volume data thus obtained was selected. The non-dimensional loss, which is the area enclosed by the p-V diagram divided by the area under the compression curve, was calculated along with the average Reynolds number for the cycle. The temperature and entropy were calculated for each p-V point and the T-S diagram plotted.

For each experiment, then, the loss, the Reynolds number and the T-S diagram were obtained. For a given gas, geometry, and average temperature, the average Reynolds number is proportional to the product of the average pressure and the average piston speed. Thus, by collecting the results of a number of experiments at several average pressures and piston speeds,

a plot of loss versus Reynolds number was made. Also a sense of the variation of the T-S diagram with Reynolds number was obtained. This process was repeated to obtain results for four gases, two volume ratios, and three cylinder liner materials.

Several preliminary series of experiments, of a similar general nature, were done prior to those reported in this chapter. The same apparatus was used, but in a cruder version. The volume instrumentation, data acquisition and data reduction were less accurate than those reported in this chapter. The parametric variations were similar in some cases, and different in others, and wall temperature measurements were made in some cases. This work is reported in Appendix D.

3.2 Apparatus

3.2.1 Configuration

The basic mechanism was adapted from a Quincy model 230 air compressor (Fig. 3.1). The cylinder head was removed, and the cylinder used in this experiment was bolted in its place. The piston used in this experiment was attached by a short rod to the compressor piston, which functioned as a crosshead. The bore and stroke were 2 in. by 3 in. The piston seal was a rubber O-ring running against the steel cylinder. With this seal the leakage was negligible, but the friction was significant. To prevent heat from this friction from affecting the results, the piston was made tall enough so that the area wiped by the seal was separated from the swept volume (see Appendix A2). Interchangeable liners for the upper part of the cylinder, including the swept and clearance
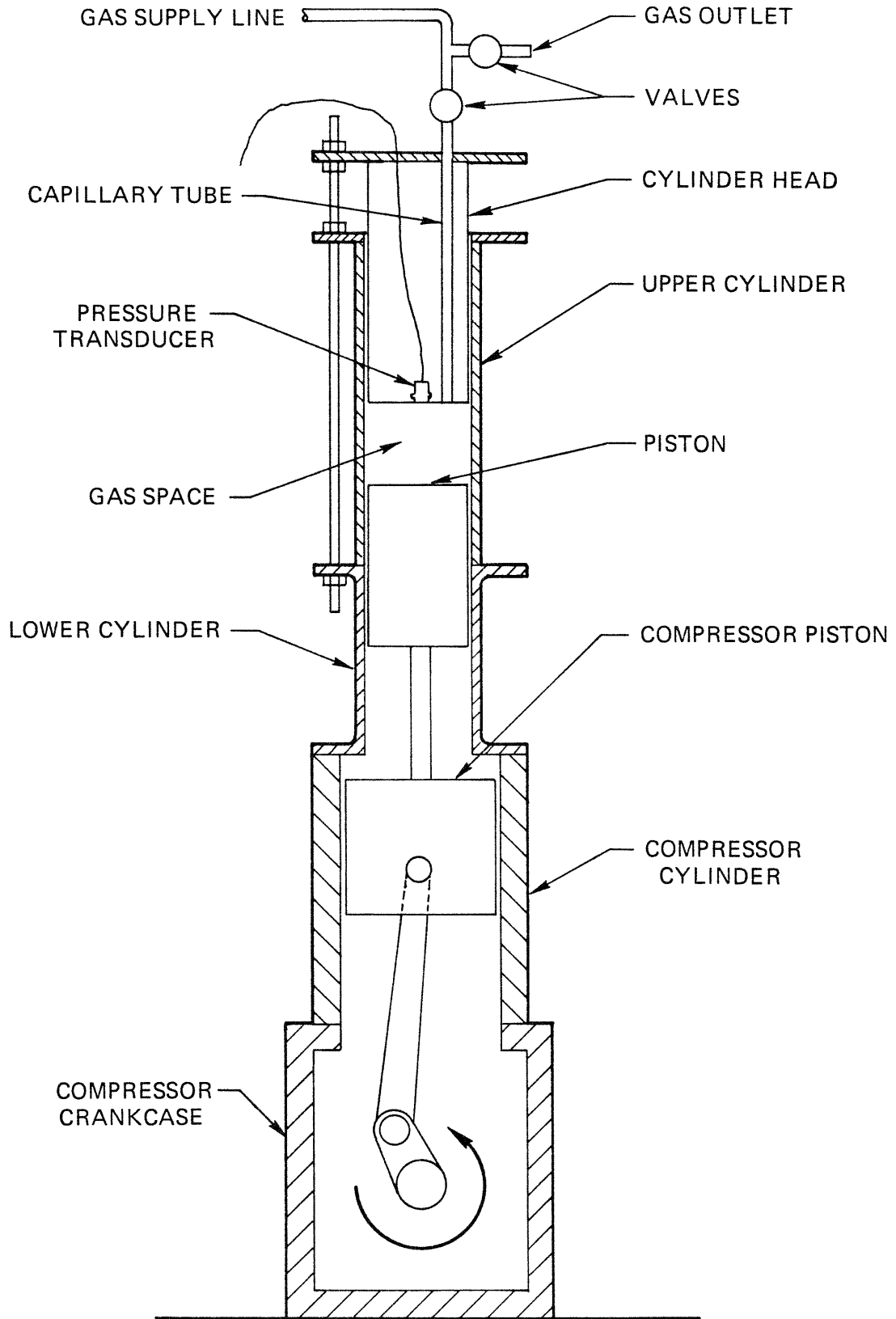
Fig. 3-1. Basic Mechanism Schematic.

volumes, were made from copper, steel and micarta (see Appendix A3).
The steel cylinder head was in the form of a stationary piston, in the
top of the cylinder, whose position could be adjusted to obtain volume
ratios from two to ten (see Appendix A4). The crankshaft was turned by
various motors and pulleys at seven speeds from 9 to 950 rpm. Vibration
prevented the use of higher speeds (see Appendix A1).

3.2.2 Gases

Results were obtained using four different gases in the
cylinder. The properties of the gases are listed in Table 3.1. The
four were selected to give a spread of molecular weight, M, and specific
heat ratio, γ . An attempt was made to select gases which were far
from the critical state, and hence more nearly perfect in their behavior,
at all conditions encountered in the experiments. This was not possible
in the case of the gas of highest molecular weight, Freon 13. The cylin-
der was filled by pressurizing with the gas to be used to the limit of
the pressure transducer being used, and then venting down to a pressure
close to atmospheric. This was repeated until no more than 1% residual
gas remained in the cylinder.

3.2.3 Instrumentation

Pressure was measured with a strain gauge pressure transducer.
Comparison runs were made with a piezoelectric transducer and the pressure
swings differed by up to 1.5%, changing the enclosed area of the p-V dia-
gram by up to about 7%. It was not evident which transducer was more
accurate. The piezoelectric transducer could not be used for the experi-
ments because of excessive zero drift (see Appendix A5).

TABLE 3.1

PROPERTIES OF GASES [5]

GAS	CHEMICAL FORMULA	M	γ	c_p Btu/lbm°F	μ lbm/hrft	Pr
Helium	He	4.002	1.666	1.241	.0493	.687
Nitrogen	N_2	28.01	1.400	.2486	.0445	.733
Argon	A	39.95	1.666	.1246	.0566	.667
Freon 13	$CClF_3$	104.5	1.138	.1571	.0358	.757

Volume was calculated from a stream of electrical pulses, generated by 16 metal tabs on the compressor flywheel passing through a photo-interrupter module. The pulse times were used to generate the crank angle as a continuous fraction of time by means of linear regression curve fit. Then the cylinder volume was calculated from the crank angle. (See Appendices A6 and B3.)

3.3 Data Reduction

The pressure and volume pulse signals were recorded on a digital oscilloscope and later transmitted to a computer for data reduction. A cycle consisted of 400 to 1000 data points, at which the pressure and volume were calculated (see Appendix B).

3.3.1 Cycle Parameters

Knowing the pressure and volume around a cycle, various parameters which characterize the complete cycle can be calculated. When the calculations are completed, the results are displayed at the computer terminal in the format shown in Fig. 3.2.

First, as a check, the pressure closure error is evaluated,

$$\text{Error} = \frac{2(P_{start} - P_{end})}{P_{start} + P_{end}} \tag{3.1}$$

where

P_{start} = pressure at the start of the cycle

P_{end} = pressure at the end of the cycle.

Next the approximate average mixed mean temperature ratio is calculated,

PRESSURE ERROR = 0.004

COMPRESSION AND EXPANSION CYCLIC HEAT TRANSFER EXPERIMENT

10-18-82   RUN 01

CYLINDER WALL MATERIAL   STEEL

WORKING GAS   HELIUM

MEAN COMPRESSION PRESSURE, PSI   12.57

CRANKSHAFT SPEED, RPM   126.8

	MAX	MIN	RATIO
PRESSURE, PSI	22.10	7.16	3.086
VOLUME, CU IN	16.21	6.79	2.389
APPROXIMATE TEMPERATURE RATIO			1.277

COMPRESSION WORK, FT-LBF   9.9

AVERAGE REYNOLDS NUMBER   0.1079E+03

NON-DIMENSIONAL LOSS   0.0975

Fig. 3-2 Example of Cycle Parameters as Displayed by Computer

$$r_{ta} = \frac{P_{tdc} V_{tdc}}{P_{bdc} V_{bdc}} \qquad (3.2)$$

Then the work input to the gas from the piston is calculated. The integral,

$$W_c = \int_c pdV \qquad (3.3)$$

is evaluated by the trapezoidal approximation using as the increment,

$$\Delta W_c = \tfrac{1}{2} (P_i + P_{i+1})(V_i - V_{i+1}) \qquad (3.4)$$

Similarly the work output to the piston from the gas is calculated. The work lost during the cycle is made non-dimensional by dividing by the work input during compression,

$$L = \frac{W_c - W_e}{W_c} \qquad (3.5)$$

This is also the area of the opening of the p-V diagram divided by the area under the compression curve. Next the mean pressure during compression is calculated,

$$P_{mc} = \frac{W_c}{V_D} \qquad (3.6)$$

Finally the average Reynolds number is found. The density is based on

the mean pressure in compression and an assumed mean temperature,

$$\rho = \frac{P_{mc}}{RT_{mean}} \qquad (3.7)$$

T_{mean} is assumed to be 560°R for all experiments. The velocity is the average piston speed,

$$v = 2Ns \qquad (3.8)$$

The characteristic length is the cylinder bore, and the viscosity is the mean gas viscosity shown in Table 3.1. Then the average Reynolds number is,

$$Re = \frac{\rho v \ell}{\mu} = \frac{2 \, P_{mc} \, Nsb}{R \, T_{mean} \, \mu} \qquad (3.9)$$

3.3.2 p-V and T-S Diagrams

The p-V diagram proved to be a much less useful tool in under-standing the results than the T-S diagram. Therefore the p-V diagram was generally not retained as part of the results of each experiment. To facilitate comparisons between cycles occurring under a variety of con-ditions, the p-V and T-S diagrams were made non-dimensional,

$$p^{*} = \frac{P}{P_{mc}}$$

$$\qquad (3.10)$$

$$v^{*} = \frac{V}{V_{D}}$$

$$T^* = \frac{T}{T_0}$$

$$S^* = \frac{T_0}{W_c} S$$

where the mixed mean subscript used in Chapter 2 is dropped. The reference state P_0, V_0, T_0, S_0 is arbitrarily selected as the state at bottom dead center. These relations are chosen so that the enclosed areas of the non-dimensional diagrams are equal to the non-dimensional loss,

$$L = \frac{\oint p dV}{\int_c p dV} = \frac{\oint T dS}{W_c} = \int T^* dS^* = \int p^* dV^* \tag{3.11}$$

Calculation of p^* and V^* is straightforward. It is not necessary to know the temperature or the mass to calculate the non-dimensional temperature and entropy,

$$T^* = \frac{T}{T_0} = \frac{PV}{P_0 V_0}$$

$$S^* - S_0^* = \frac{mT_0}{W_c} (C_v \ln \frac{P}{P_0} + C_p \ln \frac{V}{V_0}) \tag{3.12}$$

$$= \frac{P_0 V_0}{W_c R} (C_v \ln \frac{P}{P_0} + C_p \ln \frac{V}{V_0})$$

The isentropic and isothermal extremes are calculated and shown as a box on the T-S diagram as discussed in Section 2.3. Also, the points of

maximum and minimum pressure are marked on the T-S diagram by vertical
tic marks and the points of maximum and minimum volume are marked by
horizontal tic marks.

3.4 Loss vs. Reynolds Number

For a baseline case of one specific gas, volume ratio and cylinder
liner material, a range of average Reynolds numbers was obtained by
collecting the results of experiments run at various average pressure
levels and various average piston speeds. Then a log-log plot of the
non-dimensional loss versus average Reynolds number was made. This
process was repeated for three other gases having a variety of molecular
weights and specific heat ratios. For the baseline gas, the process
was further repeated for a higher volume ratio, and for two other cylin-
der liner materials. The plots are shown in Figs. 3.3 to 3.9. The sig-
nificance of the labeled points is discussed further in Section 3.5.
Table 3.2 shows the more complete results from which the data of Fig. 3.3
are taken. Tables corresponding to the other plots are given in Appendix
C.

3.4.1 Baseline Case

The gas was helium, the volume ratio was 2.39, and the cylinder
liner was steel for the baseline case. The plot of loss vs. Reynolds
number for this case is shown in Fig. 3.3.

The loss has a maximum at a Reynolds number of approximately 100
and falls off monotonically as Reynolds number is increased or decreased
from this point.
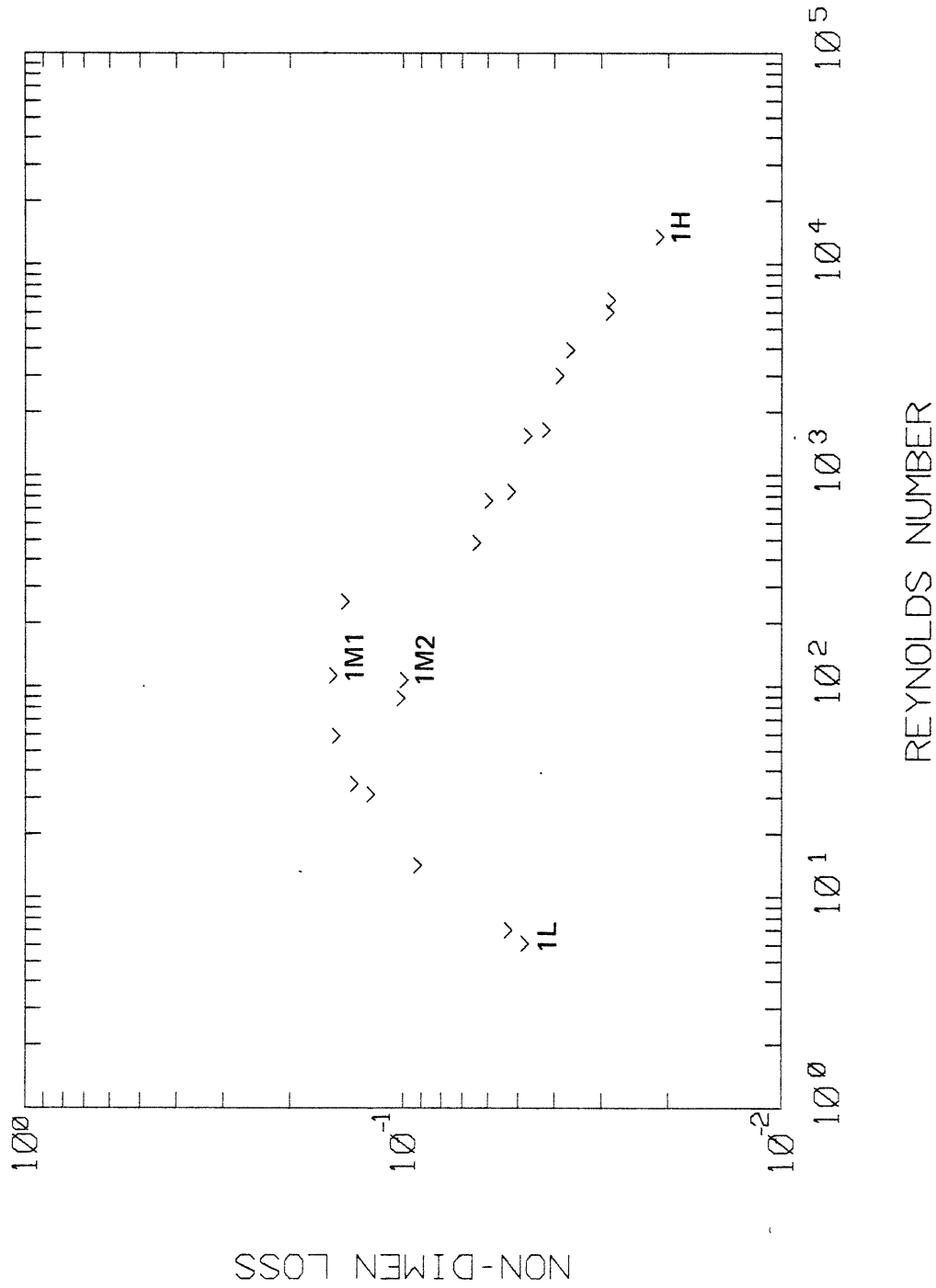
Fig. 3-3. Loss vs. Reynolds Number for Helium, Volume Ratio 2.39, Steel Liner.

Table 3-3 Results for Helium, Volume Ratio 2.39, Steel Liner

(for interpretation of headings see Appendix C)

DATE	RUN	VR	C	G	PMC	N	RE	L	PMAX	PMIN	CWORK
10-01	01	2.389	S	H	249.85	14.9	0.2513E+03	0.1399	435.80	132.66	196.2
10-01	02	2.389	S	H	227.89	258.1	0.3978E+04	0.0354	452.30	116.49	179.0
10-01	03	2.389	S	H	214.12	930.2	0.1347E+05	0.0207	417.08	115.16	168.2
10-13	01	2.389	S	H	47.73	921.7	0.2975E+04	0.0378	93.85	24.92	37.5
10-13	02	2.389	S	H	46.42	266.7	0.8374E+03	0.0507	89.40	24.56	36.5
10-13	03	2.389	S	H	56.09	15.3	0.5815E+02	0.1473	91.81	31.83	44.1
10-13	04	2.389	S	H	11.74	8.8	0.7028E+01	0.0518	18.36	7.70	9.2
10-13	05	2.389	S	H	12.72	102.0	0.8781E+02	0.0997	21.92	7.42	10.0
10-13	06	2.389	S	H	12.11	937.5	0.7679E+03	0.0586	22.66	6.81	9.5
10-18	01	2.389	S	H	12.57	126.8	0.1079E+03	0.0975	22.10	7.16	9.9
10-18	02	2.389	S	H	26.73	266.1	0.4811E+03	0.0626	50.49	14.47	21.0
10-18	03	2.389	S	H	48.78	467.3	0.1542E+04	0.0459	95.73	25.36	38.3
10-18	04	2.389	S	H	10.19	8.8	0.6091E+01	0.0469	15.90	6.72	8.0
10-18	05	2.389	S	H	13.62	15.4	0.1416E+02	0.0899	21.35	8.68	10.7
10-18	06	2.389	S	H	14.33	31.9	0.3097E+02	0.1199	23.04	8.72	11.3
10-18	07	2.389	S	H	33.28	15.3	0.3454E+02	0.1322	53.24	19.83	26.1
10-19	08	2.389	S	H	109.38	15.3	0.1130E+03	0.1508	181.15	60.91	85.9
10-19	09	2.389	S	H	98.33	249.5	0.1659E+04	0.0413	188.28	52.84	77.2
10-20	05	2.389	S	H	91.22	964.6	0.5952E+04	0.0279	179.60	47.62	71.6
10-20	06	2.389	S	H	211.78	476.9	0.6832E+04	0.0276	413.31	112.39	166.3

The points appear to define two curves which overlap but do not

join in the vicinity of a Reynolds number of 100. Consider two points

at the same Reynolds number but having different losses, such as points

1M1 and 1M2. The average pressure level and the speed are the variables

that distinguish these points since all the other experimental variables

are the same. Referring to Table 3.2, we can see that the points with

higher losses in the overlap region have higher pressures and lower

speeds than the points with lower losses. Outside the overlap region,

cycles having the same Reynolds number have very nearly the same loss

even though the combinations of pressure and speed may be quite differ-

ent. This point will be discussed further in Section 3.5.2.

3.4.2 Variation with Gas Molecular Weight and Specific Heat Ratio

Plots of loss vs. Reynolds number for nitrogen and argon are

given in Figs. 3.4 and 3.5. Properties of the gases are given in Table

3.1.

The slope of the plots above a Reynolds number of 1000 are approxi-

mately the same for helium, nitrogen and argon. Unfortunately it was

not possible to run experiments at Reynolds numbers of less than about

50 using nitrogen or argon in the apparatus used in this work. Between

Reynolds numbers of 50 and 200 the loss values for nitrogen and argon

are approximately constant, as they are for helium. This strongly

suggests that loss reaches a maximum in the vicinity of a Reynolds number

of 100 for nitrogen and argon and that the overall shapes of the plots

for these gases should be similar to that of the helium curve. If we

VAX/VMS *** PENPLOT 2.0   29-MAR-1983 16:01:27.53   RES1:[P1732.FAULKNER]HDCOPY.PLT;2 FAULKNER   ••• VAX/VMS

3-4

Fig. 3-4. Loss vs. Reynolds Number for Nitrogen, Volume Ratio 2.39, Steel Liner.

VAX/VMS *** PENPLOT 2.0   29-MAR-1983 16:01:17.46   RES1:IP1732.FAULKNER:HDCOPY.PLT;3 FAULKNER   ••• VAX/VMS
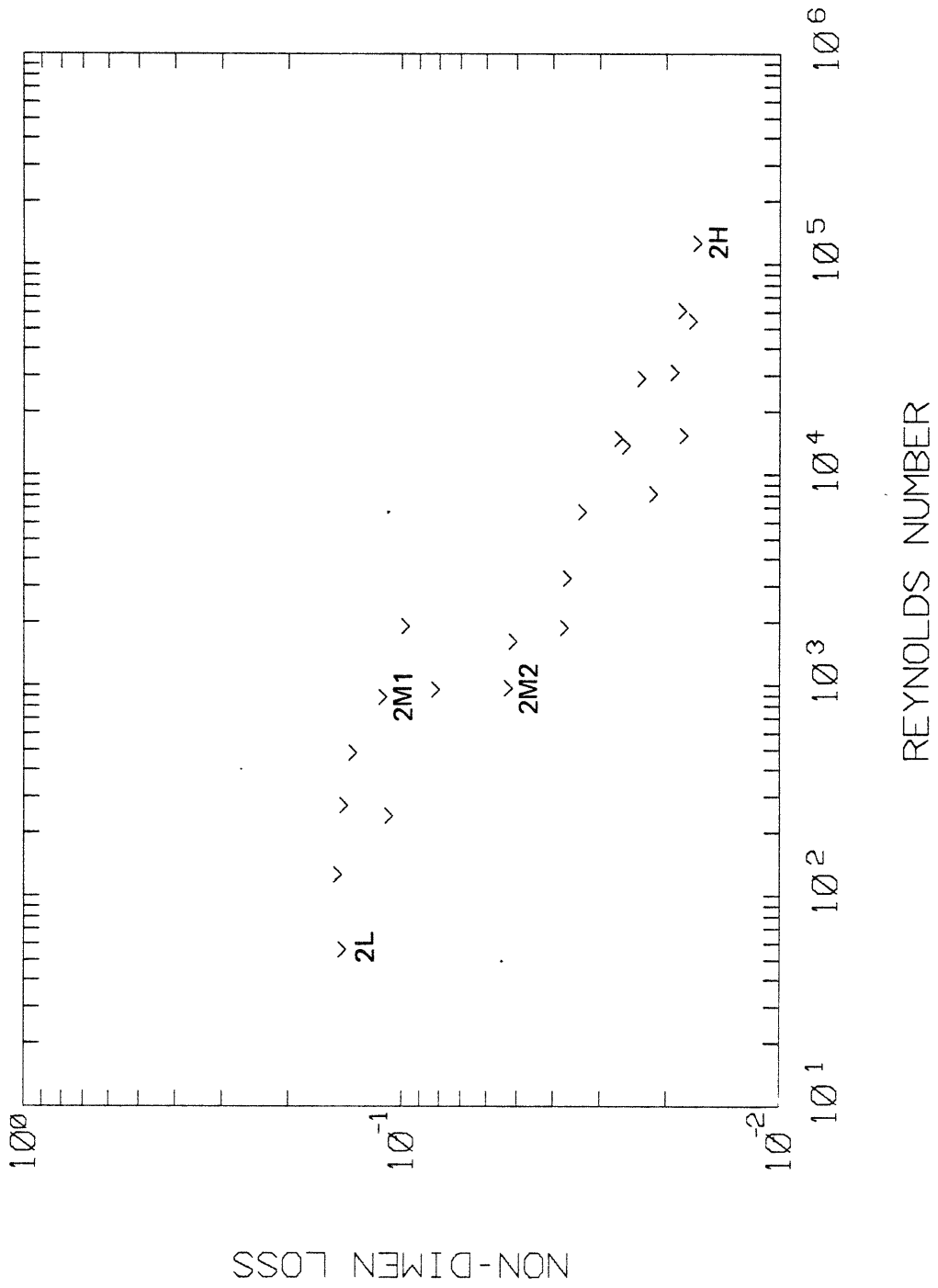
Fig. 3-5. Loss vs. Reynolds Number for Argon, Volume Ratio 2.39, Steel Liner.

assume this is true, we can make some observations about the variation of the maximum loss with the properties of the gas. The maximum loss increases with specific heat ratio but does not change with molecular weight. Also the Reynolds number at which the maximum loss occurs does not change with either specific heat ratio or molecular weight.

Like the helium case, the points for nitrogen and argon appear to define two curves which overlap but do not join. In the nitrogen and argon plots, however, the overlap region seems to be centered around a Reynolds number of 1000, instead of 100 as in the helium plot. This indicates that the Reynolds number around which the overlap region occurs increases with the molecular weight of the gas, but does not change with specific heat ratio.

Now we turn to the plot of loss vs. Reynolds number for Freon 13, shown in Fig. 3.6. In this plot many of the loss values are below 10^{-2} (1%), where, unfortunately, the accuracy of the loss becomes questionable. When the loss was below this value, the compression and expansion lines on the p-V diagram approached or crossed each other at points other than the end points. Furthermore, in six experiments above a Reynolds number of 8000, the calculated loss was negative, and therefore these points are not shown on the log-log plot. These results are not surprising in view of the level of accuracy of the pressure and volume measurements. Nevertheless, some conclusions can be drawn from the plot. A significant drop in loss is indicated in the vicinity of a Reynolds number of 10,000, suggesting an overlap region like those on the plots for the other gases. If there is an overlap region in this area, there
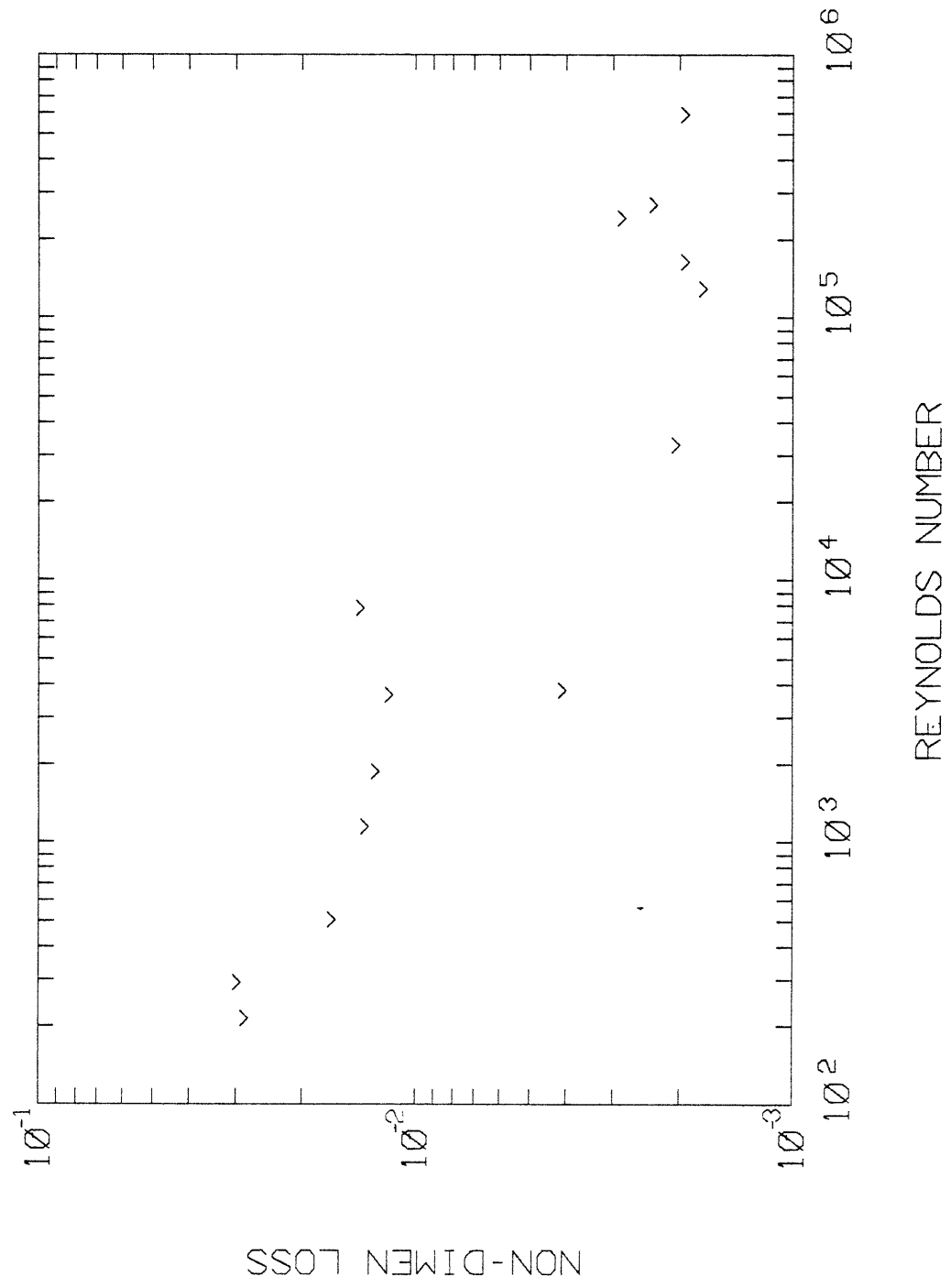
Fig. 3-6. Loss vs. Reynolds Number for Freon 13, Volume Ratio 2.39, Steel Liner.

is agreement with the conclusion above that the Reynolds number of the overlap region increases with the molecular weight of the gas. At higher Reynolds numbers, up to 10^6, the loss remains low, which tends to confirm the overall trend toward low losses at high Reynolds numbers.

3.4.3 Variation with Volume Ratio

A plot of loss vs. Reynolds number for helium at a volume ratio of 3.99 is shown in Fig. 3.7. This plot can be compared with the plot for the baseline case which had a volume ratio of 2.39. It can be seen that the maximum loss is increased with the higher volume ratio but it occurs at the same Reynolds number. The slope of the curve of loss vs. Reynolds number, on either side of the maximum loss, is less for the higher volume ratio. This is discussed further in Section 3.5.3. Two non-intersecting curves are again defined in the case of the higher volume ratio. The overlap is not as well defined because a narrower range of average pressure levels was possible with the same maximum pressure. The overlap appears to occur at the same Reynolds number.

3.4.4 Variation with Cylinder Liner Material

Plots of loss vs. Reynolds number for helium, using copper and micarta cylinder liners, are shown in Figs. 3.8 and 3.9. These plots can be compared with the plot for the baseline case which used a steel cylinder liner (Fig. 3.2). There is no significant difference between these plots. The properties of the wall should become significant when the surface temperature of the wall fluctuates significantly relative to the gas temperature fluctuation. This occurs when the cyclic heat storage

3-7

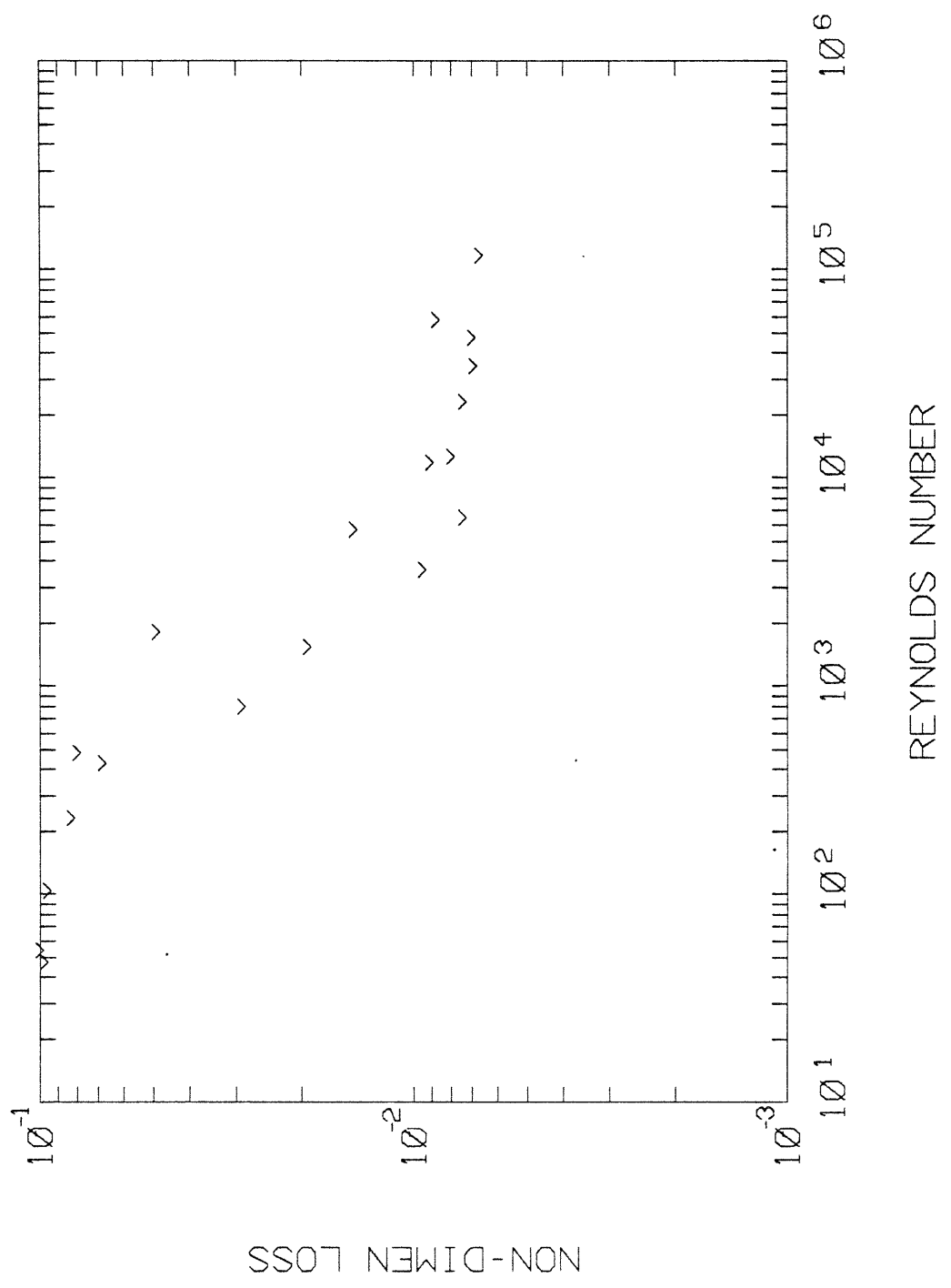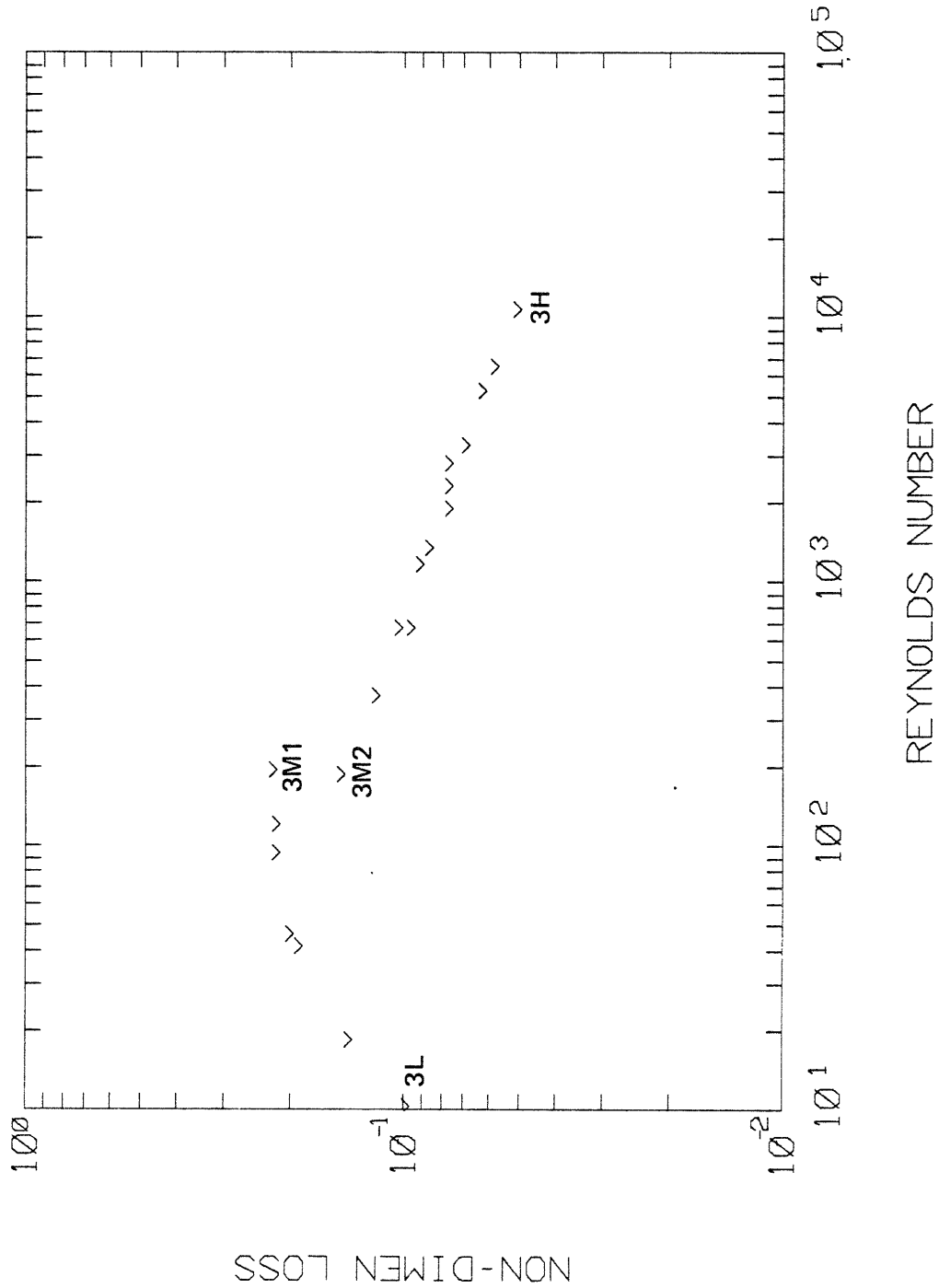
Fig. 3-7. Loss vs. Reynolds Number for Helium, Volume Ratio 3.99, Steel Liner.

3-8
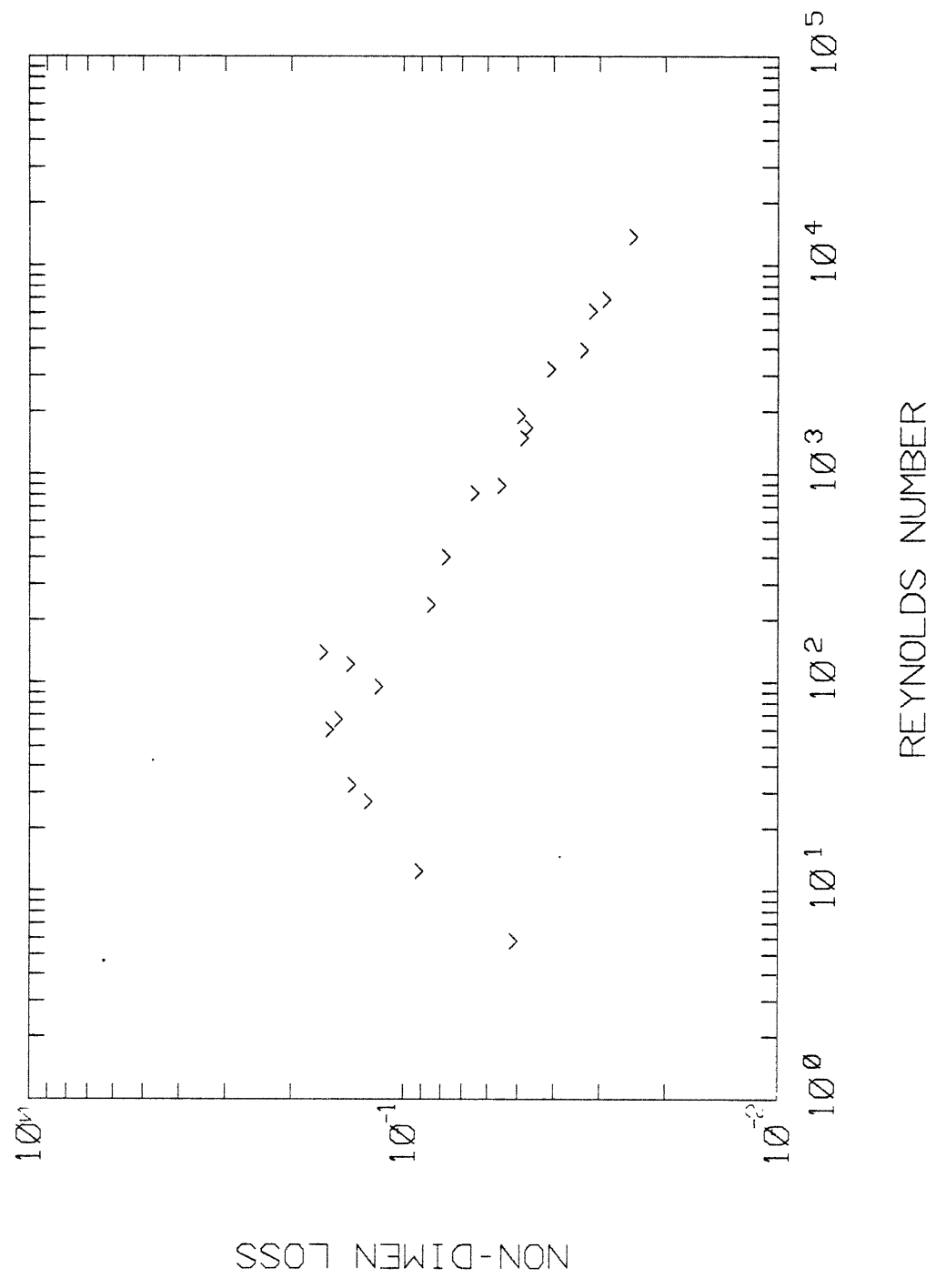
Fig. 3-8. Loss vs. Reynolds Number for Helium, Volume Ratio 2.39, Copper Liner.
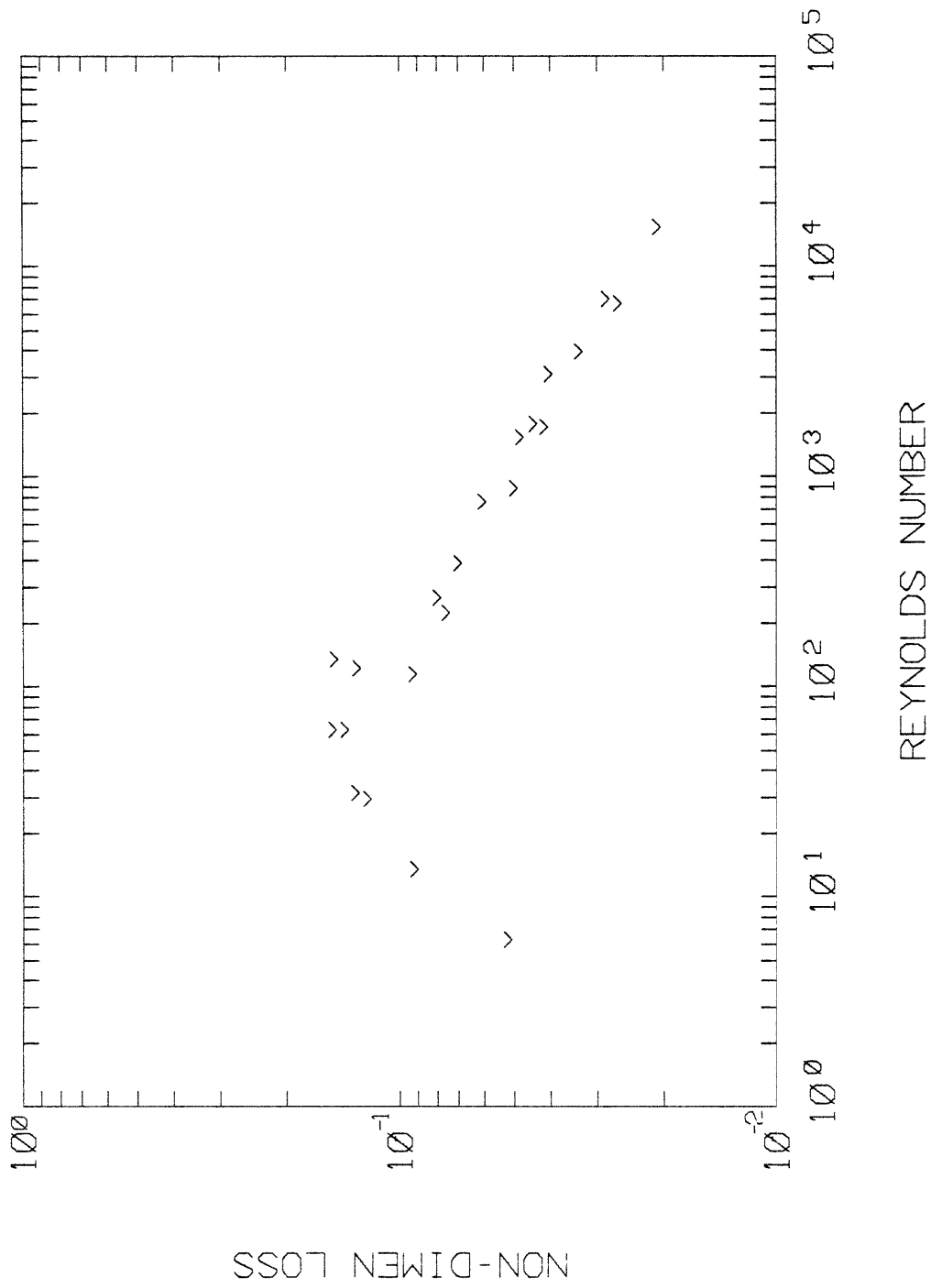
Fig. 3-9. Loss vs. Reynolds Number for Helium, Volume Ratio 2.39, Micarta Liner.

capacity of the wall is small enough. As discussed in Appendix A.3, the cyclic heat storage capacity of the wall is proportional to $\sqrt{\rho c k}$. Evidently the value of $\sqrt{\rho c k}$ for micarta is still too large for any effect to be detectable. The conclusion is that the property $\sqrt{\rho c k}$ of the cylinder wall material is not an important variable in the problem within the range values of $\sqrt{\rho c k}$ that were studied. More of an effect might have been observed if the apparatus had been run long enough to build up an axial temperature gradient in the cylinder side wall, as found in the preliminary experiments (Appendix D.2). The size of the axial temperature gradient should vary inversely with the thermal conductivity of the wall material.

3.5 T-S Diagrams

An example T-S diagram is discussed in some detail in Section 2.3. The discussion there includes the calculation of the isentropic and iso-thermal extremes, which are shown as a box on the T-S diagram. The calculation of the non-dimensional temperature and entropy is covered in Section 3.3.2. There it is mentioned that the points of maximum and minimum pressure are marked by vertical tic marks on the T-S diagrams and the points of maximum and minimum volume are marked by horizontal tic marks.

A directory of the T-S diagrams discussed in this work is given in Table 3.3. The significance of the labeled points on two diagrams is discussed in Section 3.5.1. These diagrams correspond to the four labeled points in each of three loss vs. Reynolds number plots, which were discussed in the previous section. Referring to Figs. 3.10, 3.12

TABLE 3.3

T-S DIAGRAM DIRECTORY

GAS	VOLUME RATIO	L vs. R PLOT	T-S DIAGRAMS			
Helium	2.39	Fig. 3.3	Point 1L Fig. 3.10	Point 1M1 Fig. 3.11	Point 1M2 Fig. 3.12	Point 1H Fig. 3.13
Argon	2.39	Fig. 3.5	Point 2L Fig. 3.14	Point 2M1 Fig. 3.15	Point 2M2 Fig. 3.16	Point 2H Fig. 3.17
Helium	3.99	Fig. 3.7	Point 3L Fig. 3.18	Point 3M1 Fig. 3.19	Point 3M2 Fig. 3.20	Point 3H Fig. 3.21
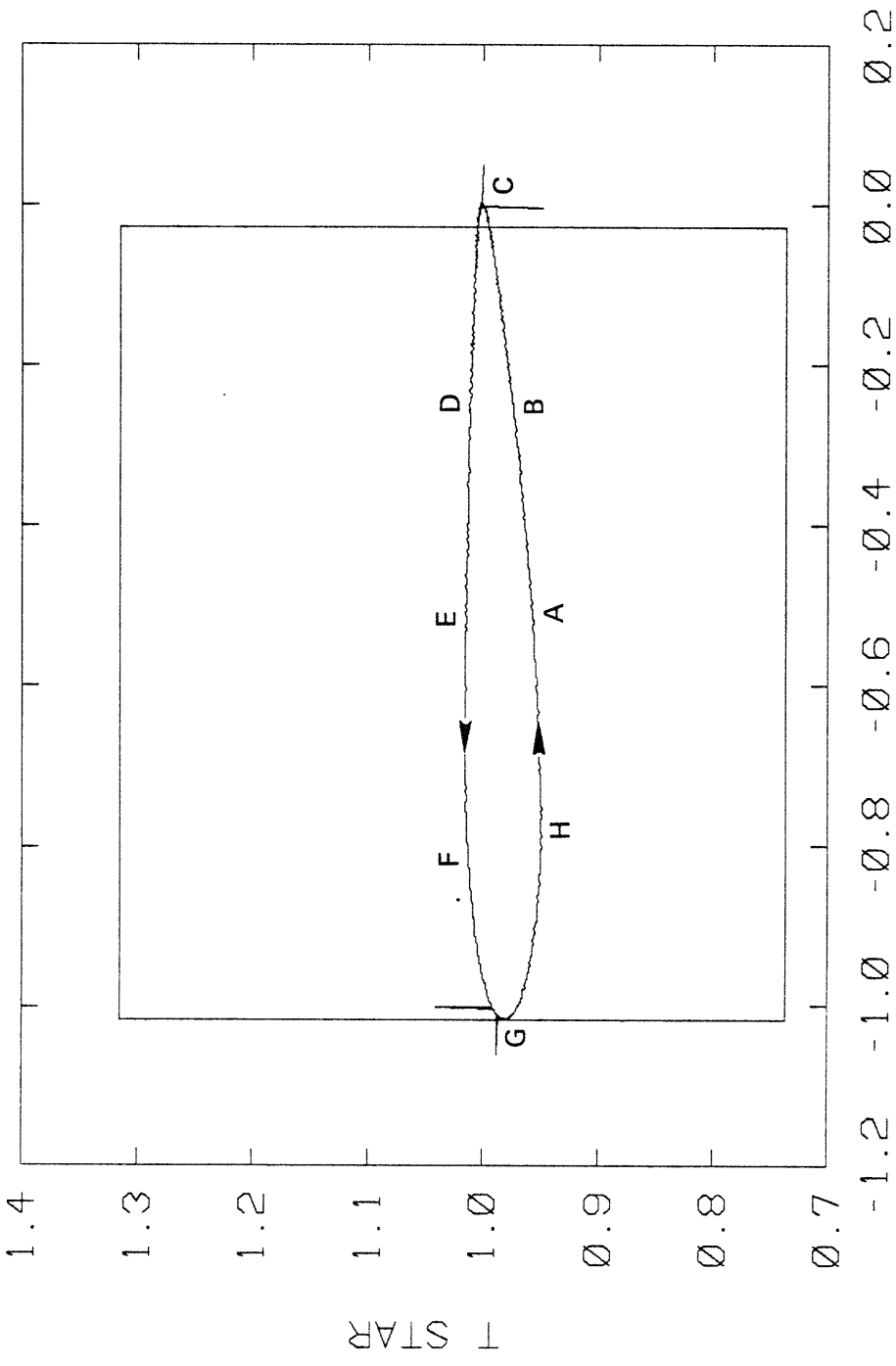
S STAR   10-18-82   RUN 04

Fig. 3-10. T-S Diagram for Helium, p_{mc} = 10.2, N = 8.8, Re = 6.09, L = .0469, Corresponding to point 1L, Fig. 3-3.
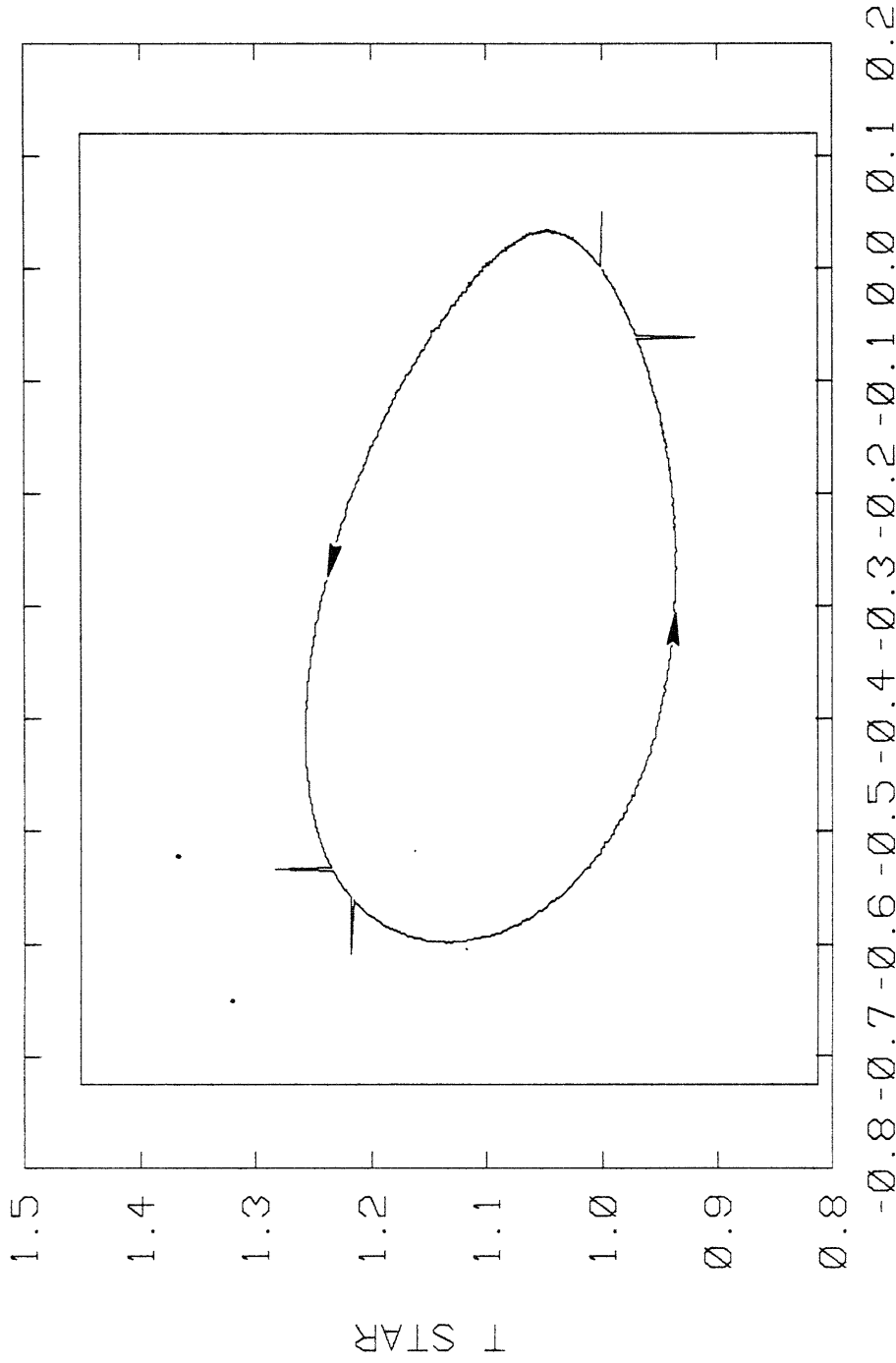
Fig. 3-11. T-S Diagram for Helium, p_{mc} = 109, N = 15.3, Re = 113, L = .151,
Corresponding to point 1M1, Fig. 3-3.

3-12
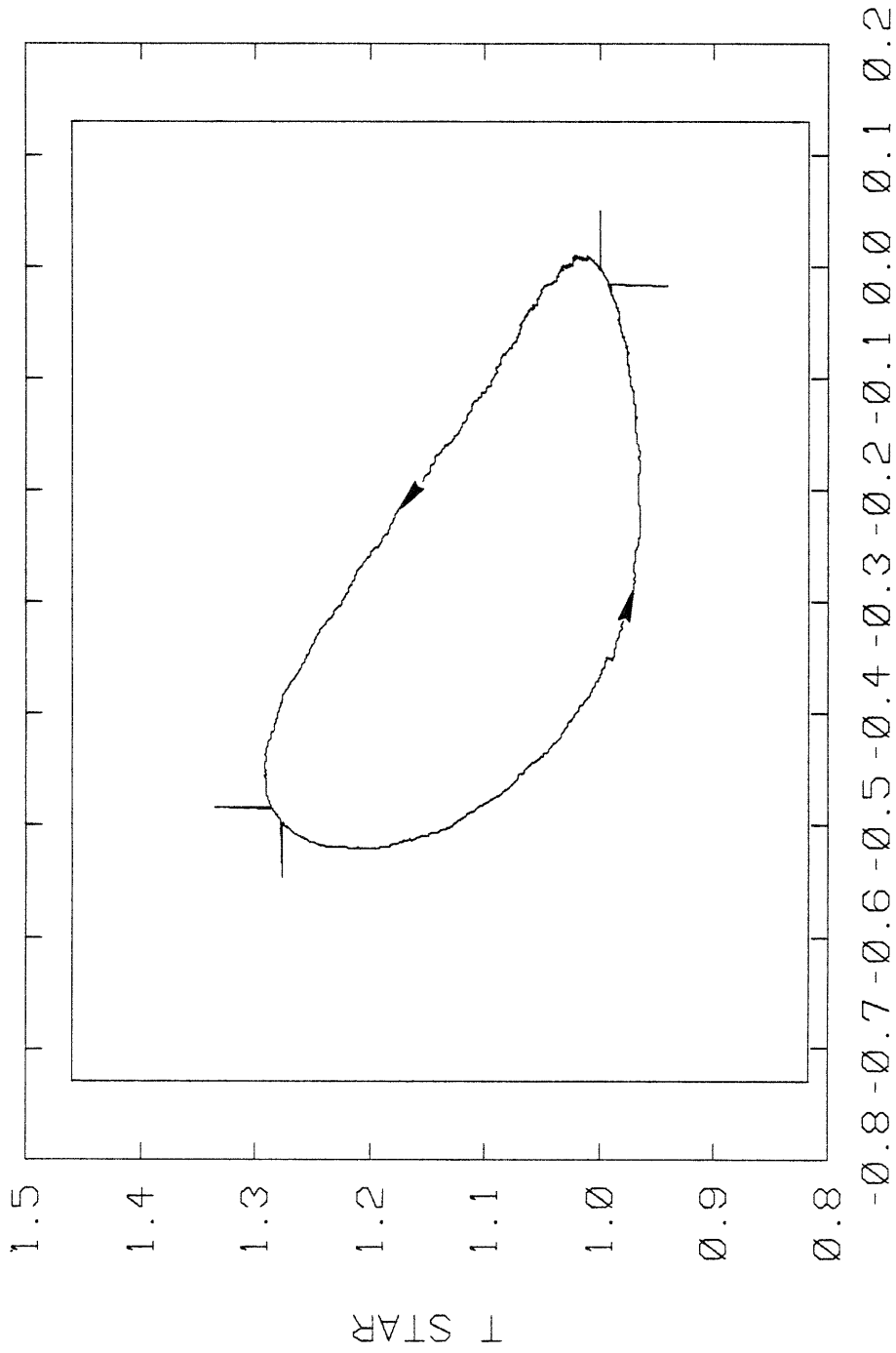
Fig. 3-12. T-S Diagram for Helium, p_{mc} = 12.6, N = 127, Re = 108, L = .0975, Corresponding to point 1M2, Fig. 3-3.

S STAR   10-01-82   RUN 03
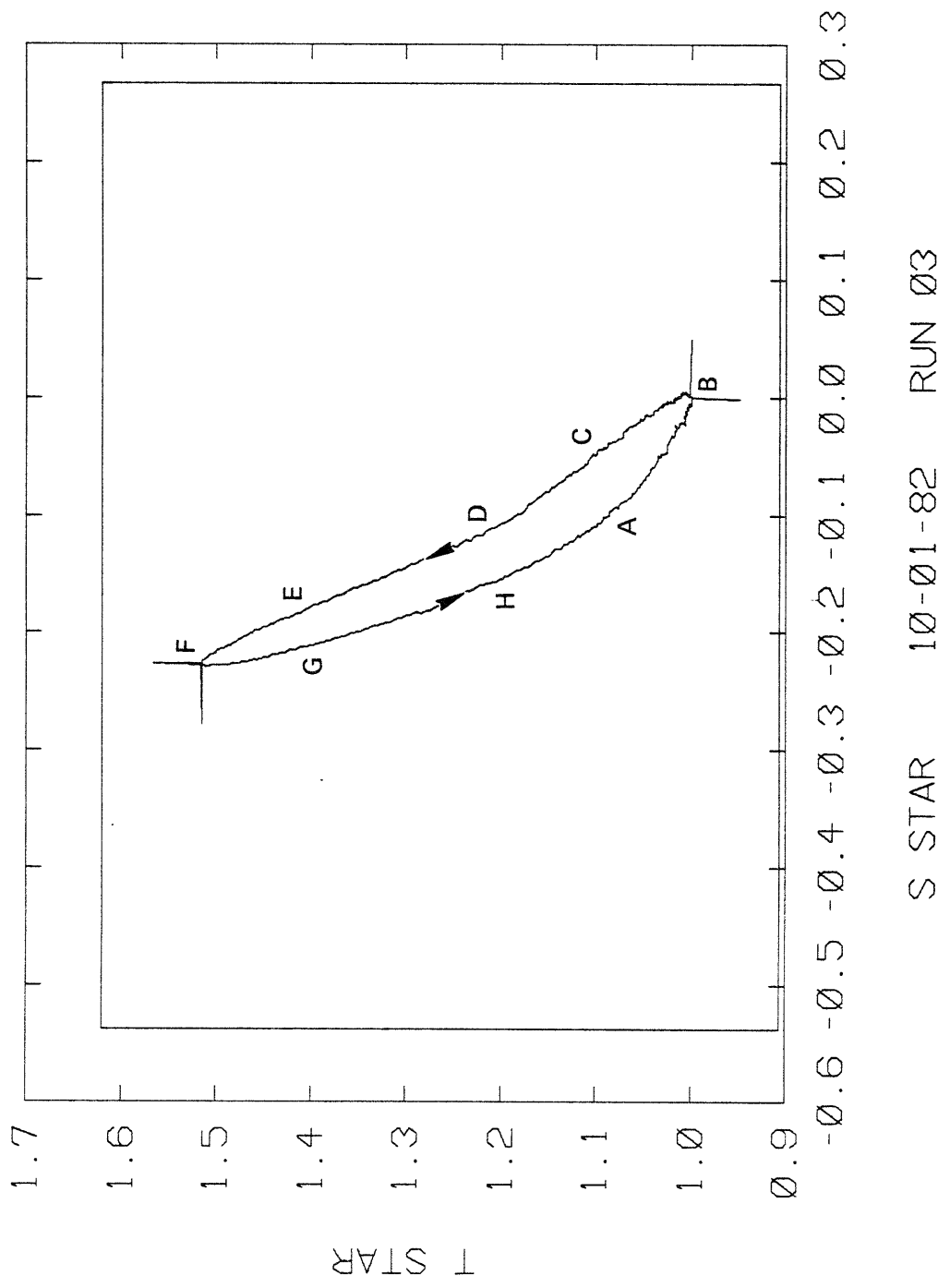
Fig. 3-13. T-S Diagram for Helium, p_{mc} = 214, N = 930, Re = 13,500, L = .0207,
Corresponding to point 1H, Fig. 3-3.

3-14
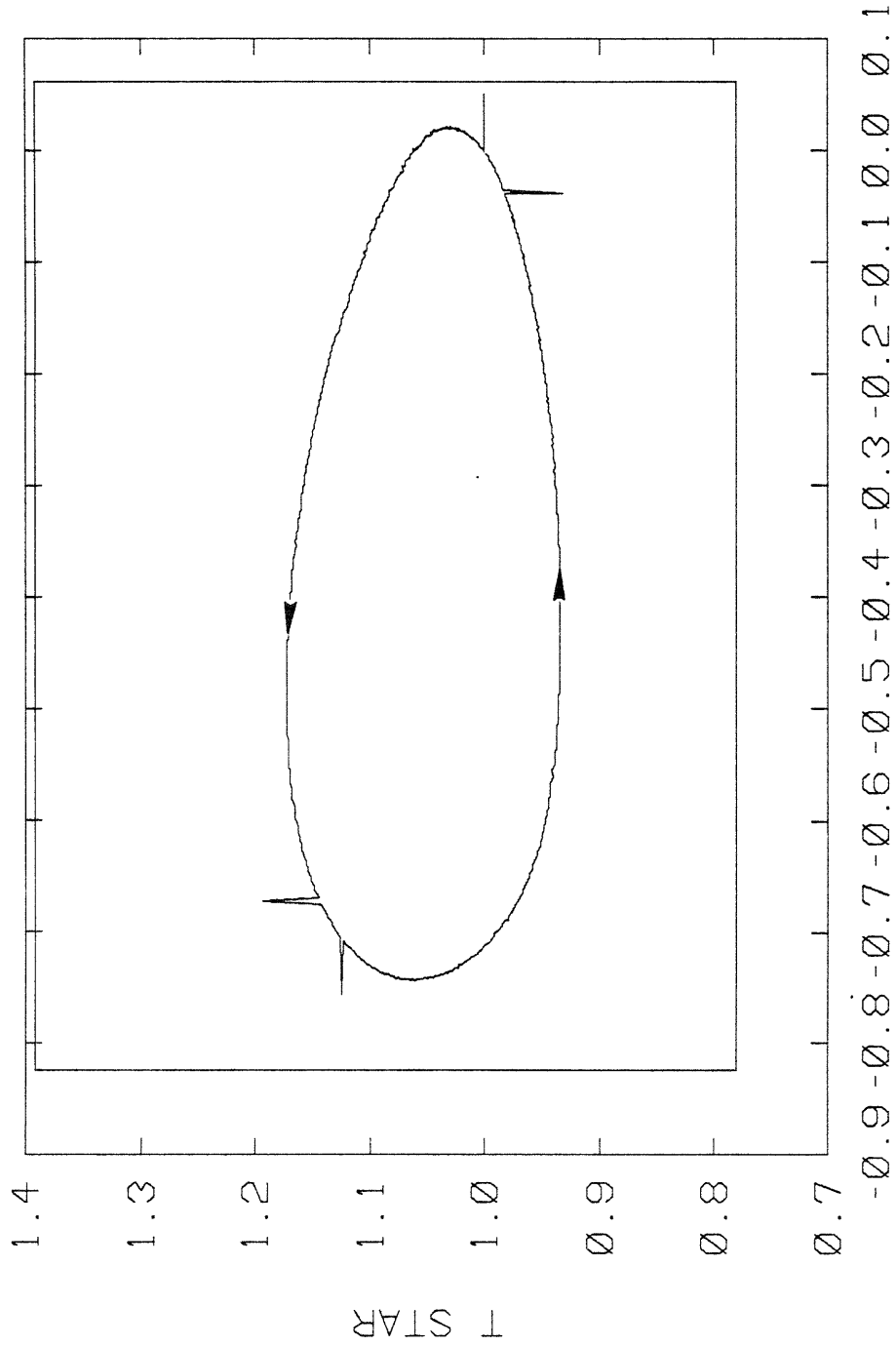
S STAR   12-30-82   RUN 11

Fig. 3-14. T-S Diagram for Argon, p_{mc} = 10.7, N = 8.8, Re = 55.5, L = .142,
Corresponding to point 2L, Fig. 3-5.
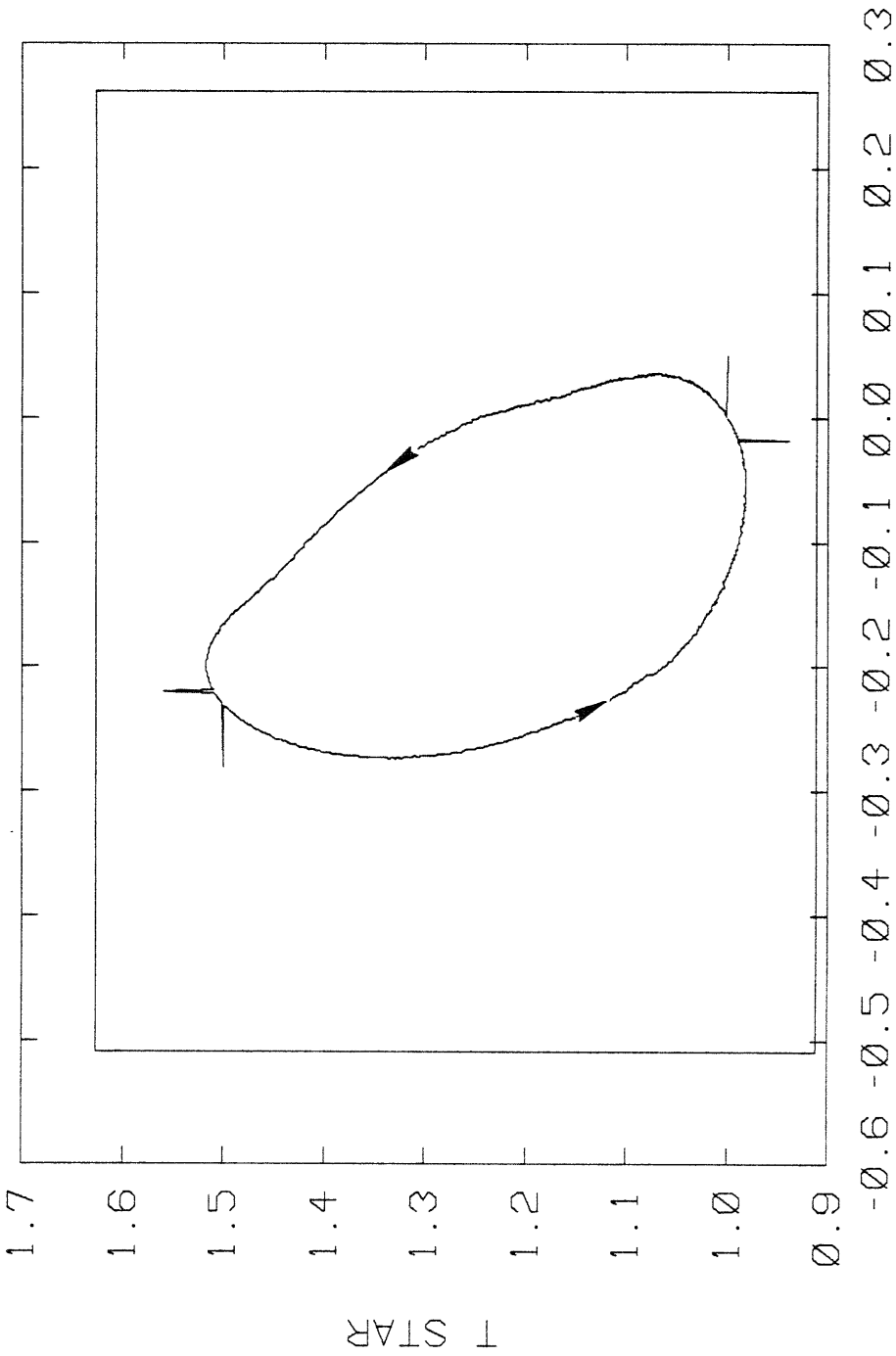
Fig. 3-15. T-S Diagram for Argon, p_{mc} = 99.8, N = 15.1, Re = 890, L = .1105, Corresponding to point 2M1, Fig. 3-5.
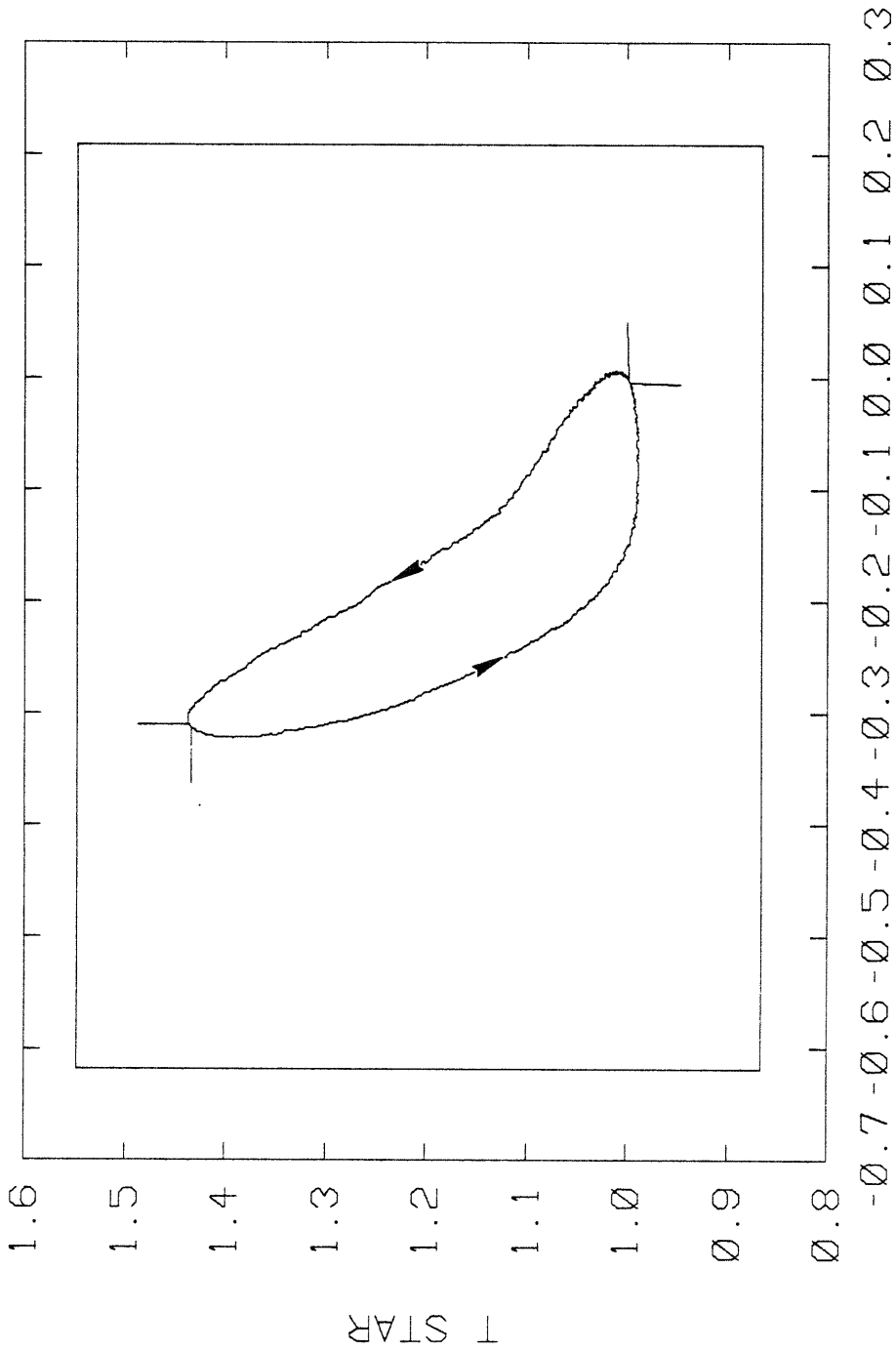
Fig. 3-16. T-S Diagram for Argon, p_{mc} = 12.6, N = 130, Re = 968, L = .0514, Corresponding to point 2M2, Fig. 3-5.
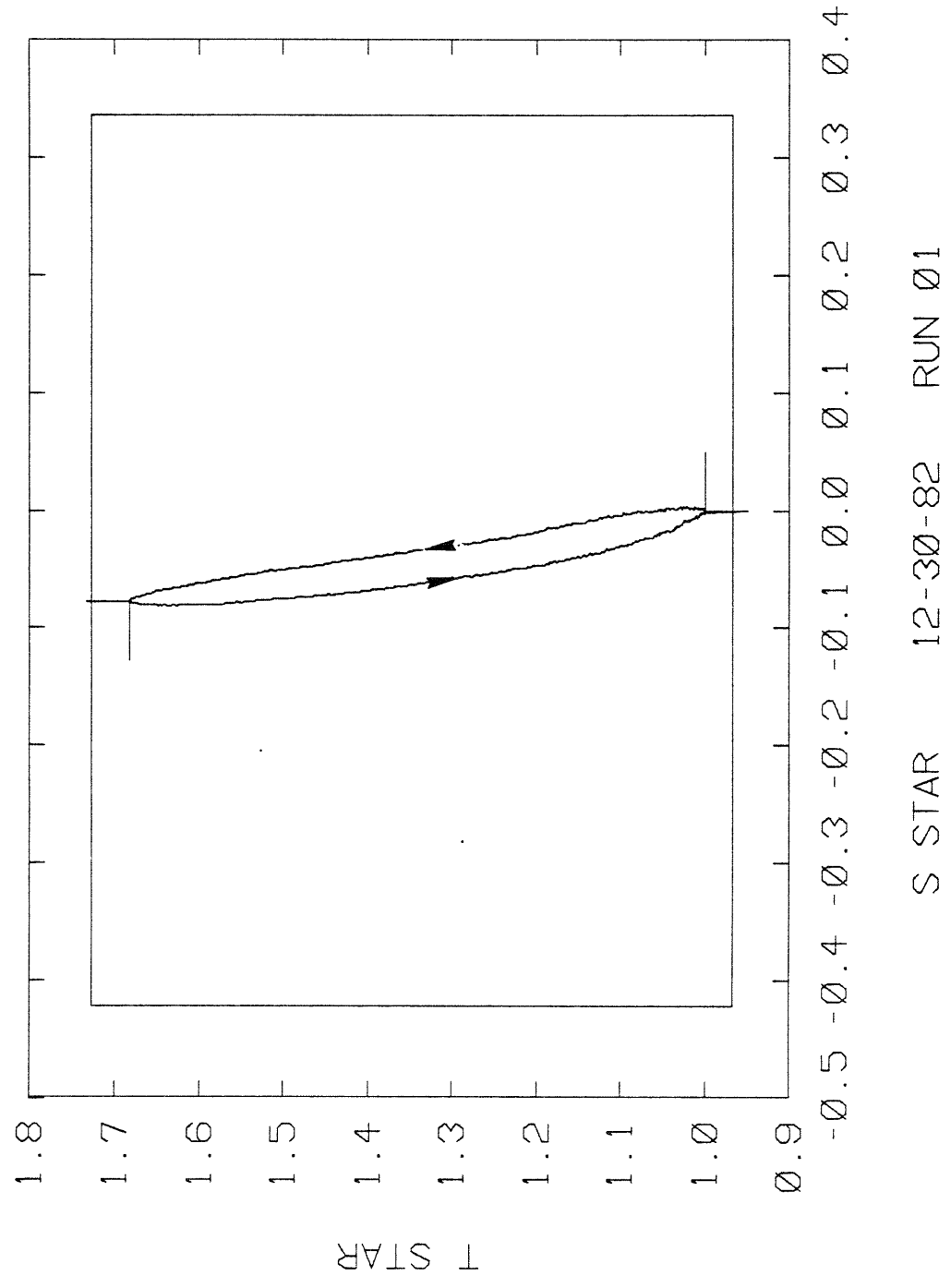
Fig. 3-17. T-S Diagram for Argon, p_{mc} = 227, N = 948, Re = 127,000, L = .0162,
Corresponding to point 2H, Fig. 3-5.

3-18
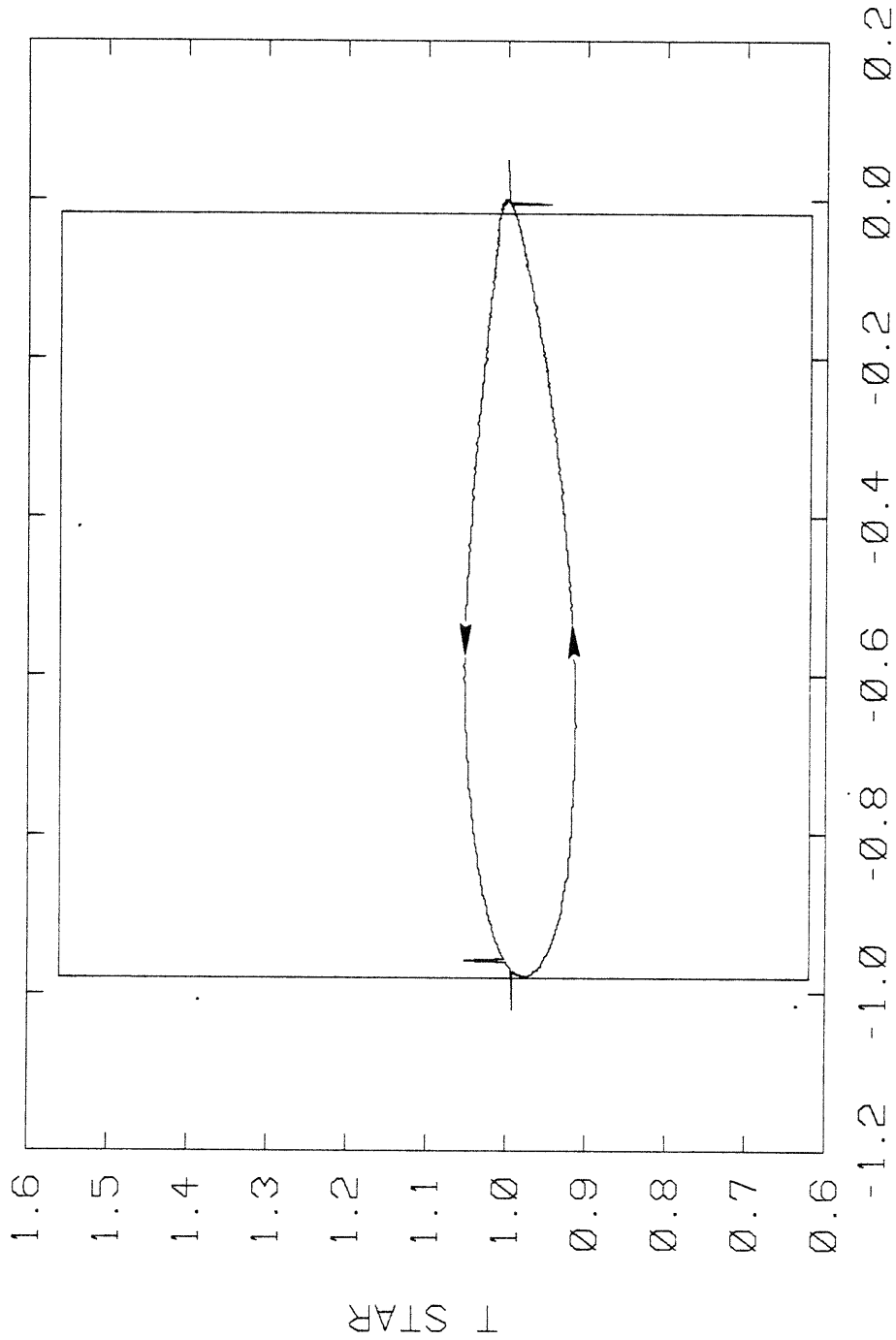
S STAR   12-10-82   RUN 05

Fig. 3-18. T-S Diagram for Helium, p_{mc} = 17.3, N = 8.8, Re = 10.3, L = .0969,
Corresponding to point 3L, Fig. 3-7.
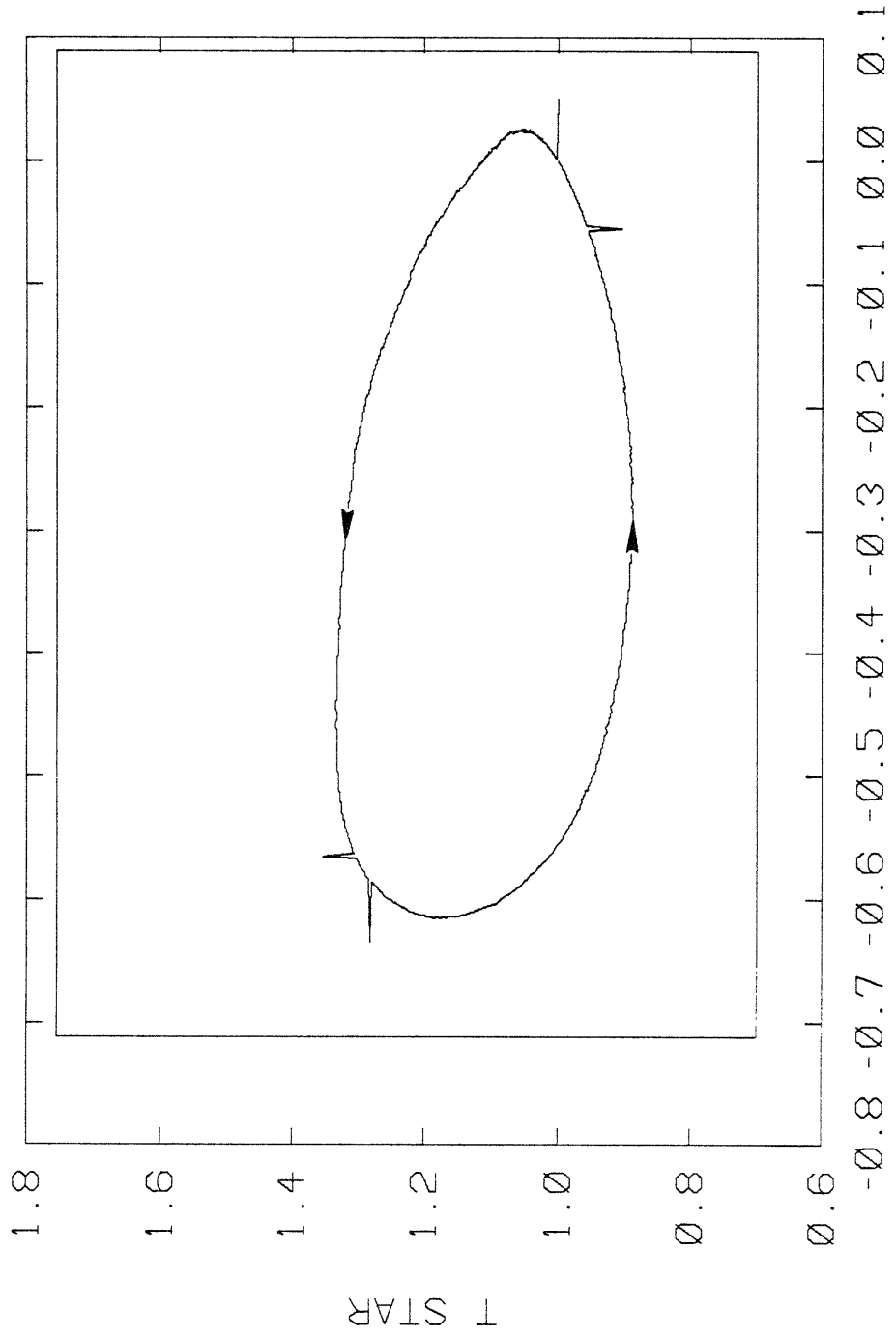
Fig. 3-19. T-S Diagram for Helium, p_{mc} = 191, N = 15.0, Re = 194, L = .218,
Corresponding to point 3M1, Fig. 3-7.
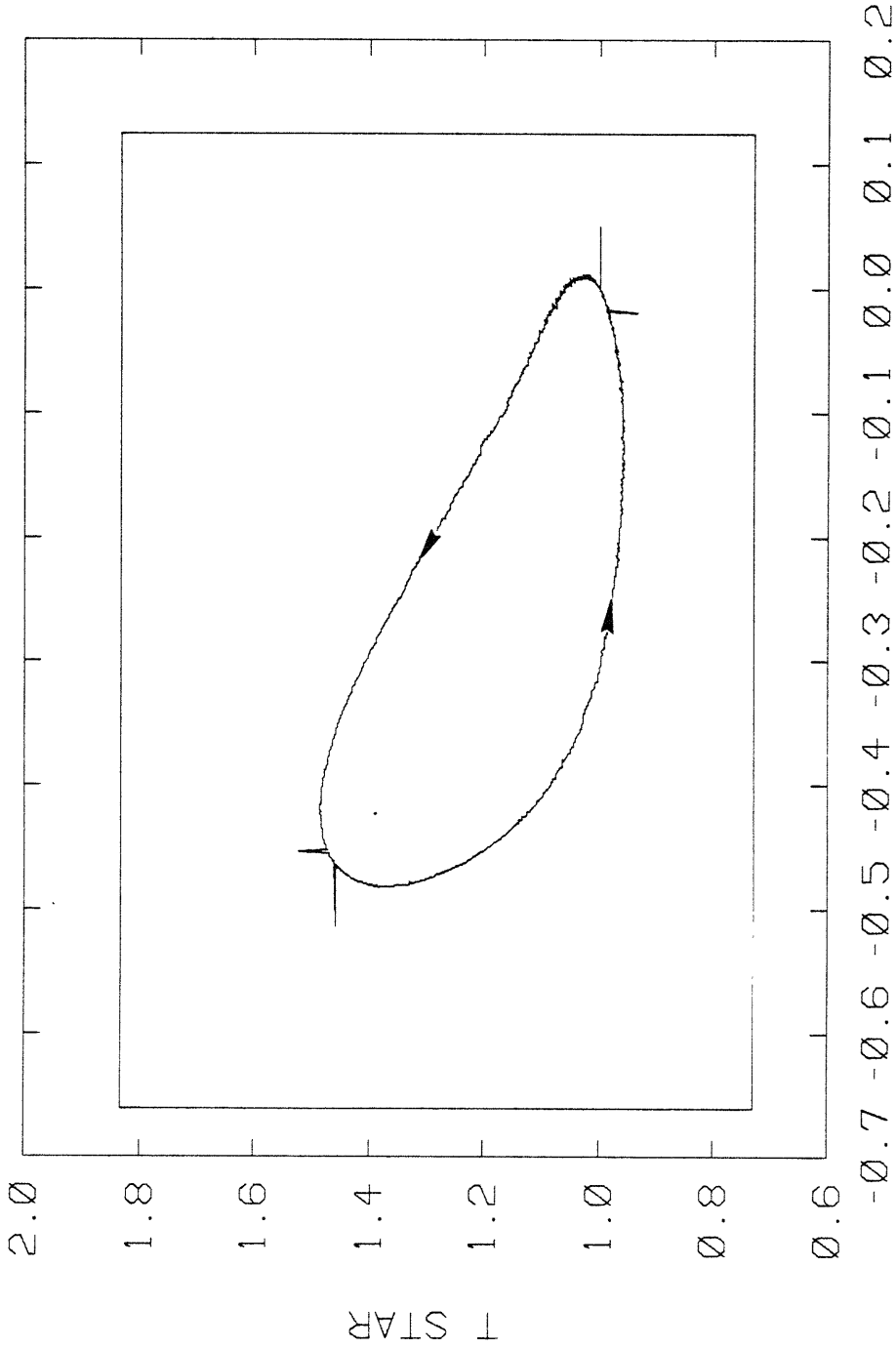
Fig. 3-20. T-S Diagram for Helium, p_{mc} = 21.7, N = 128, Re = 188, L = .144, Corresponding to point 3M2, Fig. 3-7.

3 - 21
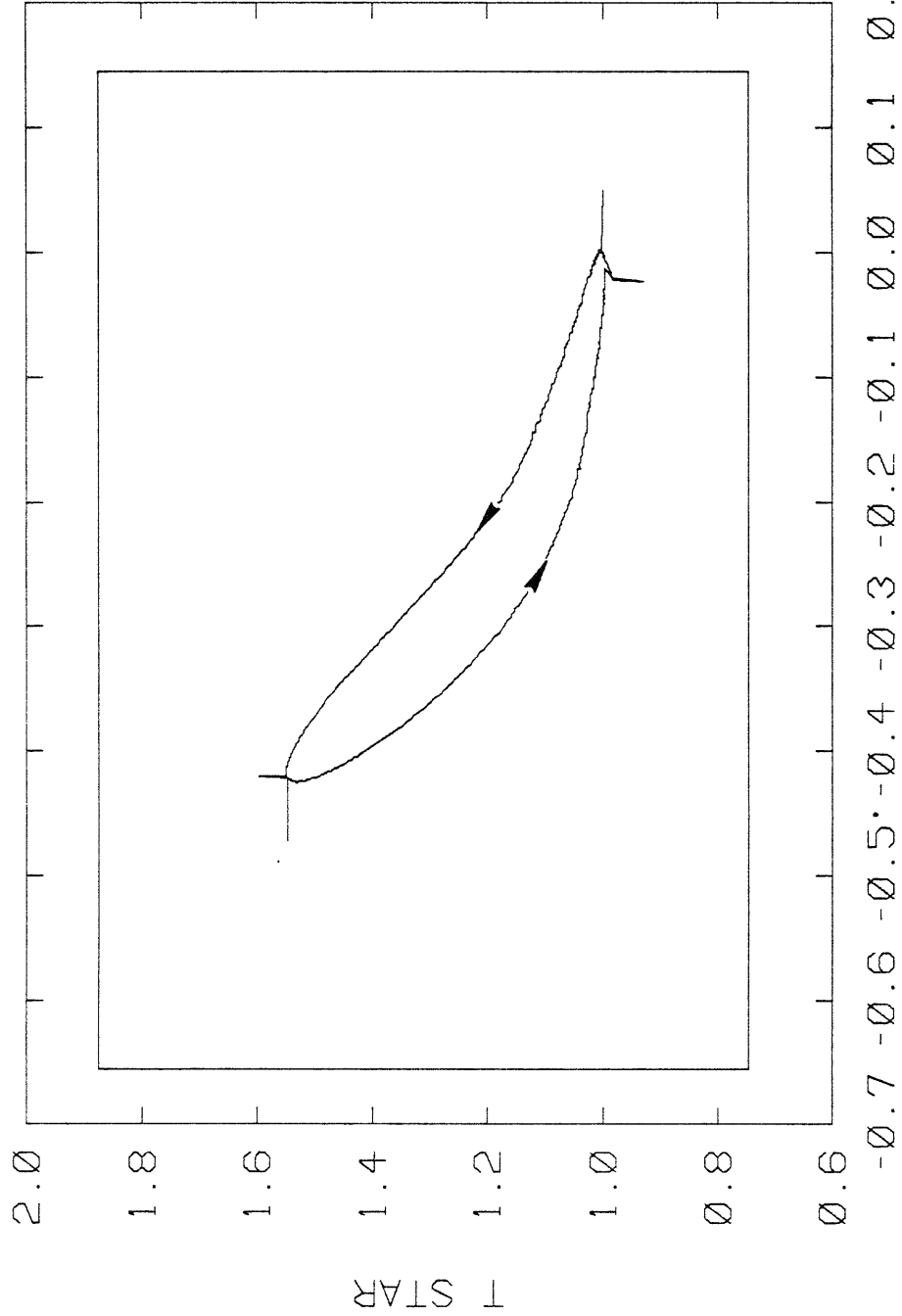
Fig. 3-21. T-S Diagram for Helium, p_{mc} = 171, N = 926, Re = 10,700, L = .0496,
Corresponding to point 3H, Fig. 3-7.

and 3.14, we see that these three sets of four points were selected each in the same way. The first point, designated L, is at the lowest Reynolds number in the plot. The second and third points, designated M1 and M2, are high loss and low loss points, respectively, at close to the same intermediate Reynolds number. The fourth point, designated H, is at the highest Reynolds number in the plot.

T-S diagrams for experiments with nitrogen are not included, because they are essentially similar to the diagrams for experiments with argon. The molecular weight of nitrogen is relatively close to that of argon. The lower specific heat ratio of nitrogen reduces the temperature swing, and hence the height of the T-S diagram, but there is no clearly discernible effect on the shape of the diagram.

T-S diagrams for experiments with Freon 13 are inherently inaccurate because the temperature and entropy are calculated using the assumption that the gas is perfect. The behavior of Freon 13 under the conditions of these experiments is far from perfect. Hence the T-S diagrams are not very meaningful and are not included.

3.5.1 Shape Change with Reynolds Number

Between points L and M1, and between points M2 and H, the shape of the T-S diagrams in each set change smoothly and continuously. By looking at the four diagrams, then, the trend of the change in shape with Reynolds number can be seen.

We now consider the diagrams for the two sets of experiments using helium. The diagrams approach isothermal at the lowest Reynolds number.

In fact the entropy reaches or slightly exceeds the isothermal extremes as shown by the sides of the box. (Overshooting at one end while just touching at the other indicates a small error in the pressure swing.) Also the heat transfer is roughly in phase with the temperature, and 90° out of phase with the pressure and volume. Thus the classical heat transfer formulation discussed in Chapter 2 would probably be appropriate at very low Reynolds numbers. At intermediate Reynolds numbers, the diagrams have an intermediate shape and enclose a greater area, representing a larger loss. A phase difference between the heat transfer and the temperature is evident, and the phase angle between the temperature and the pressure is reduced. At the highest Reynolds number the diagrams approach isentropic. The enclosed area is reduced as the loss drops. Now the temperature is in phase with the pressure and close to 90° out of phase with the heat transfer.

Now we recall the variation of the gas temperature profile with time through the cycle, as discussed in Section 2.3 and illustrated in Fig. 2.4. The experimental cycle discussed there had an intermediate average Reynolds number. We now consider how the gas temperature profile varies with time at low Reynolds number as shown in Fig. 3.22. The speed and amplitude of the pressure variation are low and hence the temperature of the gas near the wall stays in phase with the temperature of the gas far from the wall. The temperature profile changes smoothly back and forth remaining monotonic. Now consider how the profile varies with time at high Reynolds number, as shown in Fig. 3.23, where the speed
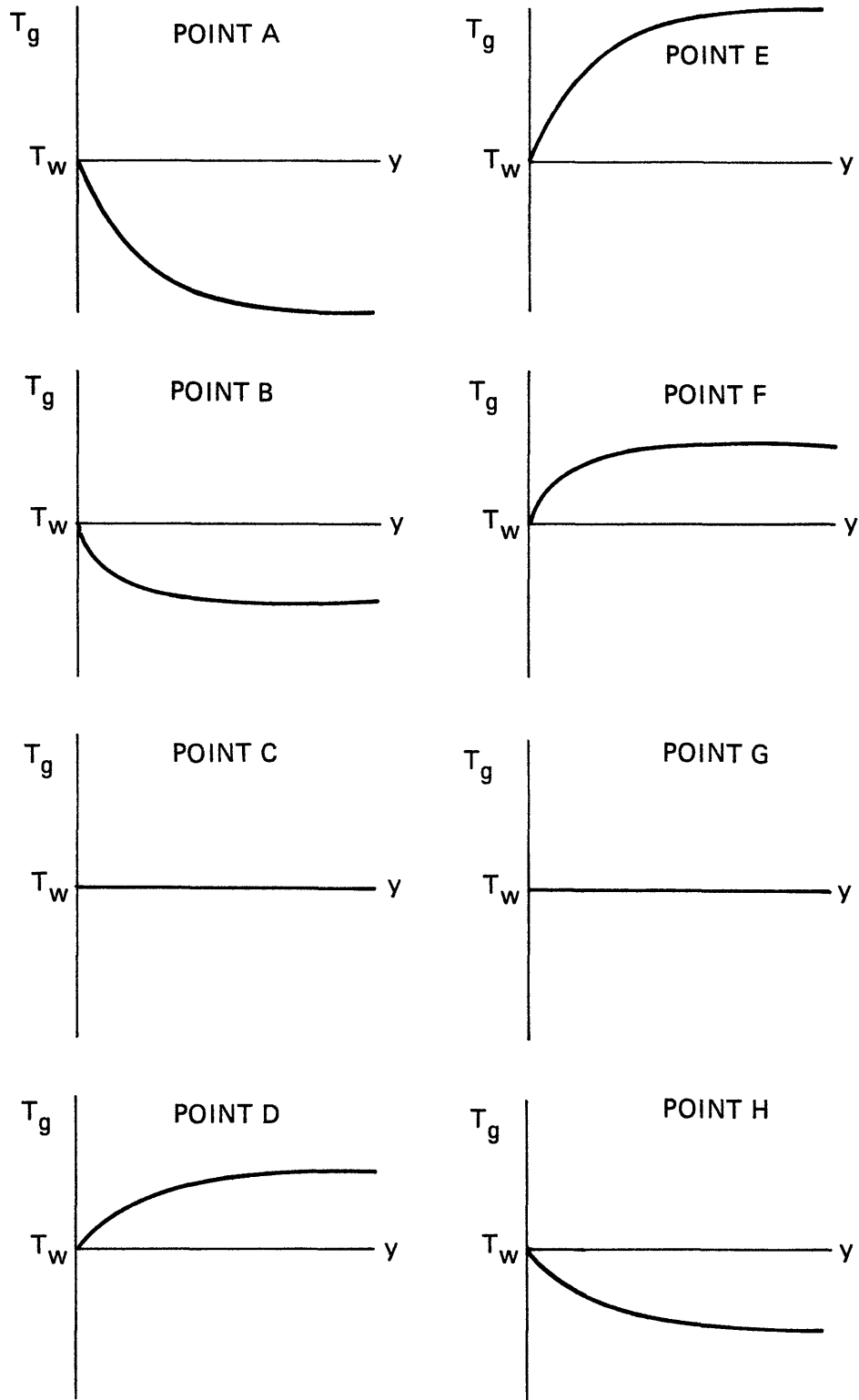
Fig. 3-22. Instantaneous Gas Temperature Profiles Corresponding to Labelled Points on T-S Diagram, Fig. 3-10.
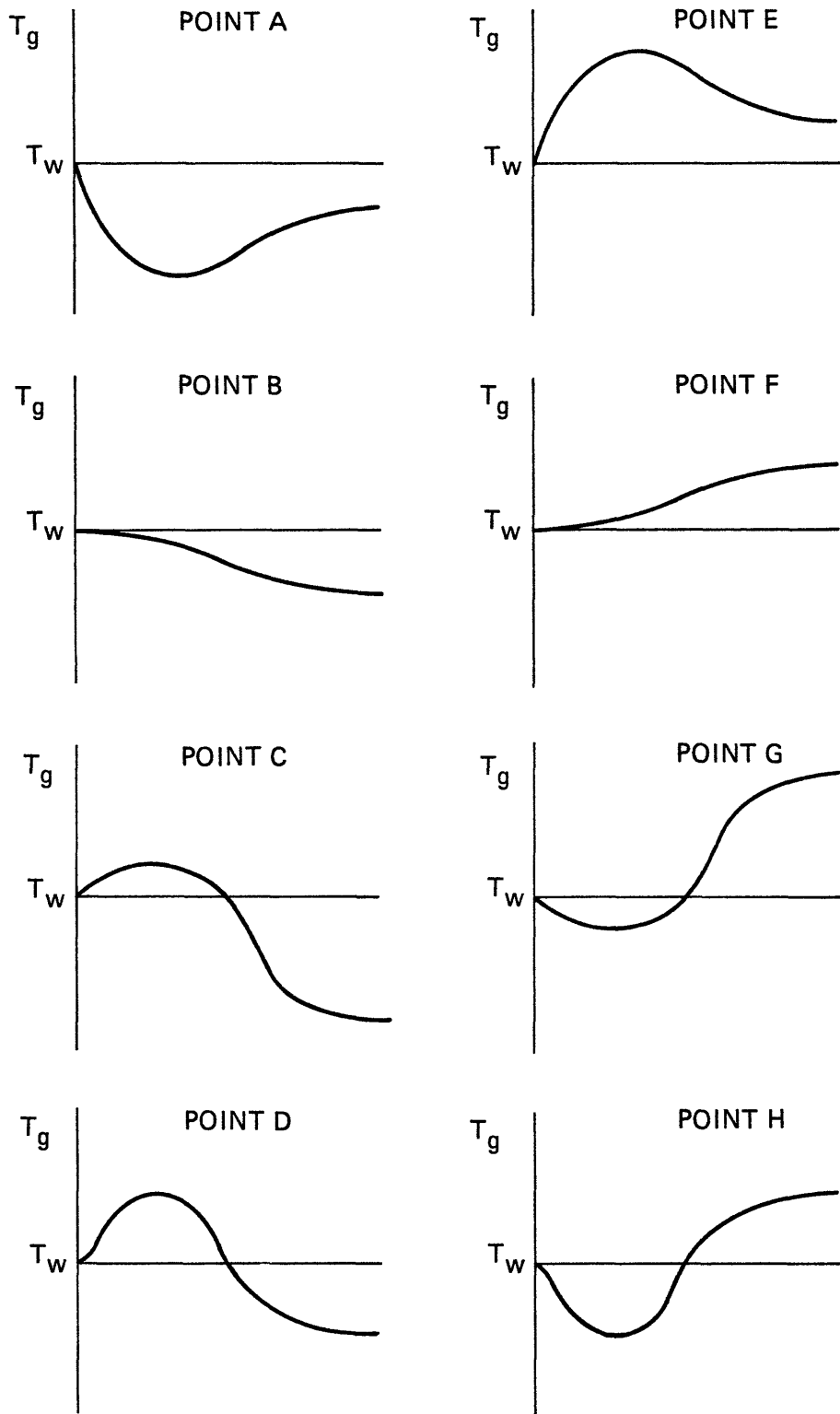
Fig. 3-23. Instantaneous Gas Temperature Profiles Corresponding to Labelled Points on T-S Diagram, Fig. 3-13.

and amplitude of the pressure variation are high. When the time deriva-
tive of pressure changes sign, the temperature of the gas near the wall
swings rapidly through the wall temperature. Thus the temperature of
the gas near the wall leads the temperature of the gas away from the wall
by about 90°.

We now turn to the diagrams for the set of experiments using argon.
These diagrams can be seen to have shapes similar to either set of helium
diagrams if we compare the first argon diagram to the second helium dia-
gram and so on. The fourth argon diagram carries the trend set in the
previous three a step further. All this indicates that the effect of the
increased molecular weight of argon over helium is well accounted for by
the increased Reynolds number of experiments done with argon at a given
average pressure and speed.

3.5.2 Shape Change with Average Pressure and
Speed at Constant Reynolds Number

In Section 3.4.1 it was observed that two experiments, falling
in the overlap region of the loss vs. Reynolds number plot, could have
rather different loss values while having Reynolds numbers that were very
close to the same. This result can be seen in the T-S diagrams by com-
paring the diagrams corresponding to points M1 and M2 in each set. There
is a characteristic change of shape common to the three sets. The upper
side of the diagram changes from concave down in the experiments at high
pressure and low speed, to straight or concave up in the experiments at
low pressure and high speed. Evidently there is a change in the processes
occurring in the cylinder, particularly in the compression part of the

cycle, which depends on the average pressure and speed at constant Reynolds number. This phenomenon could possibly be explained by some kind of abrupt and history-dependent change in the flow regime, such as the sudden onset of vortex shedding in the flow past a cylindrical body.

3.5.3 Shape Change with Volume Ratio

Comparing the T-S diagrams for the two sets of experiments done with helium, we can see that the diagrams corresponding to points L, M1 and M2 do not appear to change very much with volume ratio. Comparing the diagrams corresponding to points H, however, shows the diagram for volume ratio 3.99 to be considerably more isothermal than the diagram for volume ratio 2.39. A possible explanation for this is as follows. In the higher Reynolds number range, as the Reynolds number increases, the cycles tend to become more isentropic, i.e., heat transfer is reduced. This effect could be delayed or reduced, however, by the larger pressure swing associated with a larger volume ratio. Similarly, the diagram for point L with volume ratio 3.99 is less isothermal than the diagram for point L with volume ratio 2.39. The higher volume ratio with its greater pressure swing could delay or reduce the tendency toward constant temperature as the Reynolds number is decreased in the lower Reynolds number range. This could account for the lesser slope of the loss vs. Reynolds number plot for volume ratio 3.99 on both sides of the maximum loss.

CHAPTER 4

CONCLUSIONS

4.1 Summary of Results

The T-S diagram is a powerful tool for displaying the magnitude and timing of the instantaneous spatially averaged heat transfer around the cycle. The shape of the gas temperature profile perpendicular to the wall can be inferred from the T-S diagram. The variation of the shape of the profile with time through the cycle shows clearly why the classical heat transfer formulation is not appropriate. The time variation of the temperature profile also helps to understand why the shape of the T-S diagram changes so dramatically with Reynolds number.

With one exception, it is confirmed that the principal independent variables in the cyclic heat transfer process are the specific heat ratio of the gas and the average Reynolds number of the cycle, for a given cylinder geometry and materials. The Reynolds number seems to determine the characteristics which are likely to be related to the nature of the flow, such as the phase relationships. The gas specific heat ratio seems to determine the characteristics which are likely to be related to the temperature swing, such as the magnitude of the maximum loss. The exception is that there is a narrow band of Reynolds numbers in which the cyclic heat transfer process can vary considerably at constant Reynolds number. In this band there is another unknown determining factor, and there is likely to be some kind of flow regime transition.

The loss due to cyclic heat transfer can be quite significant. For helium at a volume ratio of 3.99, the maximum loss was 22% of the compression work. The loss due to cyclic heat transfer has a maximum at an intermediate average Reynolds number, for a given gas and cylinder. This indicates that, in designing machines in which the loss due to cyclic heat transfer is important, it is desireable to avoid intermediate Reynolds numbers. In Stirling cycle machines, the cylinders tend to operate at high average Reynolds number and the heat exchangers at low average Reynolds number. The results here suggest that the average piston speed be kept high and the gas velocity in the heat exchangers be kept low. The results also suggest minimizing the volume of connecting passages, which may operate at intermediate Reynolds number.

4.2 Suggestions for Further Research

Obviously the range of variation of the parameters could be extended. Particularly extending the pressure and speed to higher levels would be useful. Also the range of cylinder wall properties could be extended to lower $\sqrt{\rho c k}$. One way to reach the lower extreme of $\sqrt{\rho c k}$ would be to run some experiments at liquid helium temperature, where the heat capacities of metals are very small.

Another interesting set of experiments could be run in an opposed piston apparatus with the pistons about 90° out of phase. Then the small and large volume parts of the cycle would take place in different axial locations in the cylinder. The steady state axial wall temperature distribution would be interesting and could be externally altered by heating and cooling.

If an apparatus with somewhat more complicated instrumentation were built, it should be possible to begin to correlate instantaneous local heat flux measurements with the spatially averaged heat transfer obtained from p-V data. It would be necessary to measure the local heat flux by some means such as fast response surface thermocouples at a number of locations: on the head, side wall of the clearance volume, side wall of the swept volume and piston face. If this were done in a cylinder with negligible leakage while simultaneously measuring pressure and volume, a very interesting set of data would result.

A logical next step would be to begin to look at the heat transfer process through the complete cycle in a device with valves. The heat transfer in the intake and exhaust phases is different from that in compression and expansion, since the flow rate is large and the pressure change is small. Therefore, these processes should probably be studied separately from compression and expansion. An experimental compressor with a very low pressure ratio might be a useful apparatus. A considerable amount of work on exhaust heat transfer has been done by people working with reciprocating internal combustion engines. Also the interactions and transitions between the phases of the cycle would need to be considered. Clearly fluid motions generated in the intake phase may persist into the compression phase and beyond. Again this phenomenon has been studied in internal combustion engines.

Another important aspect of the processes in devices with valves is that the compression or expansion process can begin with the closing of

a valve or end with the opening of a valve. In these situations there
is a discontinuity in the time derivative of pressure, i.e. a sharp
corner in the pressure vs. time trace. The heat transfer considered in
this work is driven by a continuously varying time derivative of pressure.
Conceivably there may be additional effects and enhanced heat transfer
associated with the sudden start or stop in the rate of change of pressure.

REFERENCES

[1]   Annand, W.J.D., "Heat Transfer in the Cylinders of Reciprocating
      Internal Combustion Engines", Proc. I. Mech. E., Vol. 177,
      No. 36, pp. 973-990, 1963.

[2]   Woschni, G., "A Universally Applicable Equation for the Instan-
      taneous Heat Transfer Coefficient in the Internal Combustion
      Engine", paper 670931, SAE Trans., Vol. 76, 1967.

[3]   Wendland, D.W., "The Effect of Periodic Pressure and Temperature
      Fluctuations on Unsteady Heat Transfer in a Closed System",
      NASA CR-72323, 1968.

[4]   Vincent, R.J., Rifkin, W.D., and Benson, G.M., "Test Results of
      High Efficiency Stirling Machine Components", paper no. 829362,
      Proceedings of the 17th Intersociety Energy Conversion
      Engineering Conference, Vol. 4, pp. 1867-1874.

[5]   ASHRAE, Handbook of Fundamentals, 1972.

[6]   Jakob, M., Heat Transfer, Vol. I, Wiley, 1950.

[7]   Rohsenow, W.M., and Choi, H.Y., Heat, Mass and Momentum Transfer,
      Prentice-Hall, 1961.

[8]   Properties of micarta supplied by the manufacturer: Westinghouse,
      Hampton, South Carolina; Contact: Melvin Benson.

[9]   Taylor, C.F., The Internal Combustion Engine in Theory and
      Practice, Vol. I, 2nd edition, M.I.T. Press, 1966.

APPENDIX A

DETAILS OF APPARATUS

A.1 Speeds Used

The apparatus was driven at various speeds by the use of two electric motors and three pulley sizes as shown in Table A.1. The first motor was a 1/4 horsepower a.c. induction motor with an integral 48 to 1 worm gear reduction and the second motor was a 3 horsepower variable speed d.c. motor. Six speeds were possible using the a.c. motor and the d.c. motor at full speed, but there was a gap between 30 and 250 rpm. The speed of the d.c. motor was reduced to obtain speeds of 75-130 rpm when the pressure was below 60 psi. Higher pressures could not be used in this speed range because the d.c. motor did not develop enough torque to prevent excessive speed variation within the cycle. Speeds higher than 1000 rpm could not be used because of severe vibration from the unbalanced reciprocating mechanism of the compressor.

A.2 Lower Cylinder and Piston

The cylinder and piston is shown in Fig. A.1. The bore was two inches and the stroke was three inches. The piston was mostly made of micarta, with a steel core in the bottom part where the piston rod was attached. The piston seal was a Buna N rubber O-ring, with rubber back up rings, running in a honed steel liner in the lower part of the cylinder. This provided excellent sealing and the cycle to cycle pressure variation at mid-stroke was always less than 1%. However, the friction of the sliding seal caused noticeable heating of the cylinder wall, as reported in

TABLE A.1

SPEEDS USED

MOTOR	PULLEY DIAMETER in.	APPROXIMATE CRANKSHAFT SPEED rpm	APPROXIMATE AVERAGE PISTON SPEED ft/min
	3 1/2	9	4.5
A.C.	6 1/2	15	7.5
	13 3/4	32	16
	3 1/2	75 - 275	38 - 138
D.C.	6 1/2	460	230
	13 3/4	950	425
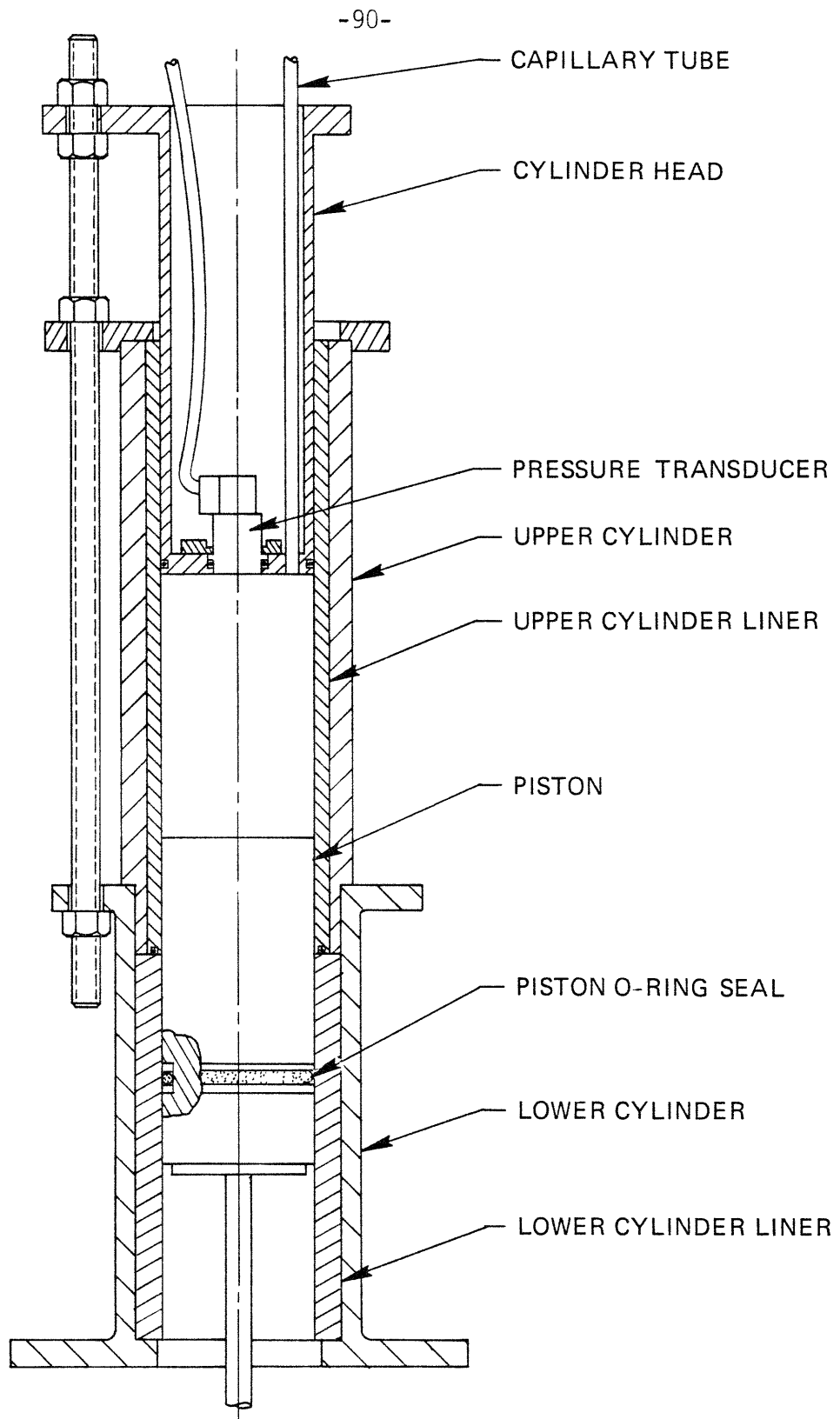
Fig. A-1. Cylinder and Piston.

Appendix D. If the working gas in the cylinder were exposed to the cylinder wall where it had been heated by piston seal friction, an un-known and undesired energy input to the gas would be created. Therefore the distance between the top of the piston and the seal was made larger than the stroke by 1/4 inch. The radial clearance between piston and the lower cylinder liner was approximately .004 inches.

A.3 Upper Cylinder

The thermal characteristics of the cylinder wall material may have an effect on the heat exchange between the wall and the gas. Reference [6] discusses the case of an infinitely thick plate in contact with a medium at oscillating temperature. The dependence of the heat energy stored in a half cycle on the characteristics of the plate material is shown to be,

$$Q \propto \sqrt{\rho c k} \qquad (A.1)$$

To study this effect, interchangeable upper cylinder liners were made of three materials, having a range of values of $\sqrt{\rho c k}$, as shown in Table A.2. The upper cylinder liner is held by a retaining plate tightly against the lower cylinder liner and this joint is sealed with an O-ring. The radial clearance between the piston and the upper cylinder liner was approximately .006 inches.

A.4 Cylinder Head

The steel cylinder head was in the form of a stationary piston fitting closely in the top of the cylinder and sealed with an O-ring (Fig. A.1).

TABLE A.2

PROPERTIES OF CYLINDER LINER MATERIALS

MATERIAL	ρ lbm/in^3	c Btu/lbm°F	k Btu/hr ft°F	$\sqrt{\rho ck}$	Ref.
Copper	.323	0.0915	233	2.57	[7]
Mild Steel	.282	0.113	25	.893	[7]
Micarta NEMA Grade C	0.050	0.38	.169	.057	[8]

The vertical position of the cylinder head was adjustable to obtain volume ratios of 2 to 10, by means of the threaded rods and nuts that hold the cylinder assembly together.

The body of the cylinder head was made from a steel tube, which was left open at the top end to allow the gas supply tube and the electrical cable from the pressure transducer to pass through. The gas supply tube between the valve and the underside of the cylinder head, was a stainless steel capillary tube to minimize gas volume not in the working space. The pressure transducer was mounted in the center, with its sensitive face flush with the bottom surface of the cylinder head, and it was sealed with an O-ring.

A.5 Pressure Instrumentation

The pressure in the cylinder was measured with a strain gauge pressure transducer. Two CEC type 4-313 transducers were used, with ranges of 0-100 psia and 0-500 psia. Thus 500 psia was the upper limit on pressure for all experiments.

An electrical schematic of the pressure instrumentation is shown in Fig. A.2. The usual balancing circuit was used to zero the output at atmospheric pressure. Originally a differential amplifier was not used, requiring the transducer power supply to be floating with respect to ground. It then acted as an antenna, adding an unacceptable level of 60 cycle noise to the output. Therefore the Analog Devices AD522 differential amplifier was used as an isolator between the transducer and the other circuitry, and incidentally provided amplification by a factor of about 100. In addition,
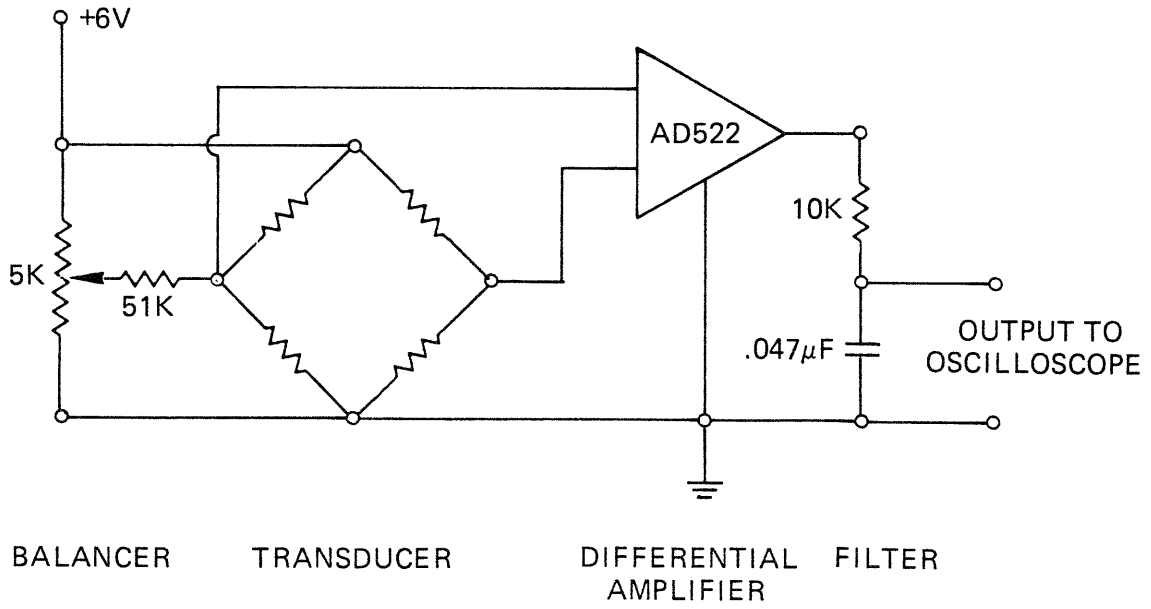
Fig. A-2. Electrical Schematic of Pressure Instrumentation.

a low pass filter was used to reduce high frequency noise to an acceptable level.

The transducers were calibrated statically from 10 psig to their upper limits using an Amthor type 452 Dead Weight Gauge Tester. The p-V and T-S diagrams are quite sensitive to relative errors in the pressure data from different parts of the cycle. Therefore two attempts were made to dynamically assess the accuracy of the transducers, the first unsuccessful and the second having limited success.

In the first attempt the instrument used for comparison was a pressure switch adapted from the M.I.T. Balanced-Diaphragm Pressure Indicator discussed in Reference [9]. In operation a static reference pressure is applied to the outer side of a small diaphragm and the cylinder pressure is applied to the inner side. As the cylinder pressure rises or falls through the reference pressure, the diaphragm deflects slightly, opening or closing the switch. An electrical signal from the switch can be displayed simultaneously with the output of the pressure transducer on an oscilloscope. The pressure indicated by the transducer at the time the switch closes can then be read and compared with the reference pressure. By repeating this procedure with various reference pressures, a comparison of the two instruments can be developed. The balanced-diaphragm indicator worked well in the past in experiments with internal combustion engines. However, the author found that the switch was too inconsistent in the pressure range used here to be useful. It is possible that greater experience with fabrication of the diaphragms and assembly of the switch would have led to greater consistency.

In the second attempt at dynamic comparison, the instrument used was a Kistler piezoelectric pressure transducer. This transducer was mounted in the side wall of the clearance volume, in the cylinder used in the earlier version of the apparatus (Appendix D). The apparatus was operated with helium at a volume ratio of 2.39, and the outputs from the piezoelectric and strain gauge transducers were simultaneously recorded with a digital oscilloscope. This was done for 13 combinations of average pressure level and speed covering the ranges used in the actual experiments.

In attempting to statically calibrate the piezoelectric transducer with the Dead Weight Gauge Tester, considerable zero drift was encountered. However, at the lowest speed used in the dynamic comparison, approximately 8 rpm, the dynamic effects on both types of transducers can be assumed to be small. Hence the low speed comparison was used as a quasi-static calibration of the two types of transducers directly against each other, with the piezoelectric drift limited to what could occur in one cycle at the lowest speed. Then the dynamic comparisons at higher speeds revealed the dynamic discrepancies between the two types of transducers.

Considering the amplitude discrepancies first, a small error in the average absolute pressure level has a small effect on the p-V and T-S diagrams, and hence this type of error was not studied. However, a small error in the pressure swing could have a significant effect on the results. The discrepancy in the pressure swing was found to be always less than 1.5%, roughly corresponding to change in the area of the p-V diagram of

about 7%. Since there was no way of telling which transducer was more accurate no attempt was made to compensate the strain gauge transducer for this discrepancy.

Turning to phase discrepancies, the dynamic comparisons showed the strain gauge transducers lagging the piezoelectric transducer. The lag was the same for both strain gauge transducers and increased with speed in the manner of a simple first order dynamic system. This lag was found to result from the electronic signal processing used with the strain gauge transducers, rather than the transducers or their bridge circuit, and is compensated in the data processing, as discussed in Appendix B.3.

A.6 Volume Instrumentation

In the early version of the apparatus (Appendix D) the piston position was indicated by a displacement transducer and cam on the crankshaft. In dynamically checking the accuracy of this system, the instrumentation used for comparison was found to be far more accurate. This second system consisted of tabs on the periphery of the compressor flywheel passing through a photo-interrupter module, thereby generating electrical pulses corresponding to known crankshaft positions. Schematics of the system are shown in Fig. A.3. From this the crank angle as a function of time can be calculated, and then in turn the piston position as a function of time can be calculated, as described in Appendix B.3. This second system was adopted for the volume instrumentation for subsequent experiments, and will now be described.

Sixteen rectangular sheet metal tabs were mounted on the flywheel. Two narrow tabs were bolted on through slots and were adjusted to corres-

FLYWHEEL

NARROW TAB

WIDE TAB

PHOTO
INTERRUPTER
MODULE

MECHANICAL SCHEMATIC

+6V

100

1K

80K

PHOTO
INTERRUPTER
MODULE

10K

OUTPUT TO
OSCILLOSCOPE
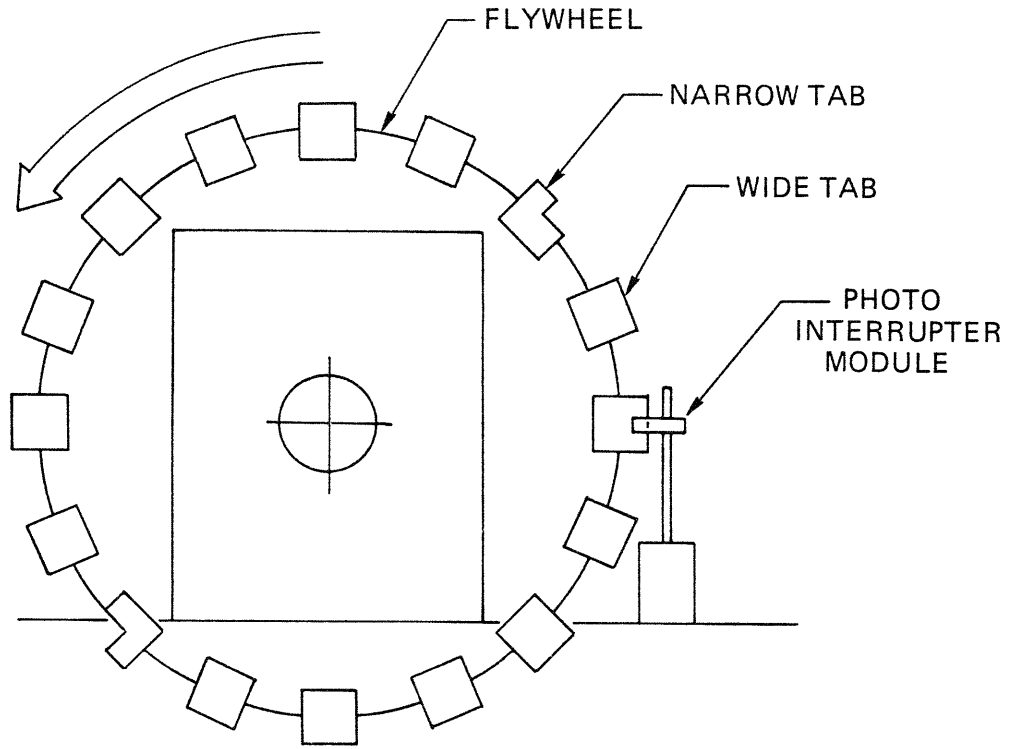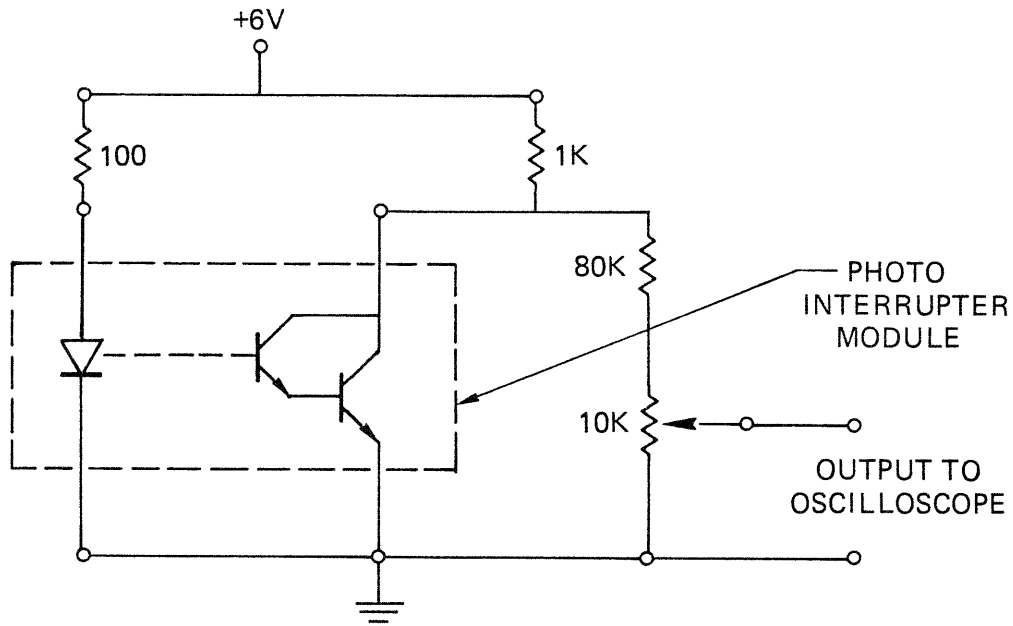
ELECTRICAL SCHEMATIC

Fig. A-3. Volume Instrumentation.

pond to the mid-stroke position of the piston, which was measured directly with a micrometer with the upper cylinder removed. If the angular velocity of the crankshaft were constant during experiments, the pulse from one of these two tabs would have been sufficient to establish the timing of the cycle relative to the pressure signal and hence determine the volume as a function of time. However the angular velocity was found to vary considerably within a cycle. Therefore the pulses from the other 14 tabs were used to calculate the crank angle as a function of time within the cycle by means of a linear regression, as described in Appendix B.3. These 14 wider tabs were attached to the flywheel with epoxy adhesive at approximately equal intervals. Their exact angular positions were established by operating the apparatus at constant angular velocity (slowly, with the cylinder head removed) and measuring the timing of the 14 pulses relative to the two pulses at known positions.

The photo interrupter module was a General Electric H13B1, consisting of a gallium arsenide infrared emitting diode coupled with a silicon photo darlington. As the crankshaft rotates, the tabs pass between the two halves of the module, preventing the infrared from reaching the photo darlington receiver, and causing the output to the oscilloscope to rise. Since the corner between the top of the pulse and the trailing edge was the most sharply defined point on the pulse shape, it was used for timing purposes. The resistances were chosen to give a rectangular pulse at the maximum speed used in the experiments, and a provision was made for pulse height adjustment. It was estimated that the maximum error that could occur in measuring the crank angle with this system was approximately 0.5 degrees.

APPENDIX B

DATA HANDLING

B.1 Experimental Procedure and Data Acquisition

A flow chart of the data acquisition process is shown in Fig. B.1. The pressure and volume signals were fed to a Nicolet Explorer III Digital Oscilloscope. The apparatus was started and the pressure and volume signals were monitored on the CRT display. When a satisfactory cycle was displayed, it was held in memory and the apparatus was stopped. The apparatus has two thermal time constants as discussed in Appendix D. The first is associated with the gas approaching steady net or average heat transfer with the wall over more than one cycle. The second is associated with the cylinder approaching steady heat transfer by natural convection with the ambient air. Data was always taken after a time that was long compared to the first time constant and short compared to the second, usually between 15 and 120 seconds. After the apparatus was stopped the data was transferred from memory to a mini-disc for storage.

B.2 Data Transfer

After a number of experiments had been recorded with the digital oscilloscope, the data was transmitted to a DEC VAX-11 computer. The data was then translated into a standard floating point format, reduced to a compact form for storage, and stored on a disc file. A cycle contained between 400 and 1000 data points depending on the frequency and time scale used on the oscilloscope. A flow chart of this process is shown in Fig. B.2 and listings of the computer programs follow.

PRESSURE
TRANSDUCER

BALANCING
CIRCUIT

DIFFERENTIAL
AMPLIFIER

FLYWHEEL

PHOTO
INTERRUPTER
MODULE

NOISE
FILTER

CIRCUIT

NICOLET
DIGITAL
OSCILLOSCOPE

CONVERT DATA TO DIGITAL

P_{signal} vs. t   1024 POINTS

V_{signal} vs. t   1024 POINTS

CRT
DISPLAY

MEMORY

MINI
DISC
STORAGE

TRANSMIT TO COMPUTER
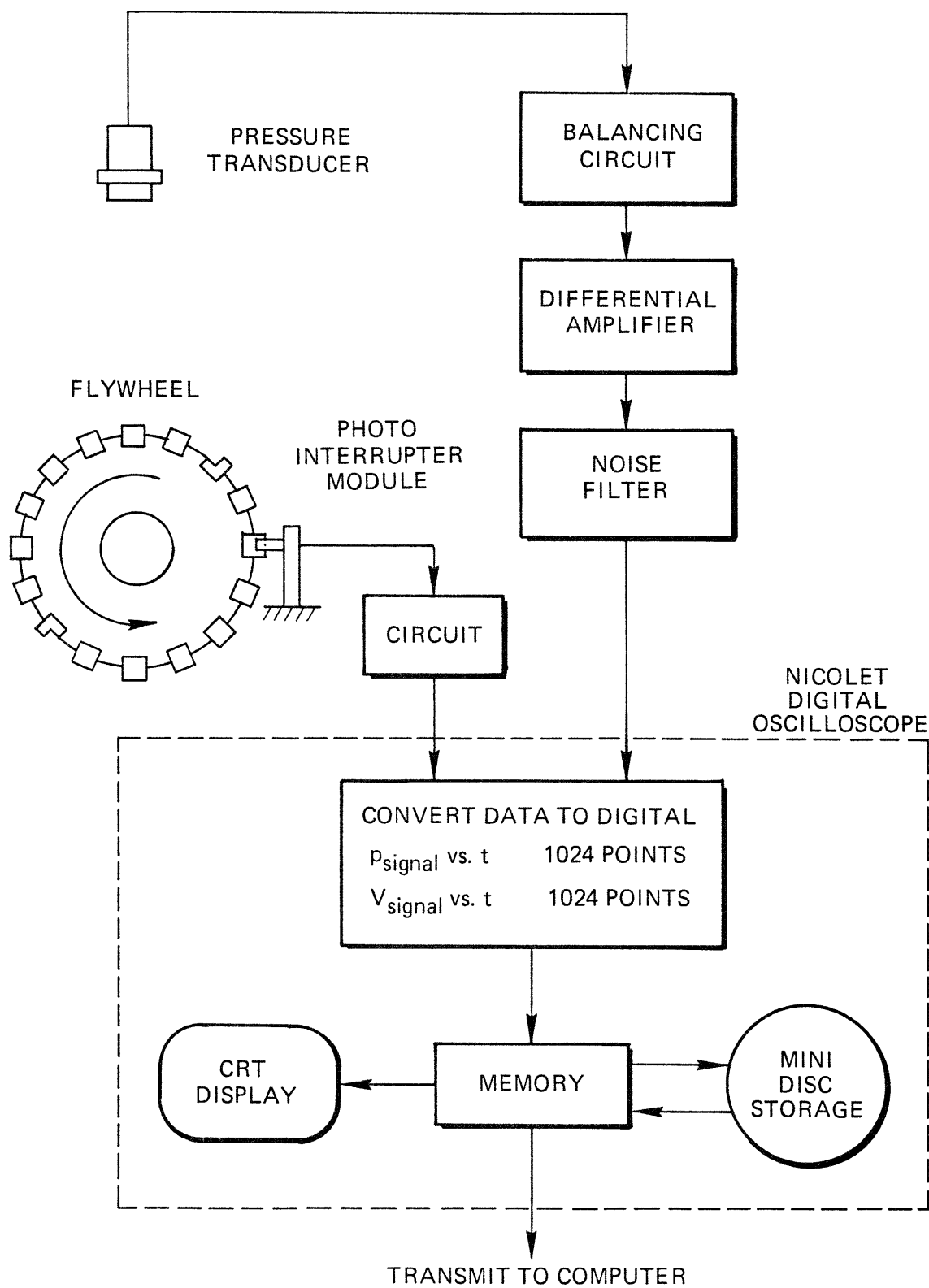
Fig. B-1. Data Acquisition Flow Chart.
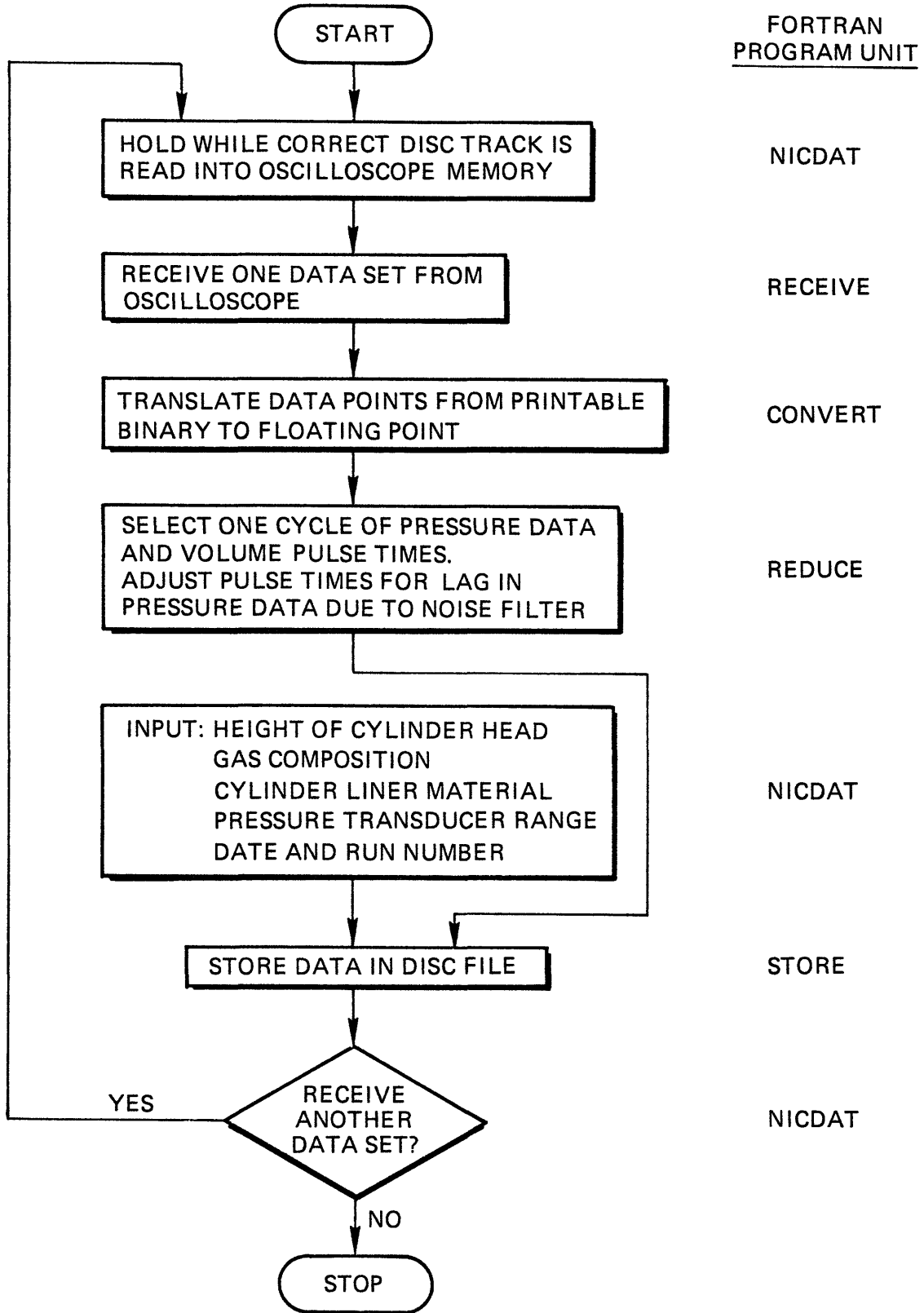
Fig. B-2. Data Transfer Flow Chart.

```
      PROGRAM NICDAT
C
C                PROGRAM TO READ DATA FROM NICOLET DIGITAL
C                OSCILLOSCOPE INTO VAX COMPUTER
C
      CHARACTER*10 FNAME
      CHARACTER*6 DIGITS
      CHARACTER*4 TYPE
      CHARACTER*3 CODE
      COMMON/FILE/ FNAME
      COMMON/CODE/ X,CODE
      WRITE (6,*) 'IS "SET TERM/NOECHO" ?'
10    WRITE (6,*) 'RECALL DATA FROM DISC TO SCOPE MEMORY'
      PAUSE 'TYPE "CONTINUE" WHEN READY'
      CALL RECEIVE
      CALL CONVERT
      WRITE (6,*) 'ENTER X, FORMAT F5.3'
      READ (5,102) X
102   FORMAT (F5.3)
      WRITE (6,*) 'ENTER THREE CHARACTERS FOR GAS, CYLINDER WALL
     1 MATERIAL, AND PRESSURE TRANSDUCER RANGE'
      READ (5,101) CODE
101   FORMAT (A3)
      CALL REDUCE
      WRITE (6,*) 'ENTER SIX DIGITS FOR MONTH, DAY, AND RUN NUMBER'
      READ (5,100) DIGITS
100   FORMAT (A6)
      TYPE = '.DAT'
      FNAME = DIGITS//TYPE
      CALL STORE
      WRITE (6,*) 'ENTER INSTRUCTION: STOP=0, ANOTHER DATA SET=1'
      READ (5,*) IANS
      IF (IANS.GT.0) GO TO 10
      WRITE (6,*) 'RESET "SET TERM/ECHO"'
      STOP
      END
```

```
      SUBROUTINE RECEIVE
C
C             SUBROUTINE TO RECEIVE NORMALIZATION INFO IN ASCII AND
C             DATA FOR ONE CURVE IN PRINTABLE BINARY FROM NICOLET
C
      CHARACTER*2 STRING(0:2047),TERM
      COMMON/REC/ IPN4,PN6,IVN4,VN6
      COMMON/STRING/ STRING
      COMMON/TIME/ VN7
C             RECEIVE TWO NORMALIZATION SETS, ONE FOR EACH CHANNEL
      WRITE (6,*) 'RECEIVING NORMALIZATION'
      WRITE (6,*) CHAR(1)
      WRITE (6,*) 'E1N2'
      WRITE (6,*) '00002'
      WRITE (6,*) CHAR(2)
      READ (5,100) IVN1,IVN2,IVN3,IVN4,IVN5,VN6,VN7
100   FORMAT (3I1,2I5,2E7.1)
      READ (5,100) IPN1,IPN2,IPN3,IPN4,IPN5,PN6,PN7
      READ (5,101) TERM
101   FORMAT (A2)
C             RECEIVE 2048 TWO CHARACTER PRINTABLE BINARY WORDS
C             IN 64 GROUPS OF 32
C             IN ORDER NOT TO EXCEED 78 CHARACTER VAX INPUT BUFFER
      WRITE (6,*) 'START RECEIVING DATA'
      I = 0
C             LOAD STARTING ADDRESS
      WRITE (6,*) CHAR(1)
      WRITE (6,*) 'E3D1'
      WRITE (6,*) 'I0001'
      WRITE (6,*) CHAR(2)
      WRITE (6,102) I
102   FORMAT (I4)
      WRITE (6,*) CHAR(3)
      READ (5,101) TERM
      DO 80 I=0,2016,32
C             RECEIVE 32 WORDS
      WRITE (6,*) CHAR(1)
      WRITE (6,*) 'E3D2'
      WRITE (6,*) '00032'
      WRITE (6,*) CHAR(2)
      READ (5,103) (STRING(J),J=I,I+31)
103   FORMAT (32A2)
      READ (5,101) TERM
80    CONTINUE
      WRITE (6,*) 'END RECEIVING DATA'
      RETURN
      END
```

```
        SUBROUTINE CONVERT
C
C               SUBROUTINE TO TAKE PRINTABLE BINARY P-V VOLTAGE DATA,
C               TRANSLATE IT TO INTEGER,
C               AND NORMALIZE IT TO FLOATING POINT
C
        DIMENSION PVOLT(0:1023),VVOLT(0:1023)
        CHARACTER*2 STRING(0:2047)
        COMMON/REC/ IPN4,PN6,IVN4,VN6
        COMMON/STRING/ STRING
        COMMON/DATA/ PVOLT,VVOLT
C               TRANSLATE PRINTABLE BINARY TO INTEGER
        WRITE (6,*) 'TRANSLATING TO INTEGER AND NORMALIZING'
        J = 0
        M = 0
        N = 0
        DO 90 I=0,2047
        IHIGH = ICHAR(STRING(I)(1:1)) - 32
        ILOW = ICHAR(STRING(I)(2:2)) - 32
        INT = 64*IHIGH + ILOW
C               NICOLET DATA WITH RANGE -2048 TO +2047 IS TWO'S
C               COMPLIMENT BINARY.  THUS IF NUMBER IS GREATER THAN
C               2047, IT IS ACTUALLY NEGATIVE AND 4096 MUST BE
C               SUBTRACTED FROM IT TO FIND ACTUAL NUMBER.
        IF (INT.GT.2047) INT=INT-4096
C               NORMALIZE INTEGERS TO FLOATING POINT
        IF (J.GE.1) GO TO 60
        J = 1
        VVOLT(M) = VN6*(INT-IVN4)
        M = M + 1
        GO TO 90
60      J = 0
        PVOLT(N) = PN6*(INT-IPN4)
        N = N + 1
90      CONTINUE
        RETURN
        END
```

```
      SUBROUTINE REDUCE
C
C             SUBROUTINE TO FIND FIRST, SECOND, AND THIRD VOLUME
C             TIMING POINTS, AND THE OTHER 14 TAB POINTS, CORRECT
C             FOR PRESSURE DATA LAG, SELECT PRESSURE VOLTAGE DATA
C             FOR ONE CYCLE BETWEEN FIRST AND THIRD TIMING POINTS.
C
      DIMENSION PVOLT(0:1023), VVOLT(0:1023), PDATA(0:1023),ITAB(17)
      COMMON/DATA/ PVOLT,VVOLT
      COMMON/FDATA/ PDATA,NP,TPERP,IMARK1,IMARK2,IMARK3,ITAB
      COMMON/TIME/ VN7
      PARAMETER (PI=3.141593,CORNER=262.)
      WRITE (6,*) 'FINDING TIMING POINTS AND PRESSURE CYCLE'
C             FIND NUMBER OF POINTS IN LONGER OF TWO ADJACENT
C             NEGATIVE PULSES IN VOLUME SIGNAL AS ROUGH
C             TYPICAL LENGTH OF LONG PULSE
      I = 20
      K = 1
      N = 0
      GO TO 6
5     I = I + 1
      IF (I.LT.1023) GO TO 6
      WRITE (6,*) 'NO PULSES FOUND'
      RETURN
6     IF (VVOLT(I-8).LT.-.150) GO TO 5
      IF (VVOLT(I-7).LT.-.150) GO TO 5
      IF (VVOLT(I-6).LT.-.150) GO TO 5
      IF (VVOLT(I-3).GT.-.150) GO TO 5
      IF (VVOLT(I-2).GT.-.150) GO TO 5
      IF (VVOLT(I-1).GT.-.150) GO TO 5
7     N = N + 1
      I = I + 1
      IF (VVOLT(I).LT.-.100) GO TO 7
      IF (K.GT.1) GO TO 9
      NP1 = N + 3
      N = 0
      K = 2
      GO TO 5
9     NP2 = N + 3
      NPULSE = NP1
      IF (NP2.GT.NP1) NPULSE=NP2
C             SEARCH VOLUME DATA FOR BEGINNING OF TRAILING EDGE
C             OF FIRST 17 NEGATIVE PULSES, BEGINNING WITH A
C             SHORT PULSE.
      I = 1
      J = 0
      GO TO 20
```

```
10      I = I + 1
        IF (I.LT.1023) GO TO 20
        WRITE (6,*) '17 VOLUME PULSES NOT FOUND'
        RETURN
20      IF (VVOLT(I-3).GT.-.150) GO TO 10
        IF (VVOLT(I-2).GT.-.150) GO TO 10
        IF (VVOLT(I-1).GT.-.150) GO TO 10
        DIFF = VVOLT(I+1) - VVOLT(I)
        IF (DIFF.LT..050) GO TO 10
        IF (VVOLT(I+2).LT.-.235) GO TO 10
        IF (VVOLT(I+3).LT.-.235) GO TO 10
        IF (VVOLT(I+4).LT.-.235) GO TO 10
        IF (J.GT.0) GO TO 30
        IF (VVOLT(I-NPULSE+6).LT.-.150) GO TO 10
        IF (VVOLT(I-NPULSE+5).LT.-.150) GO TO 10
        IF (VVOLT(I-NPULSE+4).LT.-.150) GO TO 10
        IF (I-NPULSE+2.GE.1) GO TO 30
        IF (VVOLT(1).LT.-.150) GO TO 10
        IF (VVOLT(2).LT.-.150) GO TO 10
        IF (VVOLT(3).LT.-.150) GO TO 10
30      J = J + 1
        ITAB(J) = I
        IF (J.EQ.1) IMARK1=I
        IF (J.EQ.9) IMARK2=I
        I = I + 10
        IF (J.LT.17) GO TO 10
        IMARK3 = I - 10
C               CALCULATE POINTS PER CYCLE AND FREQUENCY
        NP = IMARK3 - IMARK1
        TPERP = VN7
        FREQ = 1./(NP*TPERP)
C               CHANGE VOLUME TIMING POINTS TO ACCOUNT FOR FIRST
C               ORDER LAG IN PRESSURE DATA
        PHI = ATAN(FREQ/CORNER)
        ILAG = ININT(PHI*NP/(2.*PI))
        IMARK1 = IMARK1 + ILAG
        IMARK2 = IMARK2 + ILAG
        IMARK3 = IMARK3 + ILAG
        DO 50 I=1,17
        ITAB(I) = ITAB(I) + ILAG
50      CONTINUE
C               SELECT ONE CYCLE OF PRESSURE DATA FROM FIRST TO
C               THIRD TIMING POINT
        DO 60 I=IMARK1,IMARK3
        PDATA(I) = PVOLT(I)
60      CONTINUE
        RETURN
        END
```

```
      SUBROUTINE STORE
C
C             SUBROUTINE TO STORE PRESSURE VOLTAGE DATA, VOLUME TIMING
C             POINTS, NUMBER OF POINTS, TIME BETWEEN POINTS, CODE AND
C             VOLUME ADJUSTMENT LENGTH IN A FILE
C
      DIMENSION PDATA(0:1023), ITAB(17)
      CHARACTER*10 FNAME
      CHARACTER*3 CODE
      COMMON/FDATA/ PDATA,NP,TPERP,IMARK1,IMARK2,IMARK3,ITAB
      COMMON/FILE/ FNAME
      COMMON/CODE/ X,CODE
      OPEN (UNIT=10,NAME=FNAME,TYPE='NEW')
      WRITE (6,100) FNAME
100   FORMAT (' STORING DATA IN FILE ',A10)
      WRITE (10,101) NP,TPERP,IMARK1,IMARK2,IMARK3,X,CODE
101   FORMAT (I4,E8.1,3I4,F6.3,A3)
      WRITE (10,103) (ITAB(I),I=1,17)
103   FORMAT (17I4)
      WRITE (10,102) (PDATA(I),I=IMARK1,IMARK3)
102   FORMAT (F7.4)
      RETURN
      END
```

B.3 Data Reduction

The data for one experiment was recalled from the disc file and used to calculate the pressure and volume at each point in the cycle. Then various parameters characterizing the complete cycle were calculated and stored in a disc file. Then the non-dimensional pressure, volume, temperature and entropy were calculated and the p-V and T-S diagrams plotted. A flow chart of this process is shown in Fig. B.3. A separate program, LRPLOT, was used to recall the cycle parameters for many experiments from the disc file and make a log-log plot of non-dimensional loss versus average Reynolds number. Listings of the computer programs follow. The pressure and volume calculations will now be described in more detail. The other calculations are discussed in Section 3.3.

The first step is to find the crank angle as a function of time. The true function is approximated by using the zeroth, first and second harmonics of the cycle frequency,

$$\theta = \omega t + a_0 + a_1 \sin \omega t + a_2 \cos \omega t + a_3 \sin 2\omega t + a_4 \cos 2\omega t \quad (B.1)$$

From the 16 volume pulses, 16 pairs of crank angles and times are known. For each time, ωt , $\sin \omega t$, etc. can be calculated. Then Eq. (B.1) can be rewritten,

$$z = a_0 + a_1 x_1 + a_2 x_2 + a_3 x_3 + a_4 x_4 \quad (B.2)$$

FORTRAN
PROGRAM UNIT

START — PROCESS

RECALL DATA FROM DISC FILE — RECALL

DO CURVE FIT TO OBRAIN CRANK ANGLE vs. TIME
FOR EACH DATA POINT CALCULATE:
      CRANK ANGLE
      VOLUME
      PRESSURE
— PV

CALCULATE AND DISPLAY CYCLE PARAMETERS
INCLUDING:
      REYNOLDS NUMBER
      COMPRESSION WORK
      NON-DIMENSIONAL LOSS
— CALC

STORE CYCLE PARAMETERS IN TABLE ON DISC FILE — LRFILE

FOR EACH DATA POINT CALCULATE
NON-DIMENSIONAL PROPERTIES:
      PRESSURE,   P*
      VOLUME,   V*
      TEMPERATURE, T*
      ENTROPY,   S*
PLOT:
      P* - V* DIAGRAM
      T* - S* DIAGRAM
— TS

STOP — PROCESS

Fig. B-3. Data Reduction Flow Chart.

where

$$z = \theta - \omega t$$

$$x_1 = \sin\omega t \quad \text{etc.}$$

Thus 16 sets of (z, x_1, x_2, x_3, x_4) are known. A linear least squares algorithm was used to obtain the coefficients a_0, a_1, a_2, a_3 and a_4. It is estimated that the crank angle error resulting from this approximation is less than 0.5 degrees.

At each data point the pressure signal level and time are known. The crank angle is found using Eq. (B.1). The volume is found from the crank angle using the standard relation for a crank and connecting rod mechanism,

$$V = \frac{\pi b^2}{4} \left[\frac{s}{2} \left(1 + \frac{L}{r} - \cos\theta - \sqrt{\cos^2\theta - 1 + \left(\frac{L}{r}\right)^2}\right) + c\right] \qquad \text{(B.3)}$$

where

$$\frac{L}{r} = 4.80 \quad \text{for the compressor.}$$

Then the actual pressure is found,

$$p = \frac{p_{signal}}{(amp)(sens)} + p_{atm} \qquad \text{(B.4)}$$

```
      PROGRAM PROCESS
C
C               PROGRAM TO READ DATA FROM FILE, GENERATE P-V DATA,
C               CALCULATE AND PRINT EXPERIMENT PARAMETERS, CALCULATE
C               AND PLOT NON-DIMENSIONAL P-V AND T-S DIAGRAMS
C
      CHARACTER*10 FNAME
      CHARACTER*6 DIGITS
      CHARACTER*3 FN
      CHARACTER*4 TYPE
      COMMON/FILE/FNAME
      COMMON/LRNAME/FN
      WRITE (6,*) 'IS SET TERM/FT1 ?'
10    WRITE (6,*) 'ENTER SIX DIGIT FILENAME: MONTH, DAY AND RUN NUMBER'
      READ (5,100) DIGITS
100   FORMAT (A6)
      TYPE = '.DAT'
      FNAME = DIGITS//TYPE
      CALL RECALL
      CALL PV
      CALL CALC
      WRITE (6,*) 'ENTER INSTRUCTION: NOFILE=0, FILE=1'
      READ (5,*) IANS
      IF (IANS.LT.1) GO TO 80
      WRITE (6,*) 'ENTER 3 CHARACTER FILENAME'
      READ (5,101) FN
101   FORMAT (A3)
      CALL LRFILE
80    CONTINUE
      WRITE (6,*) 'ENTER INSTRUCTION: NO DIAGRAMS=0, DIAGRAMS=1'
      READ (5,*) IANS
      IF (IANS.LT.1) GO TO 90
      CALL TS
90    WRITE (6,*) 'ENTER INSTRUCTION: STOP=0, ANOTHER DATA SET=1'
      READ (5,*) IANS
      IF (IANS.GT.0) GO TO 10
      STOP
      END
```

```fortran
      SUBROUTINE RECALL
C
C             SUBROUTINE TO RECALL FROM FILE THE PRESSURE VOLTAGE DATA,
C             VOLUME TIMING POINTS, NUMBER OF POINTS, TIME BETWEEN
C             POINTS, CODE, AND VOLUME ADJUSTMENT LENGTH.
C
      DIMENSION PDATA(0:1023), ITAB(17)
      CHARACTER*10 FNAME
      CHARACTER*3 CODE
      COMMON/CODE/ XLENGTH,CODE
      COMMON/FDATA/ PDATA,IMARK1,IMARK2,IMARK3,ITAB
      COMMON/FILE/ FNAME
      COMMON/PERIOD/ NP,TPERP
      OPEN (UNIT=10,FILE=FNAME,STATUS='OLD')
      WRITE (6,100) FNAME
100   FORMAT (' RECALLING DATA IN FILE ',A10)
      READ (10,101) NP,TPERP,IMARK1,IMARK2,IMARK3,XLENGTH,CODE
101   FORMAT (I4,E8.1,3I4,F6.3,A3)
      READ (10,103) (ITAB(I),I=1,17)
103   FORMAT (17I4)
      READ (10,102) (PDATA(I),I=IMARK1,IMARK3)
102   FORMAT (F7.4)
      RETURN
      END
```

```
      SUBROUTINE PV
C
C              SUBROUTINE TO CONVERT PRESSURE VOLTAGE DATA TO PSI
C              AND GENERATE ASSOCIATED VOLUME DATA IN CU. IN.
C
      DIMENSION PDATA(0:1023),P(0:1023),V(0:1023),ITAB(17),
     1 THETA(0:1023)
      DIMENSION ANGLE(16),ATAB(16),A(16,5),B(16),IP(5),X(5),H(5)
      CHARACTER*3 CODE
      COMMON/PERIOD/ NP,TPERP
      COMMON/FDATA/ PDATA,IMARK1,IMARK2,IMARK3,ITAB
      COMMON/CODE/ XLENGTH,CODE
      COMMON/PVDATA/ P,V,ITDC
      COMMON/GEOM/ AL,STROKE,BORE
C              DEFINE CONSTANTS
      PARAMETER (CRCR=4.8,AMP=91.01,PI=3.141593,PAMB=14.7)
      DATA AL,STROKE,BORE/1.020,3.0,2.0/
      DATA ANGLE/-1.4662,-1.0028,-.6296,-.2544,.0894,.4771,
     1 .8159,1.2472,1.4662,1.9448,2.3450,2.7530,
     2 -3.1366,-2.6952,-2.2366,-1.7856/
      C = XLENGTH - AL
      PA = PI*BORE**2/4.
      WRITE (6,*) 'GENERATING P-V DATA'
C              CHOOSE TRANSDUCER SENSITIVITY
      IF (CODE(3:3).EQ.'L') THEN
      TRANS = 4379.
      ELSE IF (CODE(3:3).EQ.'H') THEN
      TRANS = 20160.
      ELSE
      WRITE (6,*) 'TRANSDUCER CODE NOT L OR H'
      RETURN
      END IF
C              FIND WHETHER TDC OR BDC COMES FIRST IN THE DATA
C              AND FIND CRANK ANGLES CORRESPONDING TO TABS
      IDC1 = (IMARK1+IMARK2)/2.
      IDC2 = (IMARK2+IMARK3)/2.
      IF (PDATA(IDC2).GT.PDATA(IDC1)) THEN
      ITDCE = IDC2
      DO 30 I=1,8
      ATAB(I+8) = ANGLE(I)
      ATAB(I) = ANGLE(I+8)
30    CONTINUE
      ELSE
      ITDCE = IDC1
      DO 35 I=1,16
      ATAB(I) = ANGLE(I)
35    CONTINUE
```

```
        END IF
C               USE TAB ANGLES AND TIMES TO OBTAIN AN APPROXIMATION
C               OF TRUE CRANK ANGLE VS. TIME BY A LEAST SQUARES
C               CURVE FIT USING THE ZEROETH, FIRST AND SECOND
C               HARMONICS OF CYCLE FREQUENCY.
        DTHETA = 2.*PI/NP
        DO 40 I=1,16
        T = ITAB(I) - ITDCE
        THETAE = DTHETA*T
        B(I) = ATAB(I) - THETAE
        IF (B(I).LT.-PI) B(I)=B(I)+2.*PI
        IF (B(I).GT. PI) B(I)=B(I)-2.*PI
        A(I,1) = 1.
        A(I,2) = SIN(THETAE)
        A(I,3) = COS(THETAE)
        A(I,4) = SIN(2.*THETAE)
        A(I,5) = COS(2.*THETAE)
40      CONTINUE
        IA = 16
        M = 16
        N = 5
        TOL = 0.0
        KBASIS = 5
        CALL LLSQF(A,IA,M,N,B,TOL,KBASIS,X,H,IP,IER)
C               USE THE APPROXIMATION TO GENERATE CRANK ANGLE DATA
        DO 50 I=IMARK1,IMARK3-1
        T = I - ITDCE
        THETAE = DTHETA*T
        THETA(I) = THETAE + X(1) + X(2)*SIN(THETAE) + X(3)*COS(THETAE)
     1  + X(4)*SIN(2.*THETAE) + X(5)*COS(2.*THETAE)
        IF (THETA(I).LT.-PI) THETA(I)=THETA(I)+2.*PI
        IF (THETA(I).GT.PI) THETA(I)=THETA(I)-2.*PI
        ANEW = ABS(THETA(I))
        AOLD = ABS(THETA(I-1))
        IF (ANEW.LT.AOLD.AND.ANEW.LT.0.1) ITDC=I
        IF (ANEW.GT.AOLD.AND.ANEW.GT.3.) IBDC=I
50      CONTINUE
        JTDC = ITDC - IBDC
        IF (JTDC.LT.0) JTDC=JTDC+NP
C               CALCULATE PRESSURE AND VOLUME FROM BDC TO IMARK3
        DO 60 I=IBDC,IMARK3-1
        J = I - IBDC
        P(J) = TRANS*PDATA(I)/AMP + PAMB
        COSTH = COS(THETA(I))
        AR = COSTH + SQRT(COSTH**2-1.+CRCR**2)
        XR = 1. + CRCR - AR
        V(J) = PA*(STROKE*XR/2.+C)
60      CONTINUE
```

```
C               EVALUATE PRESSURE CLOSURE ERROR AND AVERAGE END POINTS
        P1 = TRANS*PDATA(IMARK3)/AMP + PAMB
        P2 = TRANS*PDATA(IMARK1)/AMP + PAMB
        PAVG = (P1+P2)/2.
        PERROR = (P1-P2)/PAVG
        WRITE (6,100) PERROR
100     FORMAT (' PRESSURE ERROR = ',F6.3)
        P(IMARK3-IBDC) = PAVG
        COSTH = COS(THETA(IMARK1))
        AR = COSTH + SQRT(COSTH**2-1.+CRCR**2)
        XR = 1. + CRCR - AR
        V(IMARK3-IBDC) = PA*(STROKE*XR/2.+C)
C               CALCULATE PRESSURE AND VOLUME FROM IMARK1 TO BDC
        DO 70 I=IMARK1+1,IBDC-1
        J = IMARK3 - IBDC + I - IMARK1
        P(J) = TRANS*PDATA(I)/AMP + PAMB
        COSTH = COS(THETA(I))
        AR = COSTH + SQRT(COSTH**2-1.+CRCR**2)
        XR = 1. + CRCR - AR
        V(J) = PA*(STROKE*XR/2.+C)
70      CONTINUE
        ITDC = JTDC
        RETURN
        END
```

```
      SUBROUTINE CALC
C
C           SUBROUTINE TO CALCULATE VARIOUS PARAMETERS WHICH
C           CHARACTERISE THE EXPERIMENT AND PRINT THEM OUT
C
      DIMENSION P(0:1023),V(0:1023)
      CHARACTER*3 CODE
      CHARACTER*7 CYL
      CHARACTER*8 GAS
      CHARACTER*10 FNAME
      CHARACTER*17 DARUN
      COMMON/PVDATA/P,V,ITDC
      COMMON/PERIOD/ NP, TPERP
      COMMON/CODE/ XLENGTH,CODE
      COMMON/FILE/ FNAME
      COMMON/SCALE/ PMC,VD,CWORK
      COMMON/GAS/ CV,CP
      COMMON/GEOM/ AL,STROKE,BORE
      COMMON/LABEL/IPMAX,IPMIN,DARUN
      COMMON/LRDATA/VR,RPM,RE,CYCLOSS,PMAX,PMIN
      PARAMETER (TMEAN=560.,RCONST=0.0776538,PI=3.141593)
      WRITE (6,*) 'CALCULATING PARAMETERS'
C           FIND DATE AND RUN NUMBER
      DARUN = FNAME(1:2)//'-'//FNAME(3:4)//'-82   RUN '//FNAME(5:6)
C           FIND CYLINDER WALL MATERIAL
      IF (CODE(2:2).EQ.'C') THEN
      CYL = 'COPPER '
      ELSE IF (CODE(2:2).EQ.'S') THEN
      CYL = 'STEEL  '
      ELSE IF (CODE(2:2).EQ.'M') THEN
      CYL = 'MICARTA'
      ELSE
      WRITE (6,*) 'CYL WALL CODE NOT C, S, OR M'
      RETURN
      END IF
C           FIND GAS AND PROPERTIES
      IF (CODE(1:1).EQ.'H') THEN
      GAS = 'HELIUM  '
      CP = 1.241
      CV = .745
      VISCM = .0123
      ELSE IF (CODE(1:1).EQ.'N') THEN
      GAS = 'NITROGEN'
      CP = .2484
      CV = .1775
      VISCM = .00159
```

```
      ELSE IF (CODE(1:1).EQ.'A') THEN
      GAS = 'ARGON   '
      CP = .1244
      CV = .0747
      VISCM = .00141
      ELSE IF (CODE(1:1).EQ.'F') THEN
      GAS = 'FREON 13'
      CP = .157
      CV = .138
      VISCM = .000343
      ELSE
      WRITE (6,*) 'GAS CODE NOT H, N, OR F'
      RETURN
      END IF
C              CALCULATE SPEED
      RPM = 60./(NP*TPERP)
C              CALCULATE EXTREME PRESSURES
      PMAX = 0.
      PMIN = 500.
      DO 50 I=0,NP-1
      IF (PMAX.LT.P(I)) THEN
      PMAX = P(I)
      IPMAX = I
      ELSE IF (PMIN.GT.P(I)) THEN
      PMIN = P(I)
      IPMIN = I
      ELSE
      END IF
50    CONTINUE
      PR = PMAX/PMIN
C              CALCULATE EXTREME VOLUMES
      VMAX = V(0)
      VMIN = V(ITDC)
      VR = VMAX/VMIN
C              CALCULATE APPROXIMATE TEMPERATURE RATIO
      ATR = P(ITDC)*V(ITDC)/(P(0)*V(0))
C              CALCULATE WORKS OF COMPRESSION AND EXPANSION, AND LOSS
      CWORK = 0.
      DO 60 I=0,ITDC-1
      CWORK = CWORK + (P(I)+P(I+1))*(V(I)-V(I+1))/24.
60    CONTINUE
      EWORK = 0.
      DO 70 I=ITDC,NP-2
      EWORK = EWORK + (P(I)+P(I+1))*(V(I+1)-V(I))/24.
70    CONTINUE
      CYCLOSS = (CWORK-EWORK)/CWORK
```

```
C               CALCULATE MEAN COMPRESSION PRESSURE
      VD = PI*(BORE**2)*STROKE/4.
      PMC = 12.*CWORK/VD
C               CALCULATE AVERAGE REYNOLDS NUMBER
      RE = RCONST*PMC*RPM*STROKE*BORE/(VISCM*TMEAN)
C               OUTPUT
      WRITE(6,100)
100   FORMAT (1H1,'COMPRESSION AND EXPANSION CYCLIC HEAT TRANSFER EXPER
     1IMENT')
      WRITE (6,101) DARUN
101   FORMAT (1H0/1H ,A17)
      WRITE (6,102) CYL
102   FORMAT (1H0/' CYLINDER WALL MATERIAL',11X,A7)
      WRITE (6,103) GAS
103   FORMAT (1H0,'WORKING GAS',21X,A8)
      WRITE (6,104) PMC
104   FORMAT (1H0,'MEAN COMPRESSION PRESSURE, PSI',2X,F6.2)
      WRITE (6,105) RPM
105   FORMAT (1H0,'CRANKSHAFT SPEED, RPM',12X,F5.1)
      WRITE (6,106)
106   FORMAT (1H0//18X,'MAX',5X,'MIN',5X,'RATIO')
      WRITE (6,107) PMAX, PMIN, PR
107   FORMAT (1H0,'PRESSURE, PSI',2X,F6.2,2X,F6.2,3X,F6.3)
      WRITE (6,108) VMAX, VMIN, VR
108   FORMAT (1H0,'VOLUME, CU IN',3X,F5.2,3X,F5.2,4X,F5.3)
      WRITE (6,109) ATR
109   FORMAT (1H0,'APPROXIMATE TEMPERATURE RATIO',4X,F5.3)
      WRITE (6,110) CWORK
110   FORMAT (1H0//' COMPRESSION WORK, FT-LBF',9X,F5.1)
      WRITE (6,111) RE
111   FORMAT (1H0,'AVERAGE REYNOLDS NUMBER',4X,E11.4)
      WRITE (6,112) CYCLOSS
112   FORMAT (1H0,'NON-DIMENSIONAL LOSS',11X,F7.4)
      WRITE (6,113)
113   FORMAT (1H0///)
      RETURN
      END
```

```
      SUBROUTINE TS
C
C                 SUBROUTINE TO CALCULATE NON-DIMENSIONAL P-V AND T-S
C                 DATA AND PLOT P-V AND T-S DIAGRAMS
C
      DIMENSION P(0:1023),V(0:1023),PVSTAR(2,0:1023),
     1 TSSTAR(4,0:1023)
      CHARACTER*17 DARUN
      CHARACTER*27 XLAB
      CHARACTER*80 XYLAB
      INTEGER*2 IXPLOT(4)
      COMMON/PERIOD/ NP,TPERP
      COMMON/SCALE/ PMC,VD,CWORK
      COMMON/GAS/ CV,CP
      COMMON/PVDATA/ P,V,ITDC
      COMMON/LABEL/IPMAX,IPMIN,DARUN
      COMMON/LRDATA/VR,RPM,RE,CYCLOSS,PMAX,PMIN
C                 SEPARATE MAX AND MIN PRESSURE AND VOLUME POINTS
C                 BY AT LEAST ONE POINT FOR CLARITY ON DIAGRAM
      IF (NP-IPMIN.LT.2) IPMIN=NP-2
      IF (IPMIN.LT.2) IPMIN=2
      IF (ITDC-IPMAX.LT.2.AND.ITDC-IPMAX.GT.-1) IPMAX=ITDC-2
      IF (IPMAX-ITDC.LT.2.AND.IPMAX-ITDC.GT.-1) IPMAX=ITDC+2
C                 CALCULATE NON DIMENSIONAL P, V, T, AND S
C                 REFERENCE STATE IS BDC
      WRITE (6,*) 'CALCULATING P*-V* AND T*-S*'
      VDOLD = 1.
      VCTR = V(0)/SQRT(VR)
       DO 40 I=0,NP-1
       PVSTAR(1,I) = P(I)/PMC
       PVSTAR(2,I) = V(I)/VD
       TSSTAR(1,I) = P(I)*V(I)/(P(0)*V(0))
       S1 = (CV/(CP-CV))*ALOG(P(I)/P(0))
       S2 = (CP/(CP-CV))*ALOG(V(I)/V(0))
       TSSTAR(3,I) = (P(0)*V(0)/(12.*CWORK))*(S1+S2)
C                 MARK P AND V MAX AND MIN ON T*-S* DIAGRAM
       IF (I.EQ.IPMAX) TSSTAR(1,I)=TSSTAR(1,I)+0.05
       IF (I.EQ.IPMIN) TSSTAR(1,I)=TSSTAR(1,I)-0.05
       IF (I.EQ.0)     TSSTAR(3,I)=TSSTAR(3,I)+0.05
       IF (I.EQ.ITDC)  TSSTAR(3,I)=TSSTAR(3,I)-0.05
C                 FIND PRESSURES CORRESPONDING TO VCTR
       VDIFF = ABS(V(I)-VCTR)
       IF (VDIFF.GT.VDOLD) GO TO 35
       VDOLD = VDIFF
       IF (I.LT.ITDC) PCTRC=P(I)
       IF (I.GT.ITDC) PCTRE=P(I)
35     CONTINUE
```

```
         IF (I.EQ.ITDC) VDOLD=1.
40       CONTINUE
C                 PLOT NON-DIMENSIONAL P-V DIAGRAM
         WRITE (6,*) 'ENTER INSTRUCTION: SKIP=0, P-V DIAGRAM=1'
         READ (5,*) IANS
         IF (IANS.LT.1) GO TO 50
         XLAB = 'V STAR    '//DARUN
         CALL QPICTR (PVSTAR,2,NP,QX(2),QYLAB('P STAR'),
     1   QXLAB(XLAB),QLABEL(14))
50       CONTINUE
C                 GENERATE ISENTROPIC AND ISOTHERMAL BOUNDARIES
C                 FOR T*-S* DIAGRAM
         PCTR = (PCTRC+PCTRE)/2.
         EXP = ((CP/CV)-1.)/2.
         TCTRS = PCTR*VCTR/(P(0)*V(0))
         TSSTAR(2,0) = (VR**-EXP)*TCTRS
         TSSTAR(2,1) = (VR**EXP)*TCTRS
         TSSTAR(2,2) = TSSTAR(2,1)
         TSSTAR(2,3) = TSSTAR(2,0)
         TSSTAR(2,4) = TSSTAR(2,0)
         S1 = (CV/(CP-CV))*ALOG(PCTR/P(0))
         S2 = (CP/(CP-CV))*ALOG(VCTR/V(0))
         S3 = (ALOG(VR))/2.
         AA = (P(0)*V(0))/(12.*CWORK)
         TSSTAR(4,0) = AA*(S1+S2+S3)
         TSSTAR(4,1) = TSSTAR(4,0)
         TSSTAR(4,2) = AA*(S1+S2-S3)
         TSSTAR(4,3) = TSSTAR(4,2)
         TSSTAR(4,4) = TSSTAR(4,0)
         DO 60 I=5,NP-1
         TSSTAR(4,I) = 1.E+38
60       CONTINUE
C                  PLOT NON-DIMENSIONAL T-S DIAGRAM
         XYLAB(1:40) = '        S STAR      '//DARUN
         XYLAB(41:80) = '        T STAR'
         IXPLOT(1) = 3
         IXPLOT(2) = 4
         CALL PICTR (TSSTAR,4,XYLAB,XSCL,2,NP,
     1   -1,0,14,1,0,LOOK,IXPLOT)
         RETURN
         END
```

```
      SUBROUTINE LRFILE
C
C              SUBROUTINE TO ADD DATA FOR THIS RUN TO A FILE
C              CONTAINING A TABLE OF LOSS, REYNOLDS NUMBER
C              AND OTHER PERTINANT INFO FOR MANY RUNS
C
      CHARACTER*2 RUN
      CHARACTER*3 FN,CODE
      CHARACTER*5 DATE
      CHARACTER*7 FNAM
      CHARACTER*10 FNAME
      CHARACTER*80 DATA
      COMMON/FILE/FNAME
      COMMON/SCALE/PMC,VD,CWORK
      COMMON/CODE/XLENGTH,CODE
      COMMON/LRDATA/VR,RPM,RE,CYCLOSS,PMAX,PMIN
      COMMON/LRNAME/FN
C
      DATE = FNAME(1:2)//'-'//FNAME(3:4)
      RUN = FNAME(5:6)
      FNAM = FN//'.DAT'
      OPEN (UNIT=10,FILE=FNAM,STATUS='OLD')
      DO 50 I=1,1000
      READ (10,101,END=60) DATA
101   FORMAT (A80)
50    CONTINUE
60    CONTINUE
      WRITE (10,100) DATE,RUN,VR,CODE(2:2),CODE(1:1),PMC,
     1 RPM,RE,CYCLOSS,PMAX,PMIN,CWORK
100   FORMAT (/A5,1X,A2,1X,F5.3,1X,A1,1X,A1,1X,F6.2,1X,F5.1,
     1 1X,E11.4,1X,F7.4,2X,F6.2,1X,F6.2,1X,F5.1)
      RETURN
      END
```

```fortran
      PROGRAM LRPLOT
C
C                 PROGRAM TO RECALL LOSS AND REYNOLDS NUMBER DATA
C                 FOR MANY RUNS FROM A FILE AND MAKE A LOG-LOG
C                 PLOT OF LOSS VS. RE
C
      CHARACTER*3 FN
      CHARACTER*7 FNAM
      CHARACTER*80 TITLES
      DIMENSION PLOTLR(2,1000)
      WRITE (6,*) 'IS SET TERM/FT1 ?'
      WRITE (6,*) 'ENTER 3 CHARACTER FILENAME'
      READ (5,101) FN
101   FORMAT (A3)
      FNAM = FN//'.DAT'
      OPEN (UNIT=10,FILE=FNAM,STATUS='OLD')
      DO 50 I=1,1000
      READ (10,100,END=60) PLOTLR(1,I),PLOTLR(2,I)
100   FORMAT (/32X,E11.4,1X,F7.4)
50    CONTINUE
60    CONTINUE
      NPTS = I - 1
      CALL QPICTR (PLOTLR,2,NPTS,QX(1),QYLAB('NON-DIMEN LOSS'),
     1 QXLAB('REYNOLDS NUMBER'),QLABEL(1014),QISCL(31))
      STOP
      END
```

APPENDIX C

TABLES OF RESULTS OF EXPERIMENTS

Following are tables of results of all experiments discussed in Chapter 3, with the exception of the baseline case, whose results are given in Table 3.2.

Interpretation of Headings on Tables:

DATE   date of experiment

RUN   number of run on experiment date

VR   volume ratio

C   cylinder wall material: S = Steel
                                     C = Copper
                                     M = Micarta

G   gas used: H = Helium
                       N = Nitrogen
                       A = Argon
                       F = Freon 13

PMC   mean pressure in compression, psia

N   speed, rpm

RE   average Reynolds number

L   non-dimensional loss

PMAX   maximum pressure of the cycle, psia

PMIN   minimum pressure of the cycle, psia

CWORK   work of compression, ft-lbf

Table C-1 Results for Nitrogen, Volume Ratio 2.39, Steel Liner

DATE	RUN	VR	C	G	PMC	N	RE	L	PMAX	PMIN	CWORK
10-01	04	2.389	S	N	228.84	977.2	0.1170E+06	0.0066	426.72	128.78	179.7
10-01	05	2.389	S	N	236.44	279.1	0.3453E+05	0.0068	443.00	132.88	185.7
10-01	06	2.389	S	N	236.98	14.7	0.1817E+04	0.0483	424.17	134.10	186.1
10-12	01	2.389	S	N	47.39	937.5	0.2325E+05	0.0073	88.10	26.61	37.2
10-12	02	2.389	S	N	45.59	270.9	0.6462E+04	0.0073	84.68	25.69	35.8
10-12	03	2.389	S	N	53.50	15.3	0.4279E+03	0.0669	94.64	30.05	42.0
10-12	04	2.389	S	N	11.68	8.9	0.5415E+02	0.0982	18.94	7.04	9.2
10-12	05	2.389	S	N	11.51	255.3	0.1538E+04	0.0190	20.88	6.62	9.0
10-12	06	2.389	S	N	11.54	936.0	0.5652E+04	0.0143	21.09	6.60	9.1
10-18	08	2.389	S	N	10.29	8.8	0.4767E+02	0.0955	16.43	6.35	8.1
10-18	09	2.389	S	N	12.87	15.4	0.1035E+03	0.0944	21.41	7.58	10.1
10-18	10	2.389	S	N	28.98	15.3	0.2327E+03	0.0812	50.18	16.56	22.8
10-18	11	2.389	S	N	12.11	125.8	0.7969E+03	0.0285	21.73	7.02	9.5
10-18	12	2.389	S	N	26.85	260.3	0.3657E+04	0.0093	49.59	15.27	21.1
10-18	13	2.389	S	N	49.32	463.0	0.1195E+05	0.0089	91.56	27.74	38.7
10-20	01	2.389	S	N	104.46	8.8	0.4802E+03	0.0780	179.99	59.67	82.0
10-20	02	2.389	S	N	99.56	244.4	0.1273E+05	0.0078	183.05	56.83	78.2
10-20	03	2.389	S	N	99.73	910.5	0.4752E+05	0.0069	183.27	56.96	78.3
10-20	04	2.389	S	N	238.90	463.0	0.5787E+05	0.0086	443.11	134.98	187.6

Table C-2 Results for Argon, Volume Ratio 2.39, Steel Liner

DATE	RUN	VR	C	G	PMC	N	RE	L	PMAX	PMIN	CWORK
11-19	01	2.389	S	A	12.59	254.2	0.1889E+04	0.0364	24.33	6.85	9.9
11-19	02	2.389	S	A	12.62	130.0	0.9680E+03	0.0514	23.92	6.96	9.9
11-19	03	2.389	S	A	12.00	459.4	0.3254E+04	0.0359	23.22	6.56	9.4
11-19	04	2.389	S	A	11.95	943.4	0.6653E+04	0.0326	23.30	6.46	9.4
12-29	01	2.389	S	A	218.18	239.0	0.3078E+05	0.0186	442.22	110.84	171.4
12-29	02	2.389	S	A	219.93	465.1	0.6036E+05	0.0178	446.98	111.72	172.7
12-30	01	2.389	S	A	227.36	947.9	0.1272E+06	0.0162	462.27	114.94	178.6
12-30	02	2.389	S	A	96.13	958.5	0.5437E+05	0.0166	193.59	49.30	75.5
12-30	03	2.389	S	A	95.63	272.1	0.1535E+05	0.0177	192.58	49.03	75.1
12-30	04	2.389	S	A	99.84	15.1	0.8903E+03	0.1105	185.04	51.07	78.4
12-30	05	2.389	S	A	220.12	14.7	0.1912E+04	0.0957	416.97	110.62	172.9
12-30	06	2.389	S	A	53.14	15.3	0.4793E+03	0.1324	97.56	26.63	41.7
12-30	07	2.389	S	A	51.76	31.6	0.9645E+03	0.0798	99.82	26.20	40.7
12-30	08	2.389	S	A	12.96	31.8	0.2430E+03	0.1062	23.50	7.04	10.2
12-30	09	2.389	S	A	14.10	15.3	0.1274E+03	0.1452	24.03	7.77	11.1
12-30	10	2.389	S	A	29.72	15.3	0.2685E+03	0.1395	53.32	15.49	23.3
12-30	11	2.389	S	A	10.68	8.8	0.5551E+02	0.1415	17.13	6.26	8.4
12-30	12	2.389	S	A	27.45	100.0	0.1619E+04	0.0501	53.61	14.37	21.6
12-30	13	2.389	S	A	27.00	941.9	0.1501E+05	0.0263	54.11	13.98	21.2
12-30	14	2.389	S	A	50.10	975.6	0.2884E+05	0.0228	101.62	25.53	39.4
12-30	15	2.389	S	A	48.92	474.7	0.1370E+05	0.0250	98.71	25.12	38.4
12-30	16	2.389	S	A	49.98	275.9	0.8136E+04	0.0211	101.04	25.77	39.3

Table C-3 Results for Freon 13, Volume Ratio 2.39, Steel Liner

DATE	RUN	VR	C	G	PMC	N	RE	L	PMAX	PMIN	CWORK
10-04	01	2.389	S	F	216.00	15.0	0.7859E+04	0.0137	343.32	141.52	169.6
10-04	02	2.389	S	F	261.74	256.4	0.1628E+06	0.0019	416.97	173.19	205.6
10-04	03	2.389	S	F	267.65	921.7	0.5984E+06	0.0019	426.05	177.07	210.2
10-04	04	2.389	S	F	56.15	950.9	0.1295E+06	0.0017	93.51	35.49	44.1
10-04	05	2.389	S	F	53.82	270.9	0.3536E+05	-0.0042	90.02	34.21	42.3
10-04	06	2.389	S	F	50.20	15.3	0.1864E+04	0.0125	83.07	31.73	39.4
10-04	07	2.389	S	F	13.57	8.8	0.2905E+03	0.0293	21.97	8.70	10.7
10-04	08	2.389	S	F	14.35	109.3	0.3804E+04	0.0040	23.66	9.24	11.3
10-04	09	2.389	S	F	13.78	982.0	0.3281E+05	0.0020	22.76	8.89	10.8
10-19	01	2.389	S	F	53.05	463.7	0.5966E+05	-0.0016	88.51	33.63	41.7
10-19	02	2.389	S	F	51.90	265.5	0.3342E+05	-0.0063	86.87	32.94	40.8
10-19	03	2.389	S	F	31.03	267.9	0.2016E+05	-0.0037	51.94	19.70	24.4
10-19	04	2.389	S	F	13.58	269.7	0.8885E+04	-0.0038	22.56	8.74	10.7
10-19	05	2.389	S	F	13.70	15.3	0.5100E+03	0.0164	22.51	8.76	10.8
10-19	06	2.389	S	F	31.01	15.3	0.1154E+04	0.0134	51.37	19.63	24.4
10-19	07	2.389	S	F	9.98	8.8	0.2143E+03	0.0280	16.25	6.36	7.8
10-21	01	2.389	S	F	248.25	449.8	0.2708E+06	0.0023	395.37	163.78	195.0
10-21	02	2.389	S	F	101.12	978.8	0.2401E+06	0.0028	166.26	64.76	79.4
10-21	03	2.389	S	F	100.38	274.6	0.6686E+05	-0.0021	165.46	64.58	78.8
10-21	04	2.389	S	F	99.09	15.2	0.3665E+04	0.0115	161.34	63.70	77.8

Table C-4   Results for Helium, Volume Ratio 3.99, Steel Liner

DATE	RUN	VR	C	G	PMC	N	RE	L	PMAX	PMIN	CWORK
12-10	01	3.994	S	H	21.41	254.8	0.3690E+03	0.1159	56.15	8.78	16.8
12-10	02	3.994	S	H	21.73	127.7	0.1877E+03	0.1441	54.08	9.17	17.1
12-10	03	3.994	S	H	21.75	456.6	0.6719E+03	0.1018	58.05	8.93	17.1
12-10	04	3.994	S	H	21.41	933.1	0.1351E+04	0.0841	58.34	8.76	16.8
12-10	05	3.994	S	H	17.27	8.8	0.1034E+02	0.0969	35.92	8.99	13.6
12-10	06	3.994	S	H	17.85	15.3	0.1850E+02	0.1377	37.33	9.01	14.0
12-10	07	3.994	S	H	19.39	31.7	0.4164E+02	0.1863	41.86	9.12	15.2
12-10	08	3.994	S	H	44.03	31.7	0.9446E+02	0.2142	100.18	18.62	34.6
12-10	09	3.994	S	H	44.96	15.3	0.4655E+02	0.1961	96.21	20.71	35.3
12-10	10	3.994	S	H	35.93	274.6	0.6674E+03	0.0940	98.23	14.10	28.2
12-10	11	3.994	S	H	36.15	475.4	0.1163E+04	0.0889	100.18	14.07	28.4
12-10	12	3.994	S	H	35.61	956.9	0.2305E+04	0.0748	99.55	14.03	28.0
12-14	01	3.994	S	H	117.62	15.2	0.1207E+03	0.2137	254.16	53.46	92.4
12-14	02	3.994	S	H	191.49	15.0	0.1938E+03	0.2175	429.37	81.38	150.4
12-14	03	3.994	S	H	168.56	247.9	0.2827E+04	0.0750	449.31	70.74	132.4
12-14	04	3.994	S	H	173.13	451.1	0.5283E+04	0.0612	459.94	75.28	136.0
12-14	05	3.994	S	H	170.89	925.9	0.1070E+05	0.0496	458.84	73.40	134.2
12-14	06	3.994	S	H	102.93	933.1	0.6497E+04	0.0566	280.18	43.05	80.8
12-14	07	3.994	S	H	103.63	467.3	0.3275E+04	0.0675	278.41	43.72	81.4
12-14	08	3.994	S	H	104.65	267.3	0.1892E+04	0.0746	273.32	45.60	82.2

Table C-5   Results for Helium, Volume Ratio 2.39, Copper Liner

DATE	RUN	VR	C	G	PMC	N	RE	L	PMAX	PMIN	CWORK
01-04	01	2.389	C	H	52.43	247.4	0.8775E+03	0.0538	101.57	26.97	41.2
01-04	02	2.389	C	H	49.42	447.8	0.1497E+04	0.0466	97.53	25.12	38.8
01-04	03	2.389	C	H	50.44	931.7	0.3179E+04	0.0396	99.72	25.89	39.6
01-04	04	2.389	C	H	29.76	956.9	0.1926E+04	0.0475	59.06	15.01	23.4
01-04	06	2.389	C	H	13.26	107.0	0.9590E+02	0.1139	23.36	7.27	10.4
01-04	07	2.389	C	H	12.97	272.1	0.2387E+03	0.0828	24.19	6.88	10.2
01-04	08	2.389	C	H	12.53	474.7	0.4023E+03	0.0758	23.88	6.54	9.8
01-04	09	2.389	C	H	12.28	972.4	0.8076E+03	0.0636	23.96	6.31	9.6
01-04	10	2.389	C	H	12.53	31.8	0.2697E+02	0.1224	20.40	7.42	9.8
01-04	11	2.389	C	H	11.96	15.3	0.1239E+02	0.0889	19.04	7.45	9.4
01-04	12	2.389	C	H	9.76	8.8	0.5810E+01	0.0498	15.61	6.22	7.7
01-04	13	2.389	C	H	31.18	15.3	0.3229E+02	0.1343	50.11	18.44	24.5
01-04	14	2.389	C	H	57.98	15.3	0.5987E+02	0.1549	95.20	32.50	45.5
01-04	15	2.389	C	H	57.22	31.6	0.1222E+03	0.1364	100.61	30.60	44.9
01-05	01	2.389	C	H	244.45	8.5	0.1411E+03	0.1602	404.68	135.09	192.0
01-05	02	2.389	C	H	113.11	8.7	0.6653E+02	0.1469	182.87	65.74	88.8
01-05	03	2.389	C	H	96.89	254.8	0.1670E+04	0.0453	186.24	51.43	76.1
01-05	04	2.389	C	H	97.12	927.4	0.6092E+04	0.0305	189.92	51.16	76.3
01-05	05	2.389	C	H	216.71	936.0	0.1372E+05	0.0238	430.48	112.39	170.2
01-05	06	2.389	C	H	218.04	465.1	0.6860E+04	0.0283	428.93	113.83	171.2
01-05	07	2.389	C	H	217.83	269.7	0.3973E+04	0.0325	425.28	114.27	171.1

Table C-6 Results for Helium, Volume Ratio 2.39, Micarta Liner

DATE	RUN	VR	C	G	PMC	N	RE	L	PMAX	PMIN	CWORK
01-06	01	2.389	M	H	220.87	264.3	0.3949E+04	0.0329	423.39	119.37	173.5
01-06	02	2.389	M	H	222.61	463.0	0.6971E+04	0.0280	428.71	119.59	174.8
01-06	03	2.389	M	H	237.43	955.4	0.1534E+05	0.0204	459.06	128.67	186.5
01-06	04	2.389	M	H	101.82	966.2	0.6654E+04	0.0259	192.66	56.92	80.0
01-06	05	2.389	M	H	93.31	272.7	0.1721E+04	0.0408	177.47	50.67	73.3
01-06	06	2.389	M	H	106.79	8.7	0.6290E+02	0.1374	172.82	62.50	83.9
01-07	01	2.389	M	H	10.53	8.8	0.6255E+01	0.0507	16.30	6.99	8.3
01-07	02	2.389	M	H	13.64	31.8	0.2938E+02	0.1197	21.78	8.37	10.7
01-07	03	2.389	M	H	13.11	15.3	0.1359E+02	0.0898	20.37	8.44	10.3
01-07	04	2.389	M	H	30.34	15.3	0.3142E+02	0.1287	48.31	18.25	23.8
01-07	05	2.389	M	H	60.96	15.3	0.6303E+02	0.1485	100.25	34.33	47.9
01-07	06	2.389	M	H	57.84	31.6	0.1237E+03	0.1271	101.02	31.49	45.4
01-07	07	2.389	M	H	12.81	885.0	0.7665E+03	0.0592	23.92	7.19	10.1
01-07	08	2.389	M	H	12.84	447.1	0.3882E+03	0.0691	23.48	7.30	10.1
01-07	09	2.389	M	H	12.76	261.4	0.2257E+03	0.0742	22.99	7.34	10.0
01-06	07	2.389	M	H	232.61	8.5	0.1345E+03	0.1464	386.84	130.11	182.7
01-07	15	2.389	M	H	47.92	272.7	0.8841E+03	0.0491	91.90	25.67	37.6
01-07	14	2.389	M	H	48.53	469.5	0.1541E+04	0.0473	93.68	25.86	38.1
01-07	13	2.389	M	H	47.68	956.9	0.3086E+04	0.0397	92.89	25.38	37.4
01-07	12	2.389	M	H	27.66	953.9	0.1785E+04	0.0433	53.04	15.20	21.7
01-07	11	2.389	M	H	29.32	134.8	0.2674E+03	0.0785	53.62	16.23	23.0
01-07	10	2.389	M	H	12.91	131.1	0.1145E+03	0.0908	22.49	7.53	10.1

APPENDIX D

PRELIMINARY EXPERIMENTS

Several preliminary series of experiments, which were done prior to
those reported in Chapter 3, are described here. They are of a similar
general nature and used a cruder version of the same apparatus. The non-
dimensional loss was calculated and plotted against the average Reynolds
number as in later work. The analog nature of the data made calculation
of temperature and entropy data too laborious. In some experiments the
large scale flow pattern was altered by inserting obstacles at the bottom
of the clearance volume. In others wall temperature measurements were
made. The experiments are described in chronological order.

D.1 Apparatus

The apparatus was the same as that discussed in Chapter 3 except for
the piston, upper cylinder and cylinder head.

For most of the preliminary experiments the piston was 2 inches
shorter than the final version so that the area swept by the piston seal
overlapped the swept volume by 1 3/4 inches.

The upper cylinder and head had the same general arrangement as
later, but there are a number of differences, as shown in Fig. D.1. The
later cylinder is shown in Fig. A.1. The differences are as follows:

> 1. Here the cylinder does not have a removeable
>   liner , but does have a water jacket, which was
>   not used.

CYLINDER HEAD

O-RING
PISTON SEAL

PRESSURE
TRANSDUCER

GAS SPACE

GAS IN

PISTON
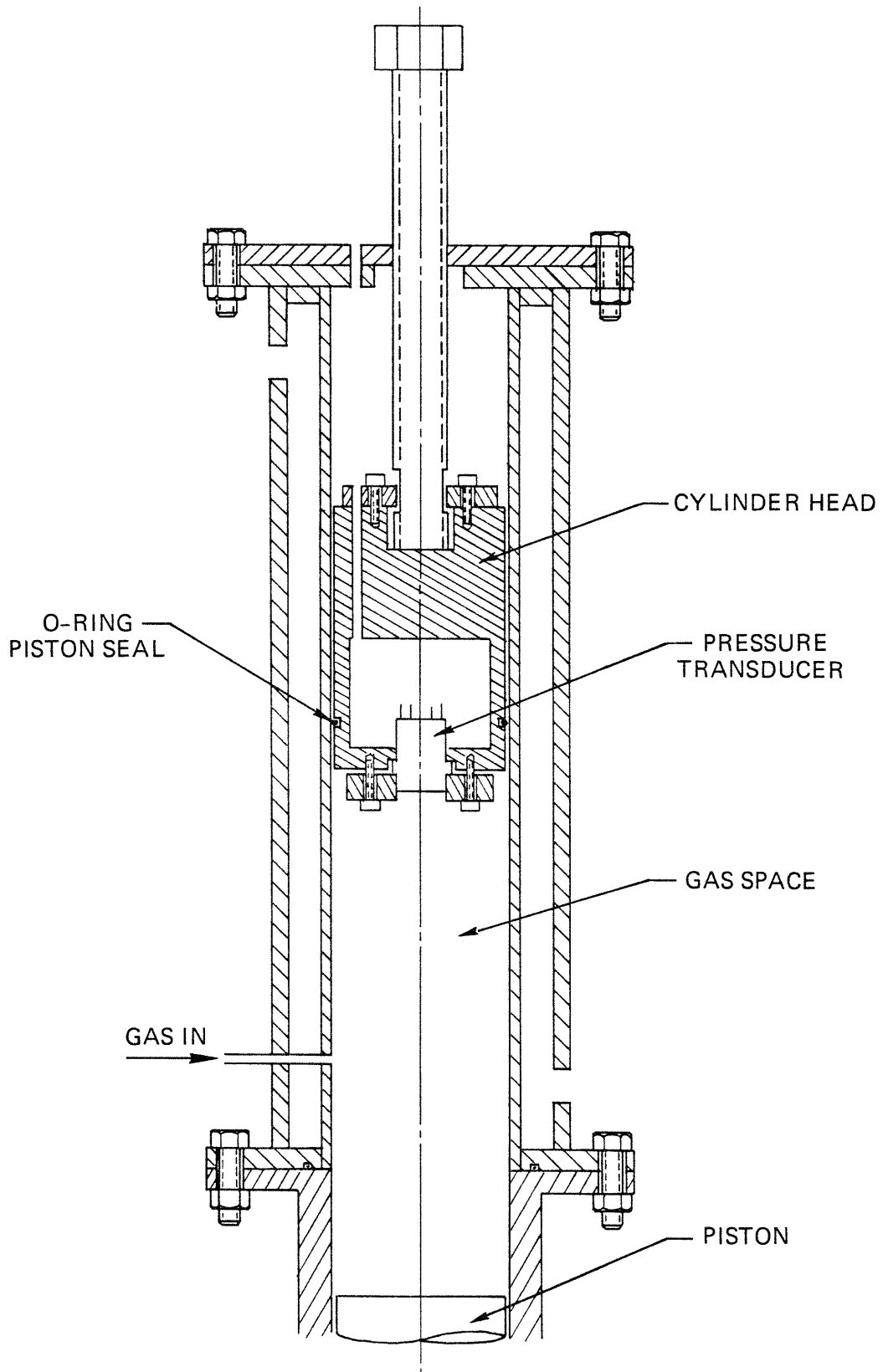
Fig. D-1. Cylinder for Early Experiments.

2. The 1/8 inch copper gas fill tube was on the side of the cylinder. Therefore the volume ratio adjustment range was 1.5 to 2.39 instead of 2 to 10.

3. The underside of the cylinder head was not smooth, as shown.

D.2 Instrumentation

The pressure transducers were the same but were only statically calibrated. It was felt that although the transducers were supposed to be compensated for temperature changes, they might not be adequately compensated for changes as rapid as the gas temperature swing in the experiments. Therefore the sensitive face of the transducer was coated with approximately 1/8 inch of RTV rubber in order to isolate the face from the gas temperature swing. After the preliminary experiments, the dynamic calibration indicated that the transducer did not seem to be significantly affected by the gas temperature swing hence the coating was not used in later experiments. The output from the transducer and balancer was fed directly to an oscilloscope without amplification or filtering. Hence there were some problems with noise.

The volume was indicated by a displacement transducer actuated by a cam on the crankshaft. The eccentric circular cam caused the transducer core to have a motion which was geometrically similar to the piston motion (Fig. D.2). The output of the transducer was fed directly to the oscilloscope. The system was statically timed by measuring the piston position directly with a micrometer. After the preliminary experiments, the system
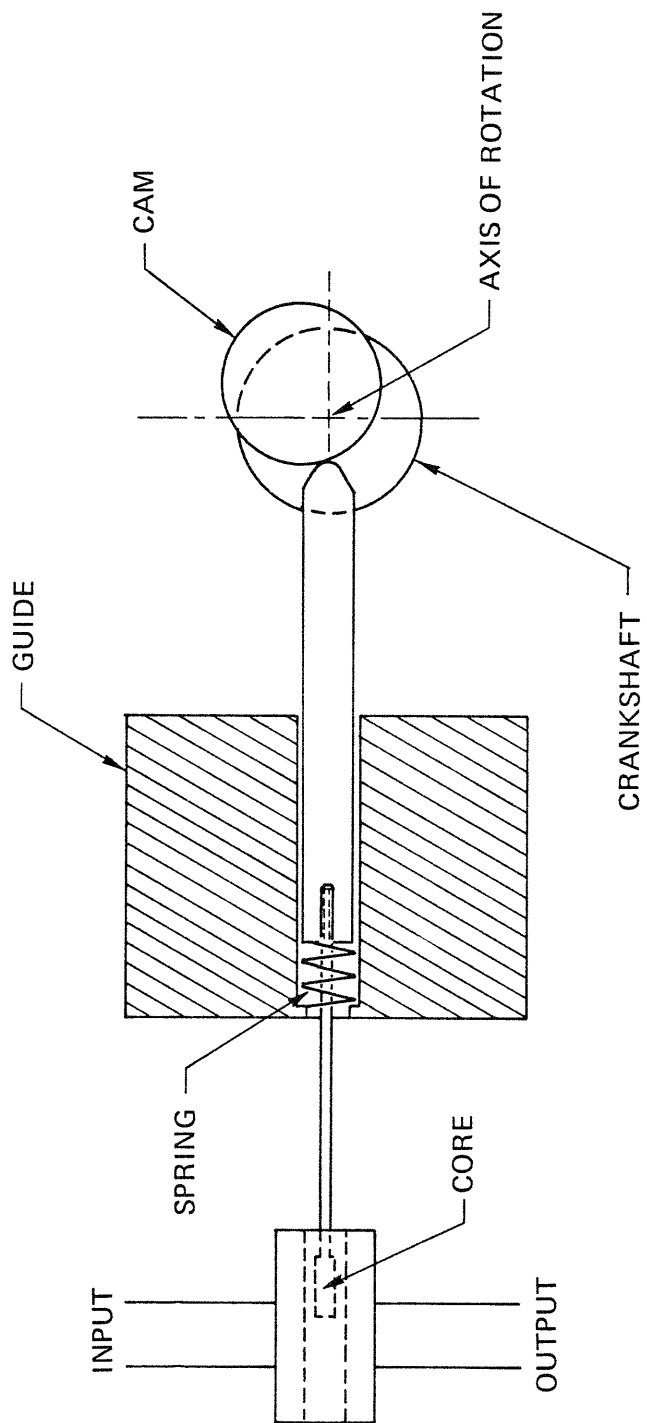
Fig. D-2. Schematic of Volume Indicator.

was calibrated dynamically by comparing with the system described in Appendix A.6. Various kinds of errors were revealed which were difficult to compensate. Hence this system was not used for later experiments.

D.3 Data Handling

The pressure and volume signals were fed to an ordinary analog oscilloscope. In X-Y mode the oscilloscope displayed the p-V diagram directly, and the diagram was photographed. The area of the opening and the area under the compression curve were measured with a planimeter to give the non-dimensional loss. The width of the lines of the p-V diagram were significant compared to the enclosed area of the diagram and the measurement of the area with a planimeter was not very accurate.

D.4 Initial Experiments

A series of experiments similar to those discussed in Chapter 3 was run initially. The volume ratio was fixed at 2.39 and the cylinder wall material was steel. The gases used were helium, nitrogen and Freon 13, whose properties are given in Table 3.1.

Plots of non-dimensional loss versus Reynolds number for these experiments are shown in Figs. D.3 to D.5. The results are generally similar to those obtained later, as shown in Figs. 3.3 to 3.6. The losses generally do not fall off as much with Reynolds number above a Reynolds number of 100. Also there is considerable scatter in the data above a Reynolds number of 1000. These discrepancies are probably attributable to errors in the volume measurement and the measurement of the opening area of the p-V diagram.

D-3 He
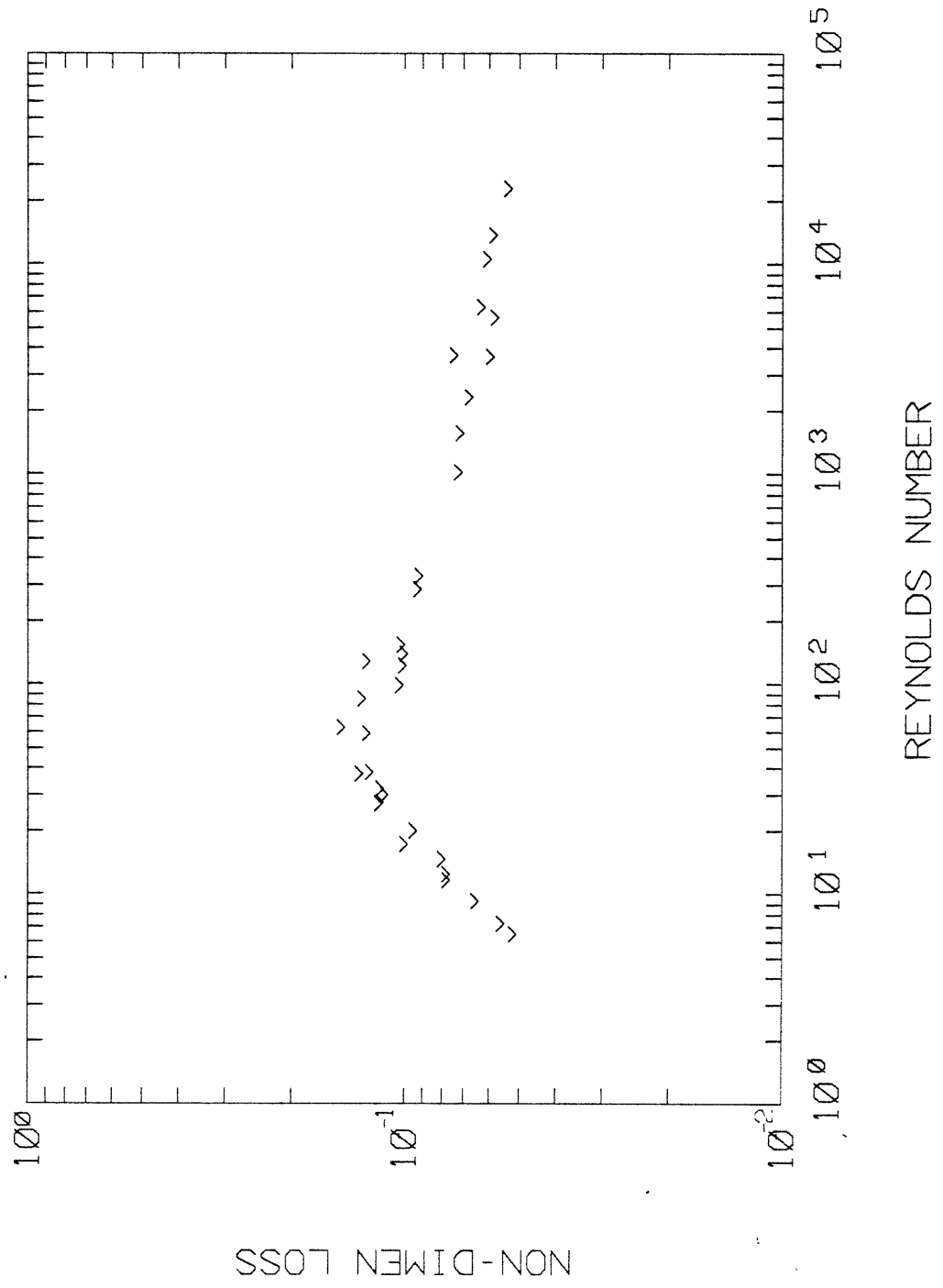
Fig. D-3. Loss vs. Reynolds Number for Helium, Volume Ratio 2.39, Steel Cylinder.
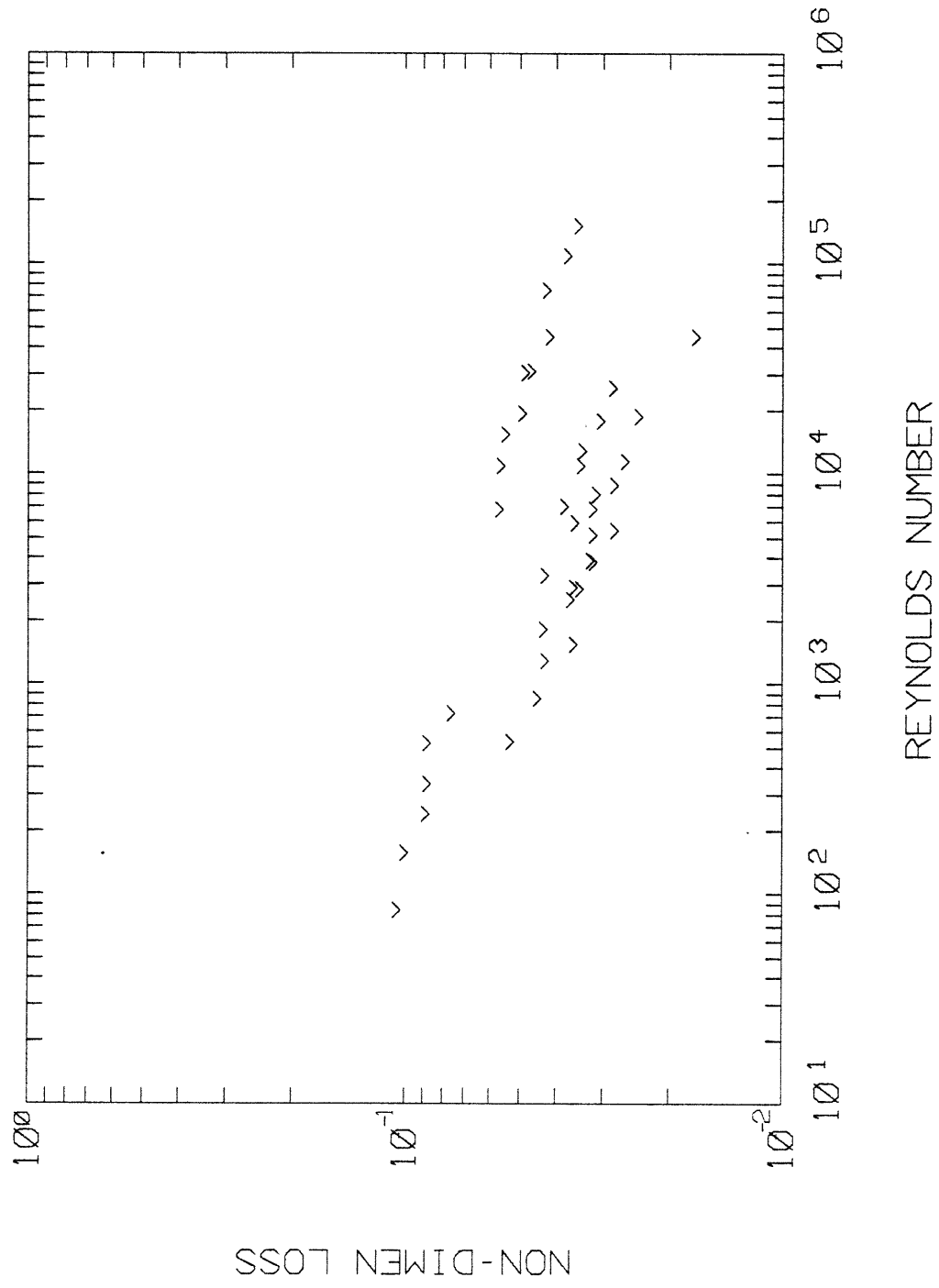
Fig. D-4. Loss vs. Reynolds Number for Nitrogen, Volume Ratio 2.39, Steel Cylinder.

D-5 CuF₃

VAX/VMS ••• PENPLOT 2.0   7-APR-1983 12:10:53.43   RES1:[P1732.FAULKNER]HDCOPY.PLT;6 FAULKNER   ••• VAX/VMS
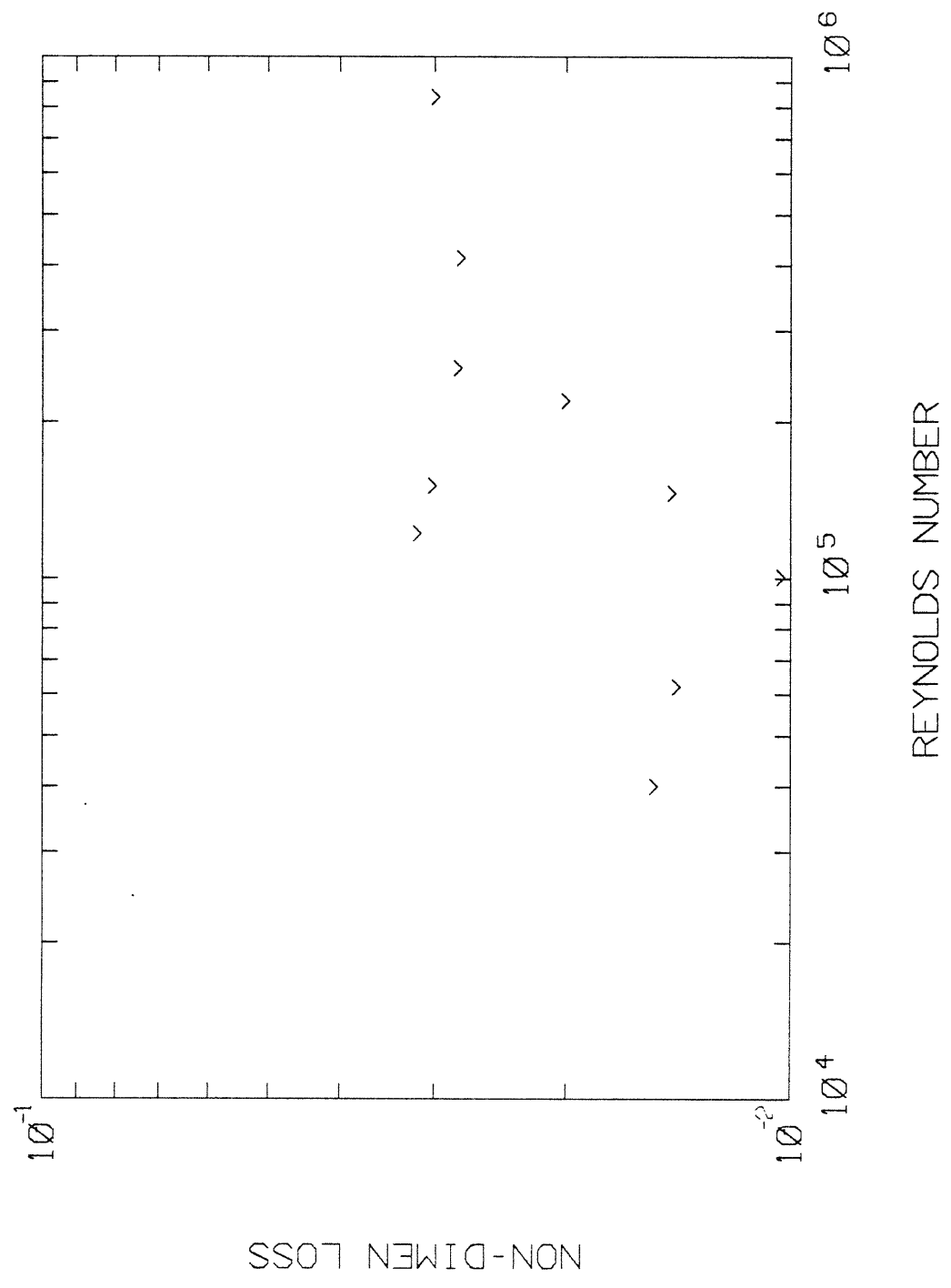
Fig. D-5. Loss vs. Reynolds Number for Freon 13, Volume Ratio 2.39, Steel Cylinder.

D.5 Large Scale Flow Modification

An attempt was made to find out if the results were strongly influenced by the large scale flow pattern in the cylinder. Experiments were run with flow obstructions installed in the cylinder just above the top dead center position of the piston, while the volume ratio was held constant at 2.39 (see Fig. D.6). One set of experiments was done with a 1/4 inch wide steel ring around the circumference of the cylinder. Another set was done with a steel plate closing off half of the cylinder cross section. These obstructions should have changed the large scale flow pattern in the cylinder markedly. A third set was done with this plate and the clearance volume packed with copper wire screens.

Figures D.7 to D.9 show plots of loss versus Reynolds number for these experiments. The three gases used in these experiments are not indicated. These results indicate that the loss versus Reynolds number relationship is not strongly influenced by the large scale flow pattern, particularly at low Reynolds number. This finding is quite remarkable and more research on this phenomenon is desireable.

The wire screens greatly increase the surface area for cyclic heat transfer and therefore the cylinder processes are more nearly isothermal. Another way to view it is that the effective average Reynolds number should be based on the screen dimensions, making the actual number much smaller than the average Reynolds number based on the bore which is used in the plot. Therefore the loss versus Reynolds number plot is shifted to the right compared to the other curves.

VOLUME RATIO HELD CONSTANT
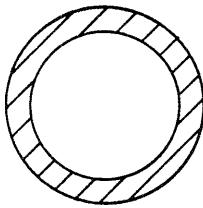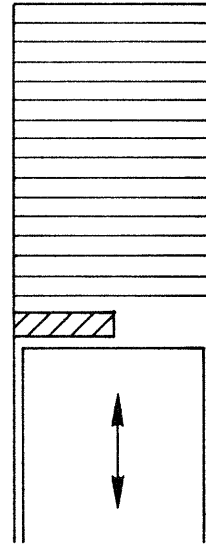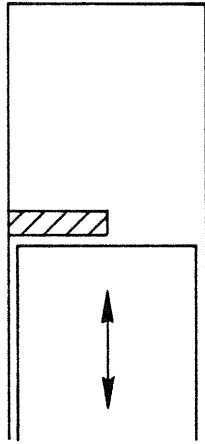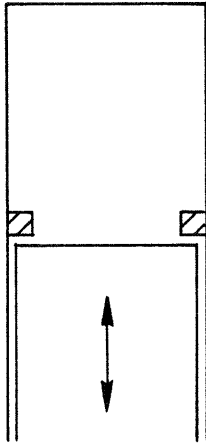
RING
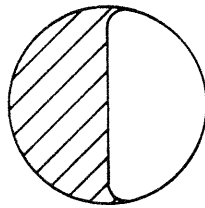
HALF OPEN PLATE
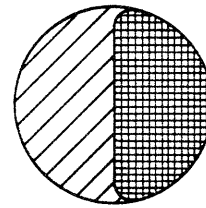
HALF OPEN PLATE
AND WIRE SCREENS

$$\frac{\text{COPPER VOL}}{\text{CLEAR VOL}} = .18$$

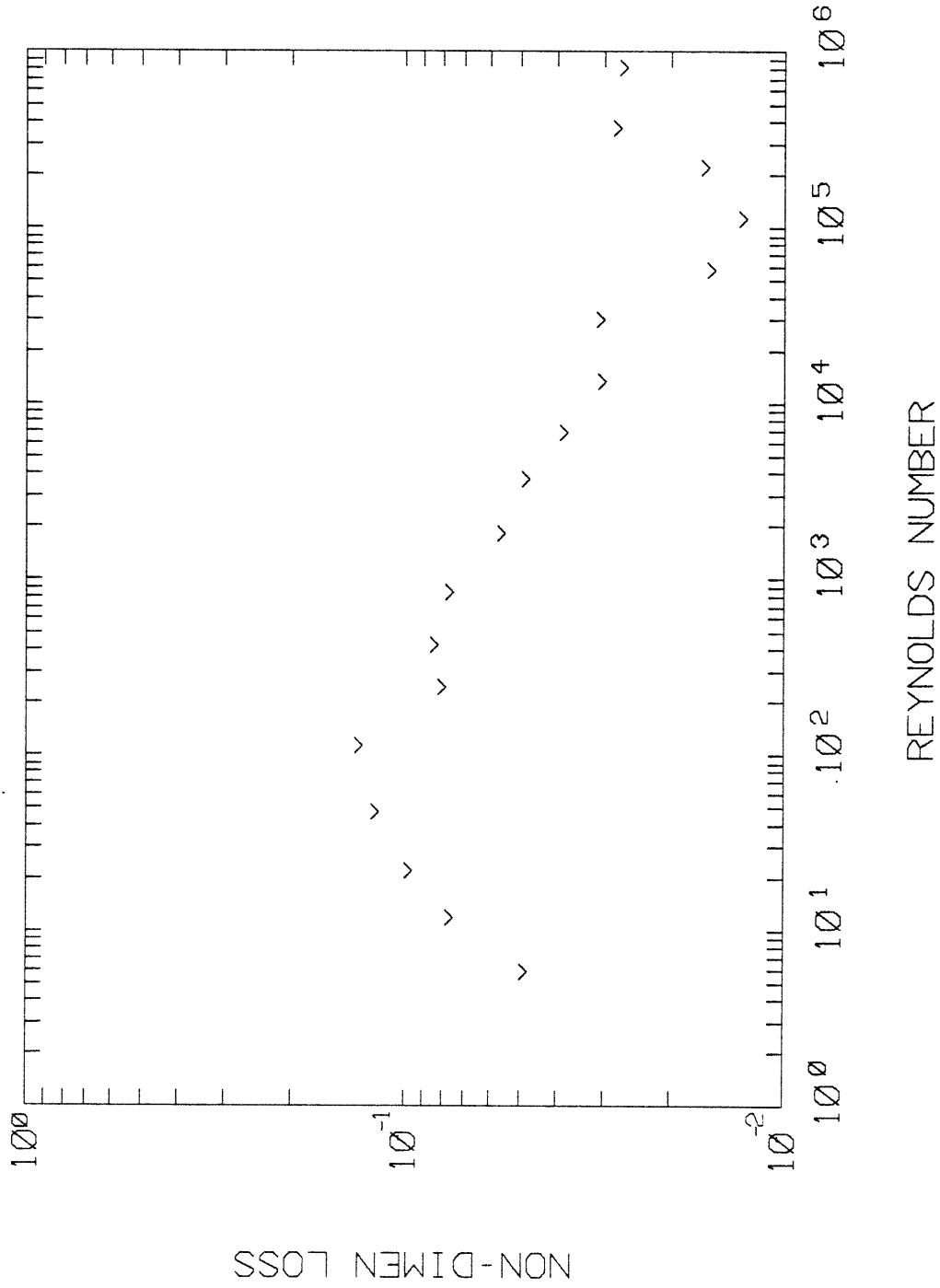20/in., .016 dia

Fig. D-6. Flow Obstructions.

D-7 King

Fig. D-7. Loss vs. Reynolds Number for 3 Gases and Ring Obstruction.
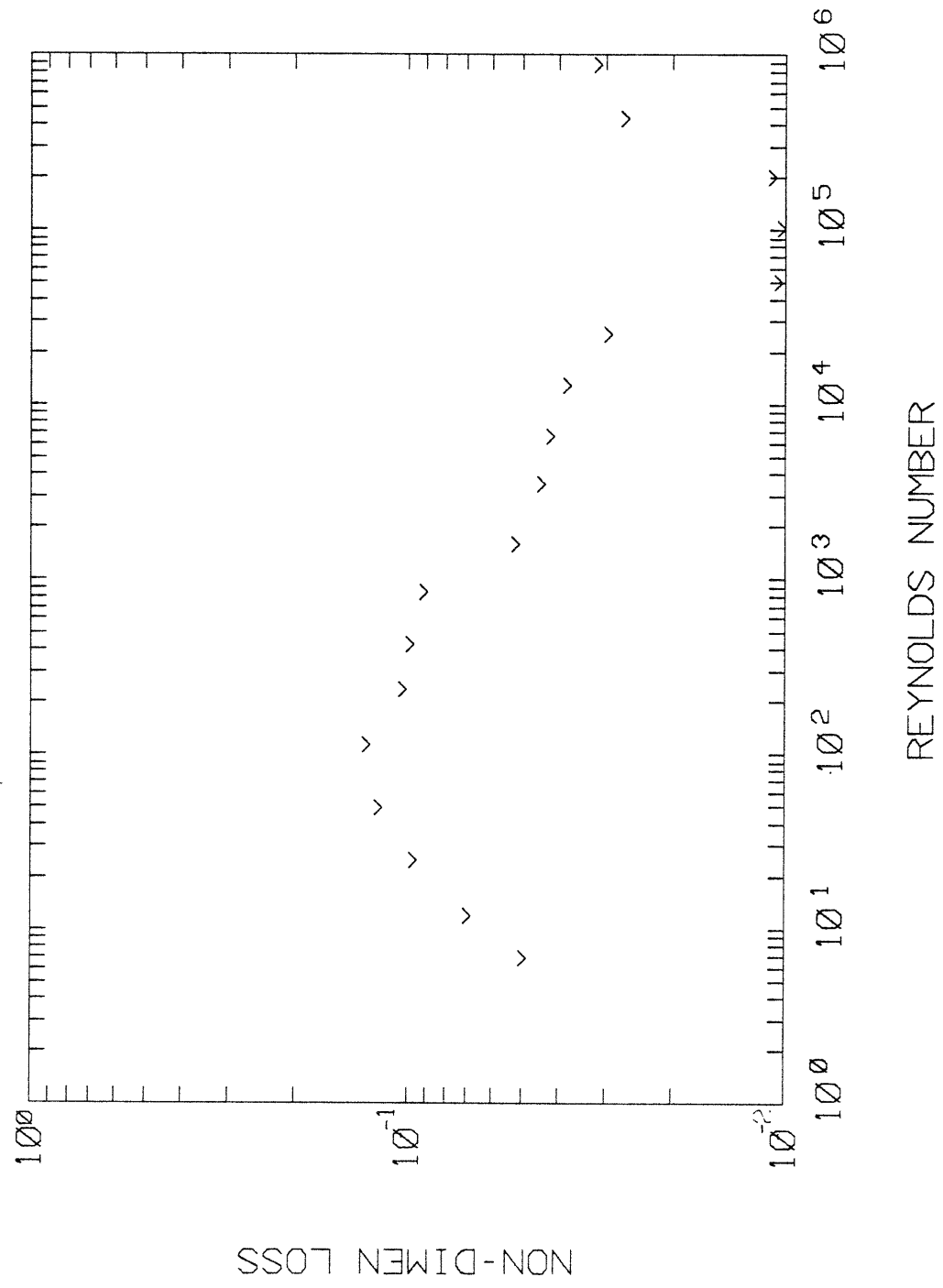
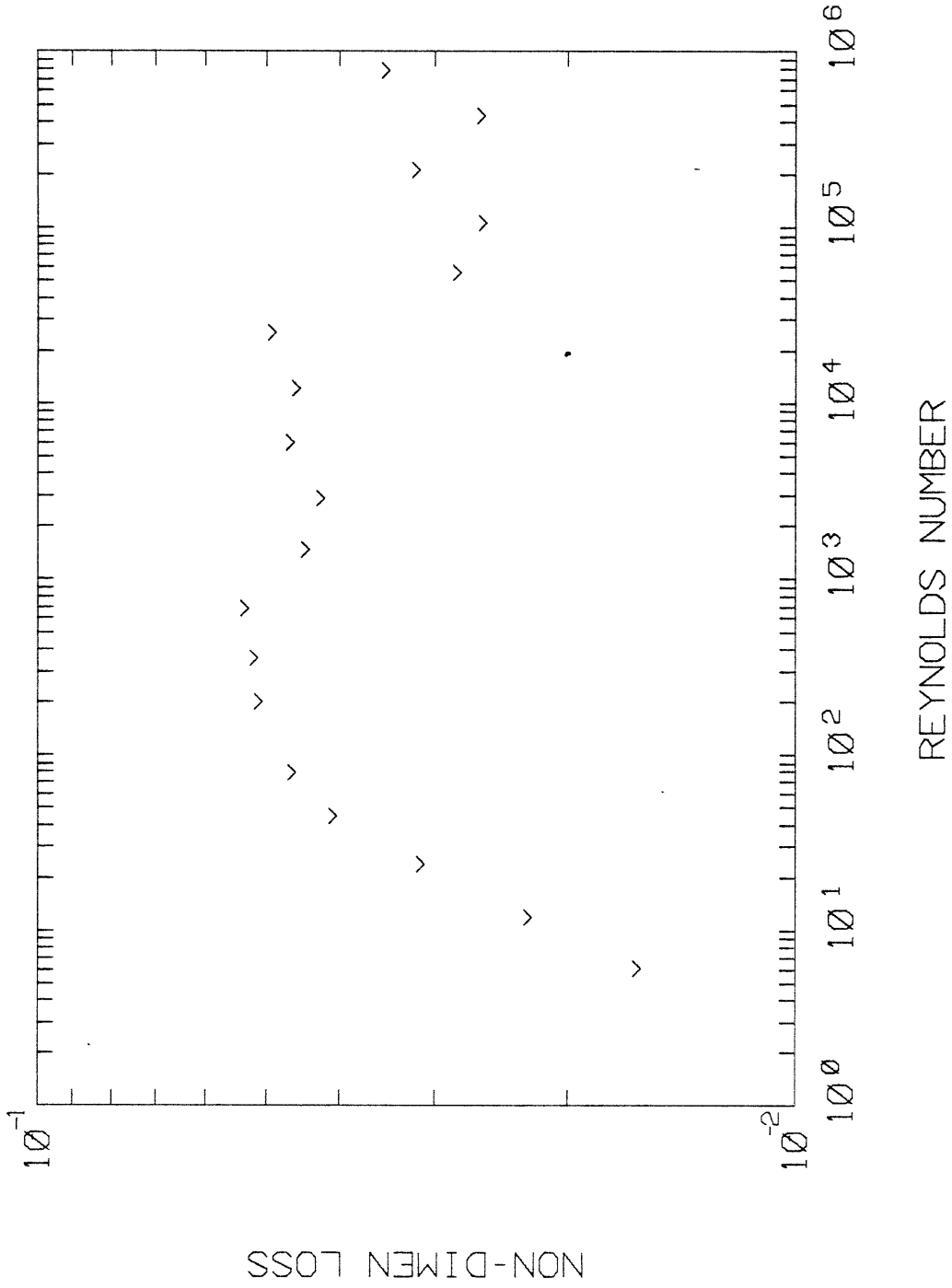Fig. D-8. Loss vs. Reynolds Number for 3 Gases and Half Open Plate Obstruction.

Fig. D-9. Loss vs. Reynolds Number for 3 Gases, Half Open Plate Obstruction, and Copper Screens.

D.6 Wall Temperature Measurements

At this point in the investigation, curiosity regarding the wall temperature developed for several reasons. It was felt that heat from piston seal friction might be getting into the gas and affecting the results. Therefore a two inch extension was put on the top of the piston, so that the gas would not be exposed to the cylinder wall where it had been wiped by the piston seal. It was also felt that there might be a significant axial variation in the wall temperature and that it might take many minutes for the cylinder to reach thermal equilibrium between the gas and the ambient air in the room. Therefore four copper-constantan thermocouples were installed on the cylinder as shown in Fig. D.10. The upper three were soft soldered in .060 inch diameter holes in the cylinder wall and then the inner surface of the cylinder was filed smooth. The fourth was soldered to the outside of the cylinder in the middle of the vertical sweep of the piston seal. The signals from the thermocouples were interpreted and recorded by an Autodata Nine data recorder.

One experiment was allowed to run over a longer time to assess the axial temperature gradient in the wall and the thermal time constant of the wall. The temperatures of the four thermocouples were recorded from start-up through one hour of running. The gas was nitrogen and the speed was 560 rpm. The average pressure started at 240 psi (Reynolds number 68,000) and declined to 105 psi (Reynolds number 31,000). The results are shown in Fig. D.11.

A significant axial temperature gradient is indicated. The gradient is in the expected direction, temperature decreasing with distance from the
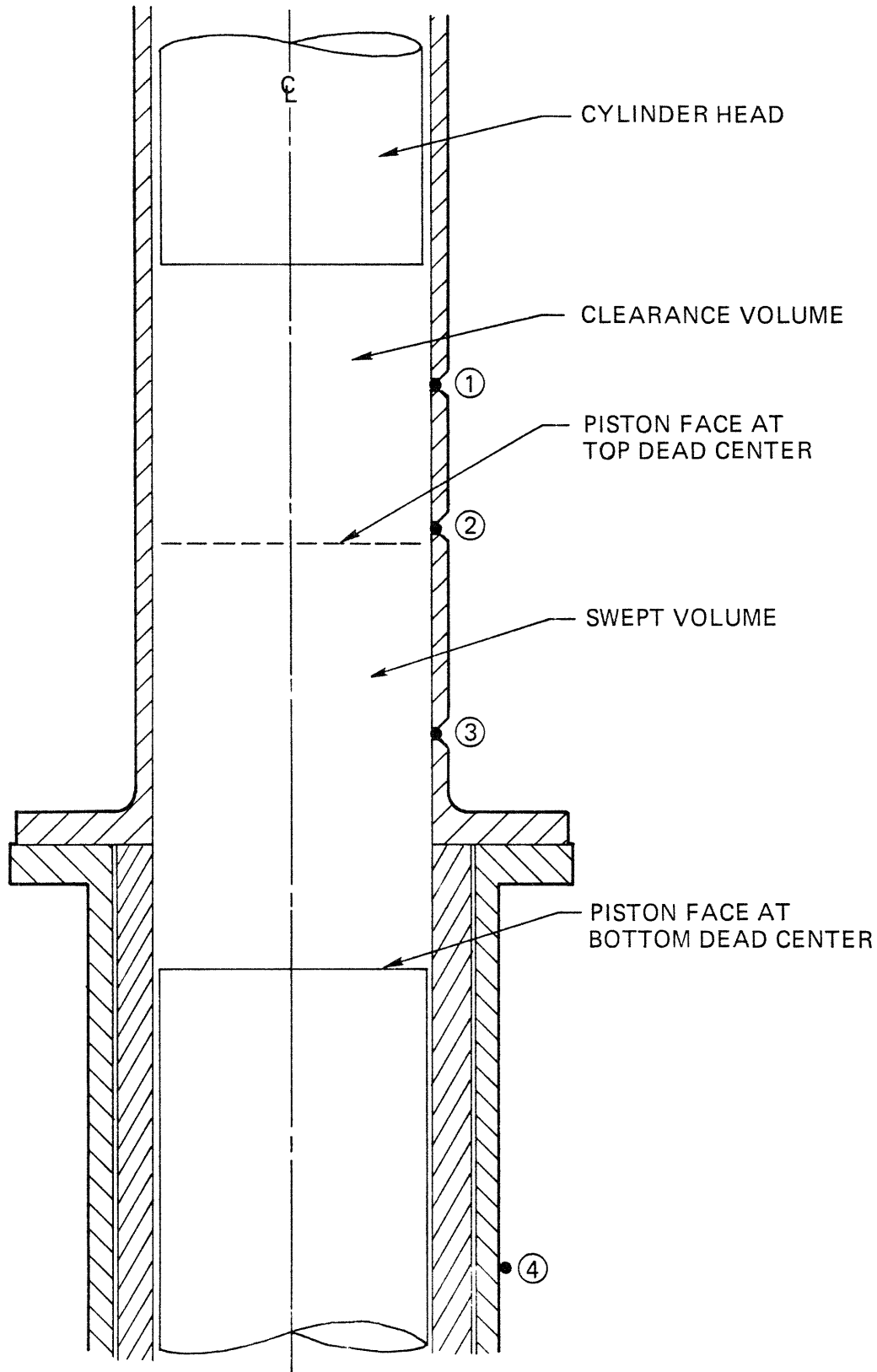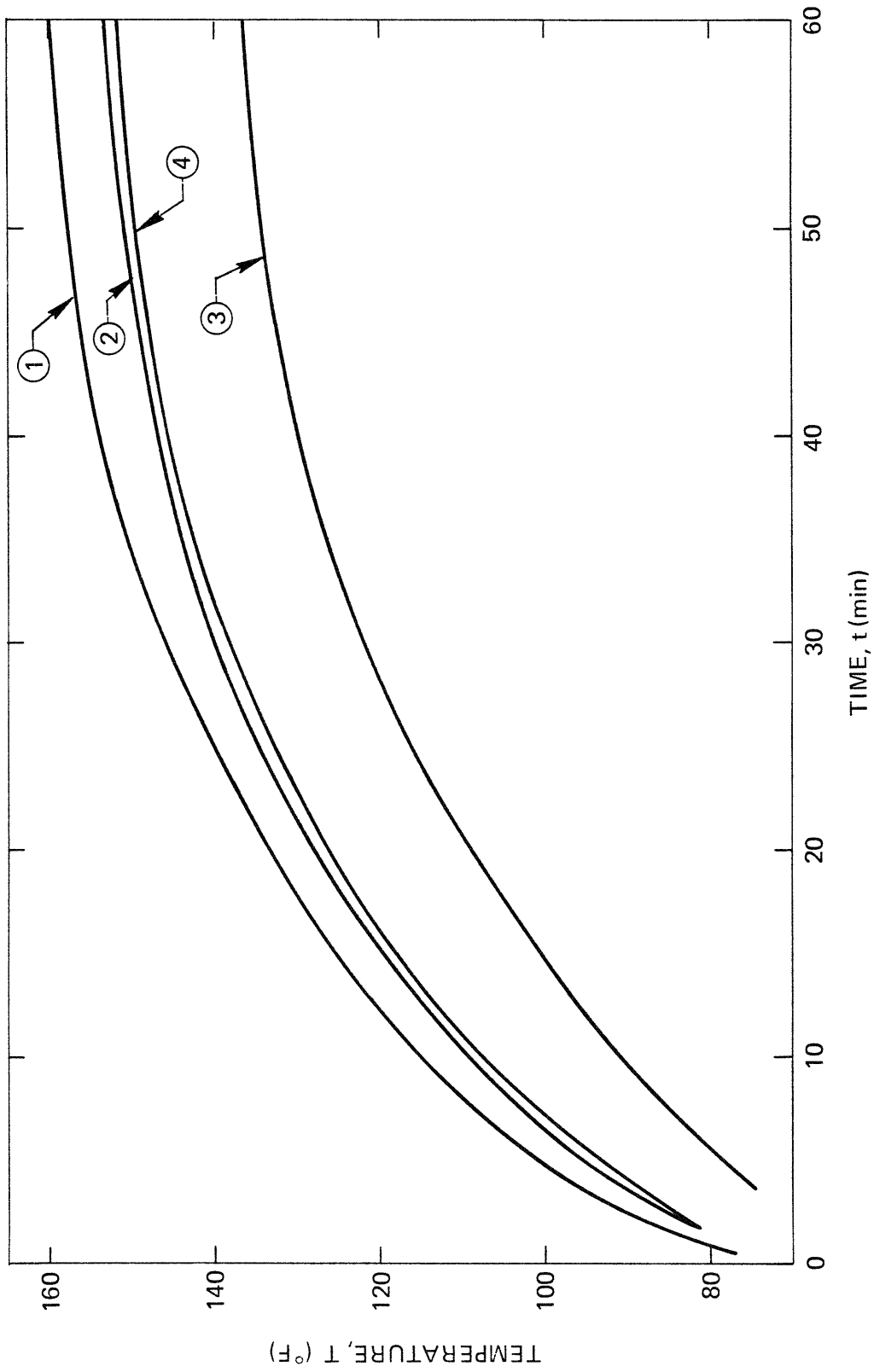
Fig. D-10. Thermocouple Locations.

Fig. D-11. Temperature vs. Time at Four Wall Locations.

cylinder head. The gradient in the swept volume suggests that heat from piston ring friction is not reaching the gas.

The thermal time constant of the cylinder is shown to be about 15 minutes. Previous experimental data had been taken after about 1 to 5 minutes of running, with no attempt to standardize the procedure, and the thermal time constant varies with Reynolds number. Thus the wall temperature varied considerably between previous experiments, introducing a random independent variable. It was decided to take all later experimental data within one minute of starting to minimize the effect of this variable. Unfortunately, the axial temperature gradient, which is likely to occur in actual reciprocating machinery, is thereby also suppressed. The other thermal time constant of the apparatus, characterizing the gas approaching equilibrium with the cylinder wall, is of the order of a few cycles. Experimental data was never taken until after this process had taken place.

Then the experiments with the unobstructed cylinder were repeated for the higher half of the Reynolds number range. The results were not noticeably different from those shown in Figs. D.3 to D.5. Thus the errors in previous experiments due to heat from piston seal friction and variation in wall temperature between experiments did not seem to be significant compared to the other errors present.

APPENDIX E

MODELS

E.1 Overview

Three kinds of analytical models of the processes in the cylinder were developed. All contributed in a general way to understanding the problem, but none were developed to the point of providing quantitative prediction of results that could be compared with the experiments. All are one-dimensional models of heat flow within a gas, which is undergoing cyclic pressure variation, while in contact with a solid wall at constant temperature. The three models will now be briefly described.

1. "Two-Space" Model

This model is discrete in time and space. Gas is lumped into two spaces of uniform temperature, one of which is in contact with the wall. Heat transfer coefficients and contact areas vary within the cycle. Since the model is non-linear, a computerized Runge-Kutta method is used to solve the differential equations, to obtain the pressure cycle for a given volume cycle. The heat transfer coefficients and mass division between the spaces are then changed to try to match a given experimentally measured p-V diagram. The Adiabatic Plane Model of Ref. [3] is a similar model with N spaces.

2. "Lumped Parameter" Model

This model is continuous in time but discrete in space. This model is similar to the two space model except the thermal resistances are

not allowed to vary with time, making it linear. Work input from the piston

is modelled as simultaneous sinusoidal heat current sources in each space.

Then conventional frequency response analysis is used to find phase

relationships and the loss as a function of speed.

3. "Entropy Generation" Model

This model is continuous in space and time. A differential

equation for the entropy as a function of position and time is developed.

Next an expression for the entropy generation rate as a function of the

instantaneous entropy distribution in space is derived. Then expressions

for the loss as a function of Reynolds number are found for two Reynolds

number regimes.

E.2 Two-Space Model

This model was developed early in the investigation. One of the initial

experiments (see Appendix D.4) was used for comparison, with parameters as

follows:

helium, volume ratio 2.39, steel cylinder

$$P_{mc} = 282 \text{ psi}, \quad N = 182 \text{ rpm},$$

$$Re = 3460 \quad, \quad L = .047.$$

As a first step, a simplified version of the model was used and results

calculated directly with a hand calculator. The gas space in contact with

the wall was assumed to be isothermal and the other space was assumed to be

adiabatic. The wall temperature was assumed to be equal to the mean tempera-

ture of the adiabatic space. The maximum and minimum pressures, as well as

volumes, were given. With this information the mass fractions in each space

and the pressure for each volume could be calculated. The masses for each

space came out about equal. Since the processes in this model are reversible, the p-V diagram is a line, which is shown in Fig. E.1, along with the experimental p-V diagram. The model line is less curved, indicating less variation in heat flux through the cycle.

In the complete model, the inputs were the speed, wall temperature, heat transfer coefficients, mass fractions, gas properties, areas of thermal contact, and volumes. The DYSIS computer program at the M.I.T. Joint Computer Facility calculated the pressure and temperature at each volume step. When the mass fractions and heat transfer coefficients were adjusted to match the experimental p-V diagram, fair agreement was obtained with the following:

$$h_1 = 1700 \text{ Btu/hrft}^2\text{°R}$$

$$h_2 = 10 \quad \text{Btu/hrft}^2\text{°R}$$

$$\frac{m_1}{m_2} = 1.70$$

where subscript 1 refers to the space in contact with the wall and subscript 2 refers to the interior space. When h_1 was made a linear function of volume with the same average value, close agreement was obtained as shown in Fig. E.2. The greater heat transfer at large volumes implied in this is also shown by the bending of the T-S diagram in Fig. 3.13.

E.3 Lumped Parameter Model

This model is shown in diagramatic and linear graph form in Fig. E.3. Here subscript 2 refers to the space in contact with the cylinder wall and
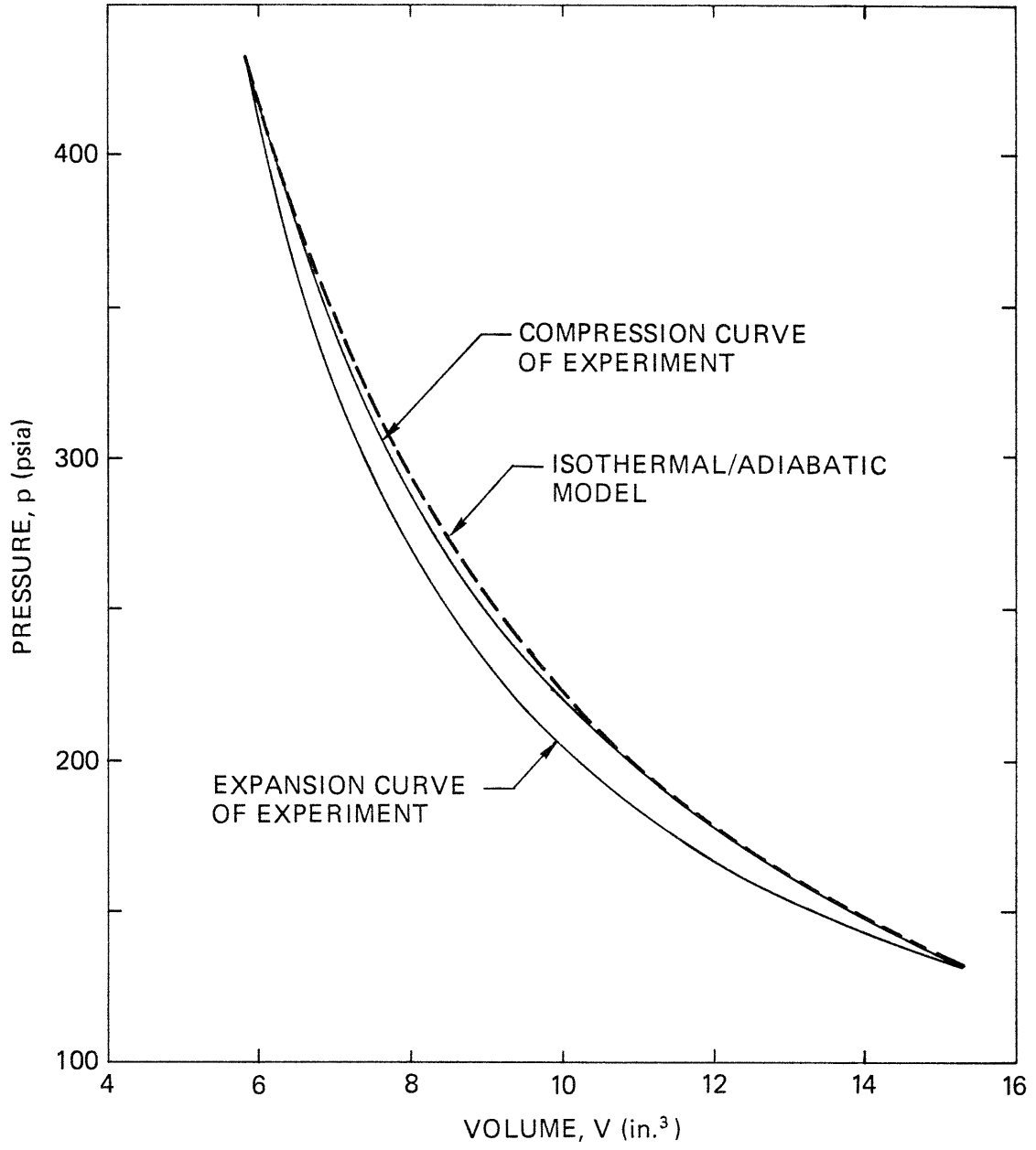
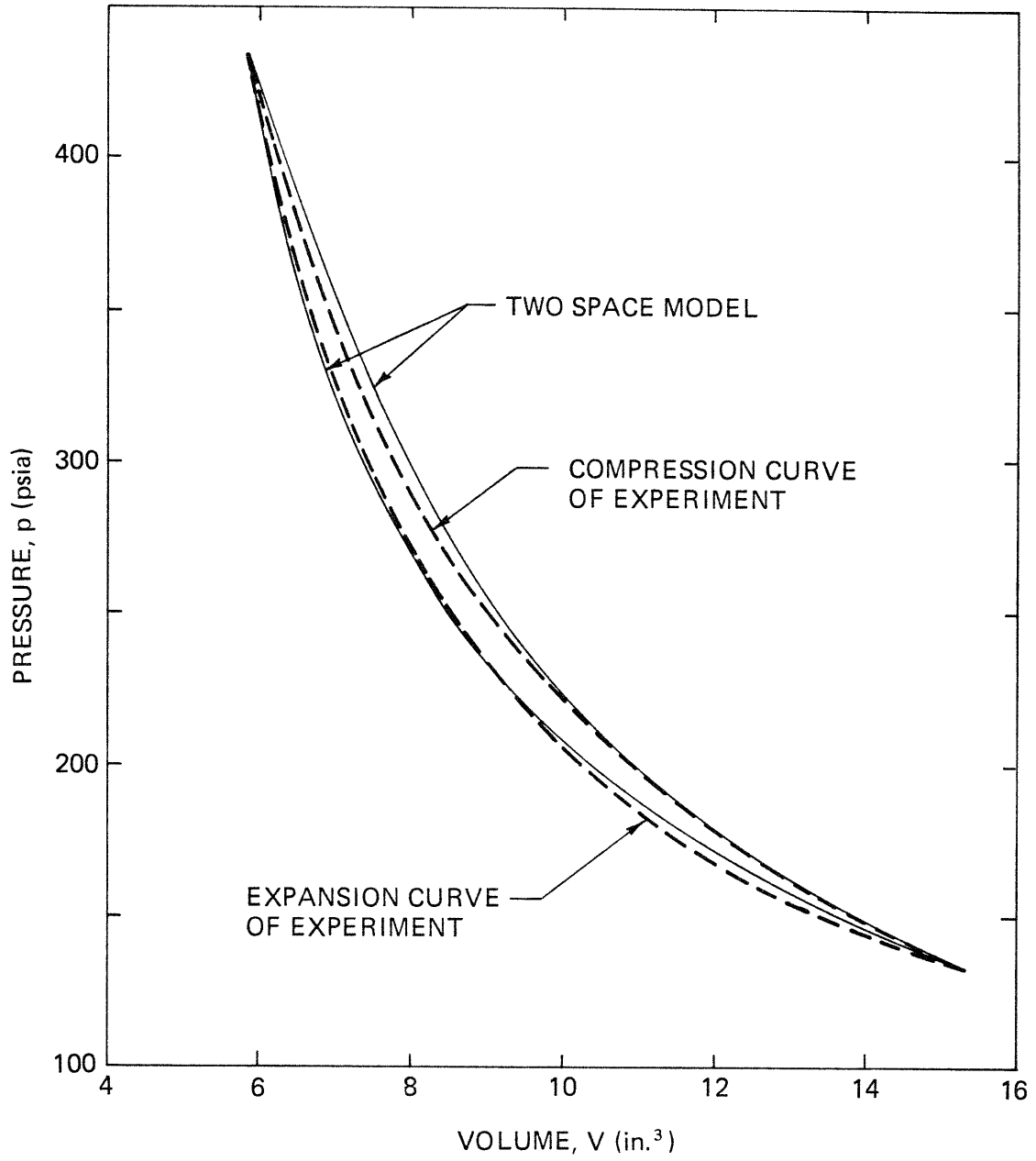Fig. E-1. Isothermal/Adiabalic Model Results.

Fig. E-2. Two Space Model Results.

subscript 1 refers to the interior space.

The system is inherently overdamped second order. For convenience we define the parameters,

$$r_R = \frac{R_1}{R_2} \quad , \quad r_c = \frac{C_1}{C_2} \quad , \quad \tau_1 = R_1 C_1 \tag{E.1}$$

Then the natural frequency and damping ratio are,

$$\omega_n = \frac{1}{\tau_1} \sqrt{r_R r_c}$$

$$\tag{E.2}$$

$$\zeta = \frac{1}{2} \sqrt{r_R r_c} \quad (1 + \frac{1 + r_c}{r_R r_c})$$

The magnitude ratio of the heat sources is assumed to be equal to the ratio of the thermal capacities

$$r_s = \left| \frac{q_{s1}}{q_{s2}} \right| = r_c \tag{E.3}$$

Example values of parameters were derived from the results of the two-space model,

$$r_R = 167, \quad r_c = .588, \quad \tau_1 = 1.11 \text{ sec},$$

$$\omega_n = 8.92 \text{ sec}^{-1}, \quad \zeta = 5.09$$

The system variables can be calculated using these values of parameters.

PISTON   SPACE 1   SPACE 2   WALL

q_{s2}

q_{s1}

q_g q_W

q_1 q_2

T_1, C_1 R_1 T_2, C_2 R_2 T_W

R_1

θ_1 θ_2

$\theta_1 = T_1 - T_W$

$\theta_2 = T_2 - T_W$

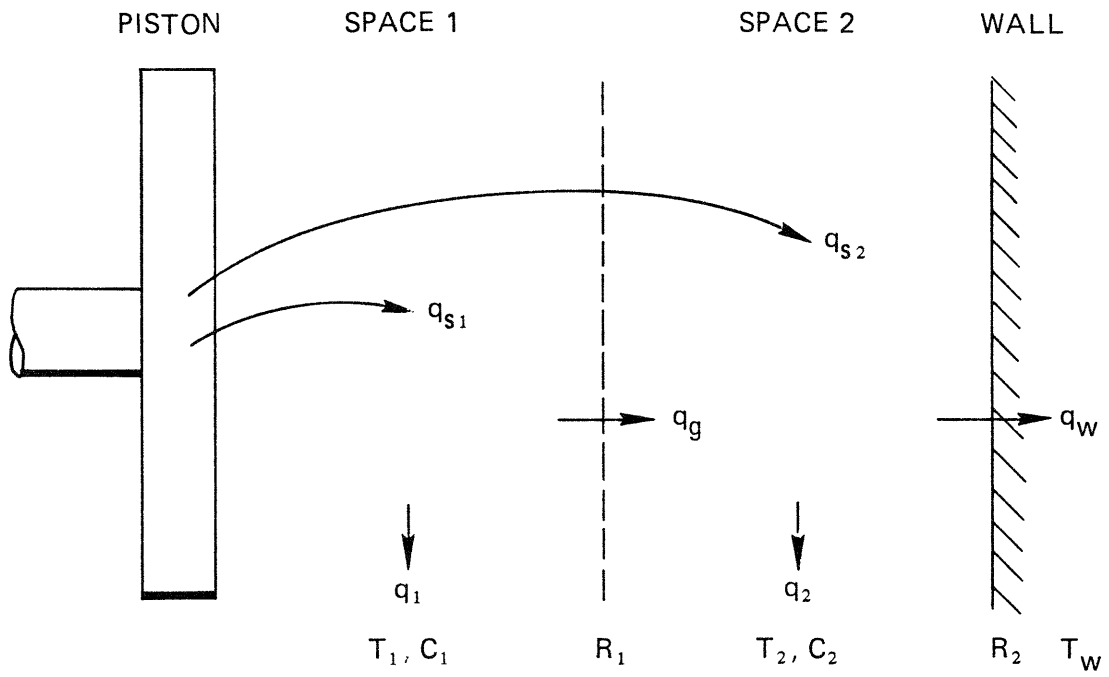q_{s1} C_1 q_{s2} C_2 R_2
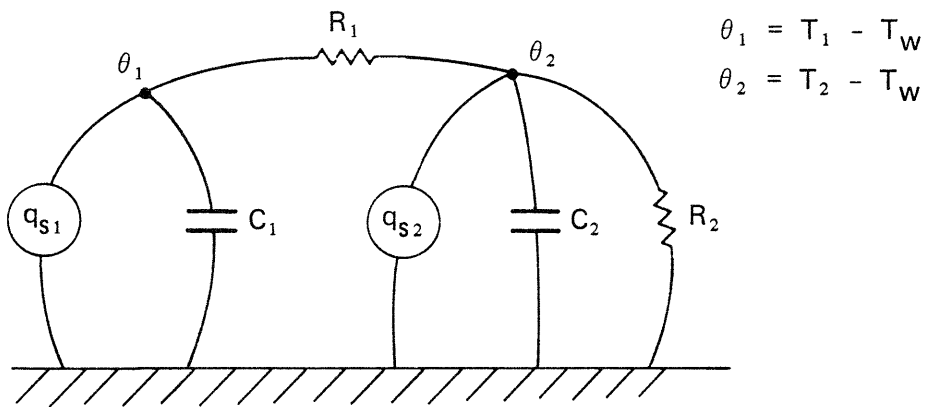
Fig. E-3. Lumped Parameter Model.

One relationship of interest is the phase difference between the temperature in the interior of the gas and the temperature next to the wall. In the terms of the model, this is the phase angle between θ_2 and θ_1,

$$\frac{\theta_2}{\theta_1} = \tan^{-1}\left(\frac{\tau_1\omega}{r_c+1}\right) - \tan^{-1}\left(\frac{\tau_1\omega}{r_R r_c + r_c + 1}\right) \tag{E.4}$$

where the individual phase angles of θ_2 and θ_1 are relative to the phase of the pressure. A Bode plot of this relationship is given in Fig. E.4. This plot suggests that the temperature near the wall leads the interior temperature by an angle increasing with frequency to more than 45° at 100 rpm, which agrees roughly with the experiments. The decline of phase difference above 100 rpm does not agree with experiments. The discrepancy is probably due to the resistances and capacities varying with frequency.

This model can be used to develop an expression for the non-dimensional loss as a function of system variables, and hence the model is potentially able to predict the loss as a function of average Reynolds number. The average pressure enters the prediction through the resistances and capacitances being functions of average pressure. The form of these functions is not clear and hence the loss has been studied only as a function of speed or frequency. The loss rate is given by,

$$\text{Loss Rate} = T_0 \dot{S}_{gen}$$

$$= T_w q_g \frac{T_1 - T_2}{T_1 T_2} + T_w q_w \frac{T_2 - T_w}{T_2 T_w} \tag{E.5}$$
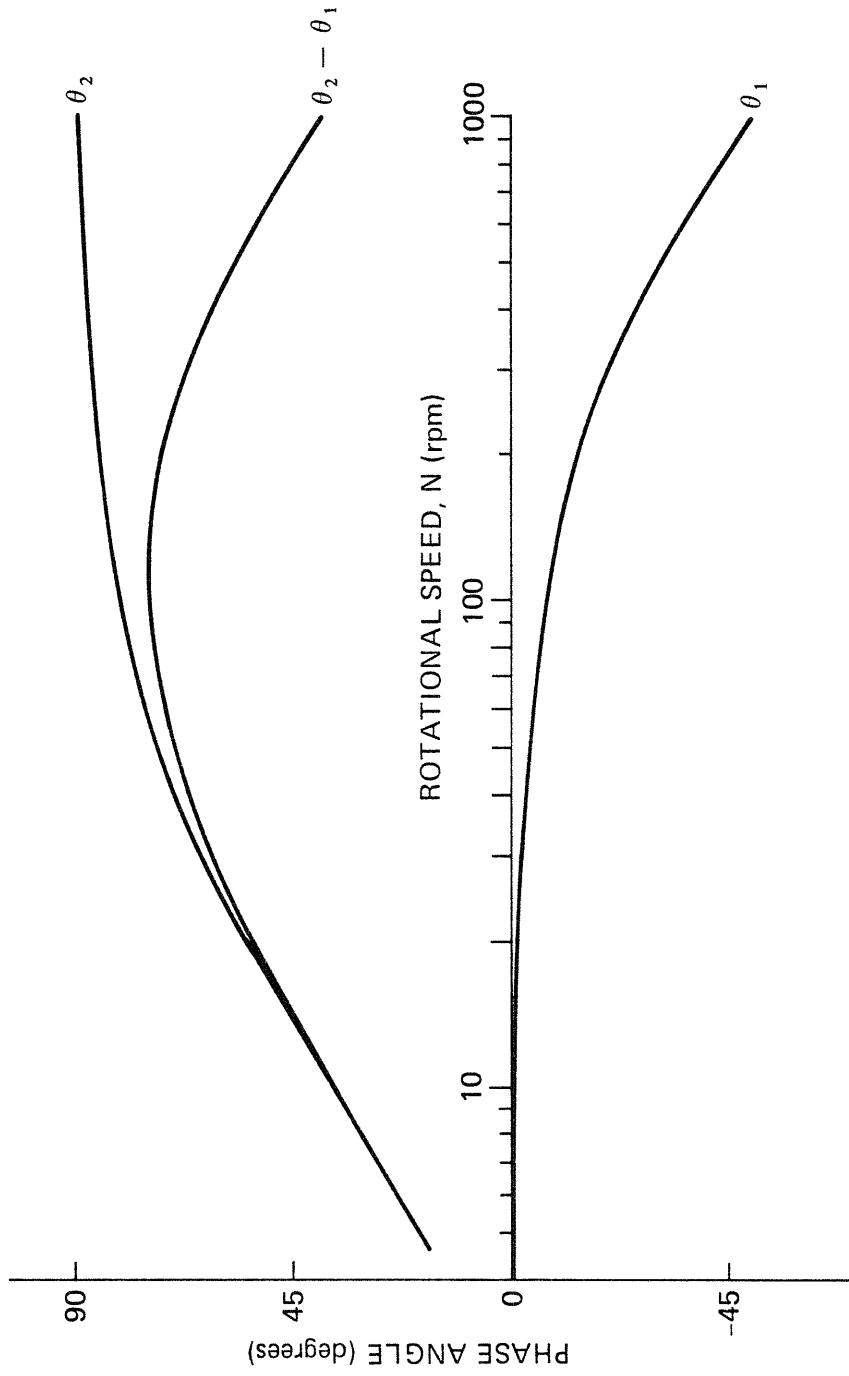
Fig. E-4. Phase Angle Between θ_2 and θ_1 vs. N from Lumped Parameter Model.

for $\dfrac{T_1 - T_w}{T_w}$ and $\dfrac{T_2 - T_w}{T_w}$ small,

$$\text{Loss Rate} = \frac{1}{T_w}(q_g^2 R_1 + q_w^2 R_2) \tag{E.6}$$

and,

$$\text{Loss per Cycle} = \frac{R_1}{T_w} \oint q_g^2 dt + \frac{R_2}{T_w} \oint q_w^2 dt \tag{E.7}$$

The work in compression is given by,

$$W_c = \int_0^{\pi/\omega} (q_{s1} + q_{s2}) dt \tag{E.8}$$

We now substitute and integrate over the sinusoidal cycle to obtain,

$$L = \frac{\text{Loss per Cycle}}{\text{Compression Work}}$$

$$= \text{constant}(R_1 \left| \frac{q_g}{q_s} \right|^2 + R_2 \left| \frac{q_w}{q_s} \right|^2) \tag{E.9}$$

When the expressions are evaluated and the example parameter values are substituted, the loss is obtained as a function of speed as plotted in Fig. E.5. The log-log plot shows a negative slope of about -1, whereas the experimental loss versus Reynolds number plot has a negative slope of about -1/3 above Reynolds number 100 (Fig. 3.3). The excess negative slope could be associated with the phase difference declining with speed, as discussed above.
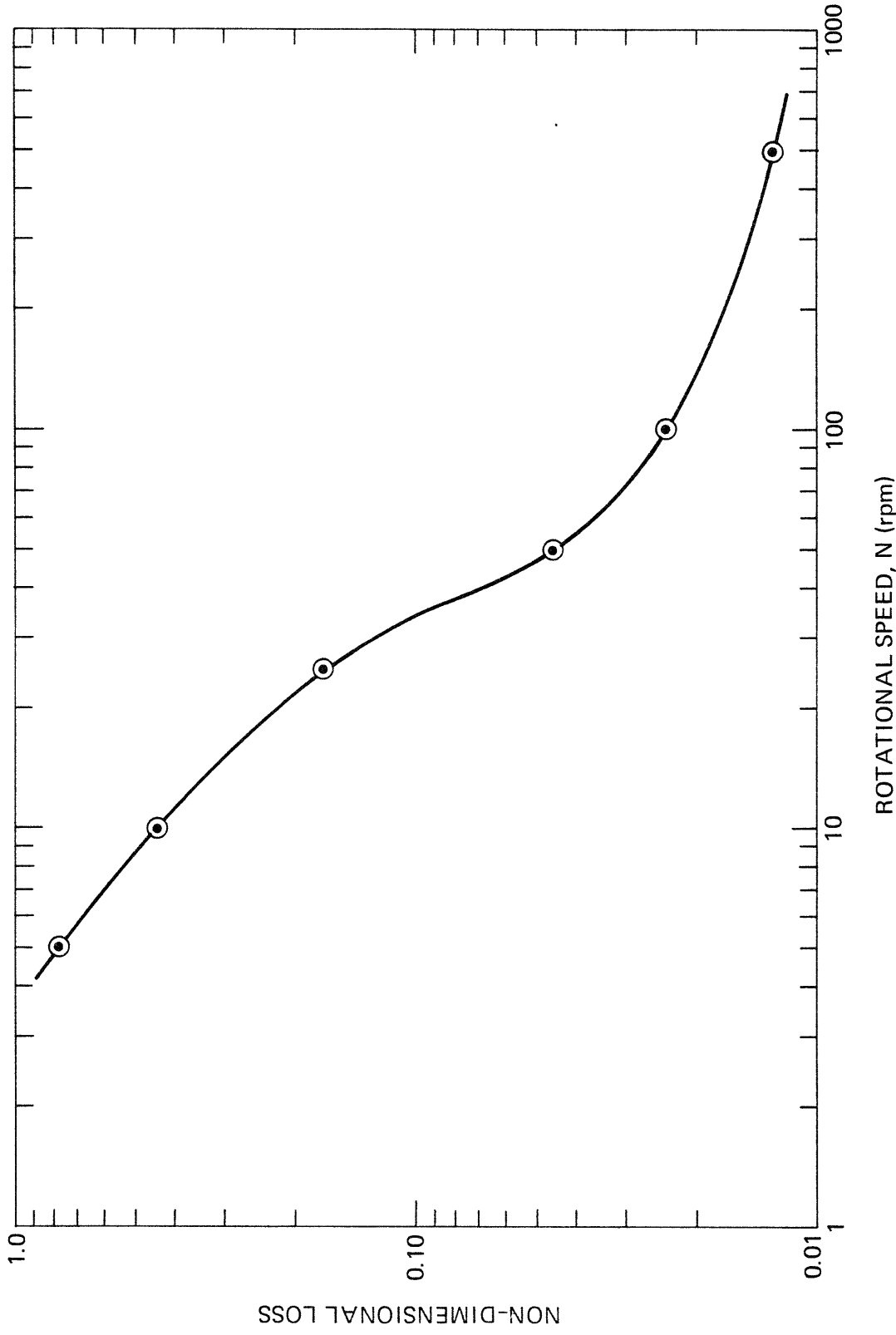
Fig. E-5. Loss vs. Speed from Lumped Parameter Model.

The lumped parameter model can also potentially predict the rough shape of the T-S diagram as a function of average Reynolds number. As in the case of the non-dimensional loss discussed above, only the variation of the shape with speed was studied. The average gas temperature is given by,

$$T = T_w + \frac{r_c \theta_1 + \theta_2}{r_c + 1} \tag{E.10}$$

and the entropy by,

$$S - S_0 = C_1 \ln \frac{T_1}{T_w} + C_2 \ln \frac{T_2}{T_w} - \int \frac{q_s}{T} dt \tag{E.11}$$

For $\dfrac{T_1 - T_w}{T_w}$ and $\dfrac{T_2 - T_w}{T_w}$ small,

$$S - S_0 = \frac{C_1}{r_c T_w} (r_c \theta_1 + \theta_2) - \frac{r_c + 1}{T_w r_c} \int q_{s1} dt \tag{E.12}$$

Then the transfer function T/S can be found as a function of frequency. A plot of T versus S will be a Lissajou figure which should have some resemblance to an experimental T-S diagram.

The shape of the figure should change with frequency in a way similar to that of the experimental T-S diagrams. The results in Fig. E.6 indicate fair agreement except for the phase lag at higher frequency.

E.4 Entropy Generation Model

The basic characteristics of this model are shown in Fig. E.7. The
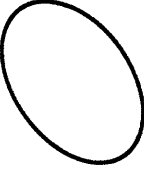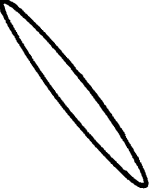
	RPM		
	10	100	1000
APPROXIMATE EXPERIMENTAL T-S DIAGRAM			
ROUGHLY EQUIVALENT LISSAJOU FIGURE			
ROUGH PHASE LAG	$90° - 135°$	$120° - 165°$	$130° - 170°$
$\left\|\dfrac{T}{S}\right\|$	LOW	MED	HIGH
MODEL PHASE LAG	124	155	107
MODEL $\left\|\dfrac{T}{S}\right\|$	.33	.57	1.78

Fig. E-6. Comparison of T-S Relationship Between Experiments and
Lumped Parameter Model.

gas does not move except back and forth as the density changes with the pressure variation. The variable x is the coordinate of a fixed position in space. The variable m is the mass of gas between a given gas particle and the wall. This is a Lagrangian coordinate, following the particle, and it becomes the position variable in the equations.

The differential equation for the entropy as a function of space and time will now be derived. The equation is initially formulated with temperature as the dependent variable but is simplifed by reformulation in terms of entropy. We start with three basic equations:
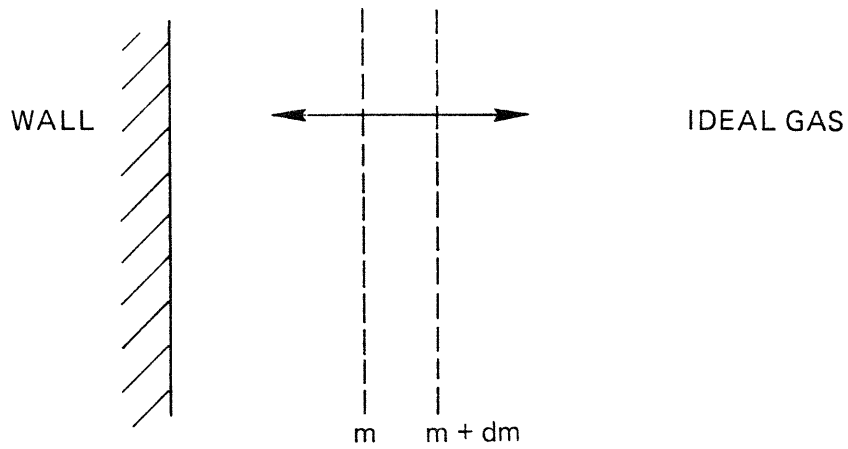
$$\text{Continuity} \quad \frac{\partial x}{\partial m}\bigg|_t = \frac{1}{\rho A} = \frac{v}{A} \qquad\qquad (E.13)$$

$$\text{Conduction} \quad q = -kA \frac{\partial T}{\partial x}\bigg|_t \qquad\qquad (E.14)$$

$$\text{Energy} \quad \delta Q - \delta W = dU \qquad\qquad (E.15)$$

The terms of the energy equation are expanded for a differential mass dm . Beginning with δQ , and using the conduction equation, we obtain

$$
\begin{aligned}
\delta Q &= \left(q_m - q_{m+dm}\right)dt \\[2mm]
&= \left[-kA \frac{\partial T}{\partial x}\bigg|_{m,t} + kA \frac{\partial T}{\partial x}\bigg|_{m+dm,t}\right]\partial t \\[2mm]
&= -kA\left[\frac{\frac{\partial T}{\partial m}}{\frac{\partial x}{\partial m}} - \frac{\frac{\partial T}{\partial m} + \frac{\partial^2 T}{\partial m^2}\,dm}{\frac{\partial x}{\partial m} + \frac{\partial^2 x}{\partial m^2}\,\partial m}\right]dt
\end{aligned}
$$

$$(E.16)$$

WALL   IDEAL GAS

m   m + dm

x

m

ONE DIMENSION IN SPACE

- DEPENDENT VARIABLE: s

- POSITION INDEPENDENT VARIABLE: m

- TIME INDEPENDENT VARIABLE: t

- PARAMETERS: ω, r_p

- CONSTANTS: $k, c_p, R, p_0, T_0, s_0, A$

- BOUNDARY CONDITIONS:

  - AT WALL: $m = 0$, $\dfrac{\partial T}{\partial t} = 0$

    $s_0 + \dfrac{R}{2} \ell n \, r_p \sin \omega u$

  - FAR FROM WALL: $m = \infty$, $\dfrac{\partial s}{\partial m} = 0$

Fig. E-7. Entropy Generation Model.

We then expand δW,

$$\delta W = - [p(dV)_m - p(dV)_{m+dm}]$$

$$= -[P\ A(x_{t_m} + dt - x_{t_m}) - P\ A(x_{t_{m+dm}}+dt - x_{t_{m+dm}})] \qquad (E.17)$$

$$= p\ A\ \frac{\partial^2 x}{\partial m \partial t}\ dmdt$$

Then we expand dU,

$$dU = dm\ c_v(T_{t+dt_m} - T_{t_m})$$

$$= c_v\ \frac{\partial T}{\partial t}\ dm\ dt \qquad (E.18)$$

We then substitute in the energy equation,

$$kA\left[\frac{\frac{\partial^2 T}{\partial m^2}}{\frac{\partial x}{\partial m}} - \frac{\frac{\partial T}{\partial m}\frac{\partial^2 x}{\partial m^2}}{(\frac{\partial x}{\partial m})^2}\right] - p\ A\ \frac{\partial^2 x}{\partial m \partial t} = c_v\ \frac{\partial T}{\partial t} \qquad (E.19)$$

From continuity and the equation of state we obtain,

$$\frac{\partial x}{\partial m} = \frac{v}{A} = \frac{RT}{Ap} \qquad (E.20)$$

Then,

$$\frac{\partial^2 x}{\partial m^2} = \frac{\partial}{\partial m}\left(\frac{RT}{Ap}\right) = \frac{R}{Ap}\ \frac{\partial T}{\partial m} \qquad (E.21)$$

and,

$$\frac{\partial^2 x}{\partial m \partial t} = \frac{\partial}{\partial t} \left(\frac{RT}{Ap} \right) = \frac{R}{A} \frac{p \frac{\partial T}{\partial t} - T \frac{\partial p}{\partial t}}{p^2} \qquad (E.22)$$

We then substitute in the energy equation,

$$kA \left[\frac{\frac{\partial^2 T}{\partial m^2}}{\frac{RT}{Ap}} - \frac{\frac{R}{Ap} \left(\frac{\partial T}{\partial m} \right)^2}{\left(\frac{RT}{Ap} \right)^2} \right] - \frac{R}{p} \left(p \frac{\partial T}{\partial t} - T \frac{\partial p}{\partial t} \right) = c_v \frac{\partial T}{\partial t} \qquad (E.23)$$

We then simplify,

$$\frac{kA^2 p}{RT^2} \left[\frac{\partial^2 T}{\partial m^2} - \frac{1}{T} \left(\frac{\partial T}{\partial m} \right)^2 \right] - \frac{c_p}{T} \frac{\partial T}{\partial t} + \frac{R}{p} \frac{\partial p}{\partial t} = 0 \qquad (E.24)$$

From perfect gas relations, we obtain,

$$ds = \frac{c_p}{T} dT - \frac{R}{p} dp \qquad (E.25)$$

Then,

$$\frac{\partial T}{\partial m} = \frac{T}{c_p} \frac{\partial s}{\partial m} \qquad (E.26)$$

and,

$$\frac{\partial^2 T}{\partial m^2} = \frac{1}{c_p} \left[T \frac{\partial^2 s}{\partial m^2} + \frac{T}{c_p} \left(\frac{\partial s}{\partial m} \right)^2 \right] \qquad (E.27)$$

Also,

$$s - s_0 = c_p \ln \frac{T}{T_0} - R \ln \frac{p}{p_0} \qquad (E.28)$$

Then,

$$\frac{T}{T_0} = \left(\frac{p}{p_0} \right)^{\frac{R}{c_p}} \exp\left(\frac{s - s_0}{c_p} \right) \qquad (E.29)$$

and,

$$\frac{p}{T} = \frac{p_0}{T_0} \left(\frac{p}{p_0} \right)^{\frac{1}{\gamma}} \exp\left(\frac{s_0 - s}{c_p} \right) \qquad (E.30)$$

We then substitute to obtain,

$$\frac{kA^2}{c_p R} \frac{p_0}{T_0} \left(\frac{p}{p_0} \right)^{\frac{1}{\gamma}} \exp\left(\frac{s_0 - s}{c_p} \right) \frac{\partial^2 s}{\partial m^2} - \frac{\partial s}{\partial t} = 0 \qquad (E.31)$$

This equation is simplified by scaling the time variable by the pressure,

$$u = \int \left(\frac{p}{p_0} \right)^{\frac{1}{\gamma}} dt \qquad (E.32)$$

Then

$$\frac{\partial s}{\partial t} = \frac{\partial s}{\partial u} \frac{du}{dt} = \left(\frac{p}{p_0} \right)^{\frac{1}{\gamma}} \frac{\partial s}{\partial u} \qquad (E.33)$$

We then substitute to obtain,

$$\frac{\partial^2 s}{\partial m^2} - \exp\left(\frac{s - s_0}{c_p} \right) \frac{\partial s}{\partial u} = 0 \qquad (E.34)$$

Now this equation is made linear by the approximation,

$$\frac{s - s_0}{c_p} \ll 1$$

For a sample of 17 preliminary experiments over the full range of Reynolds numbers (see Appendix D), $s-s_0/c_p$ was always less than 0.26. The linear equation,

$$\frac{\partial^2 s}{\partial m^2} - \frac{c_p R}{kA^2} \frac{T_0}{P_0} \frac{\partial s}{\partial u} = 0 \qquad (E.35)$$

is completely analogous to the one-dimensional heat conduction equation. The solution of this equation for two Reynolds number regimes is discussed below.

The solution of this equation will give the entropy distribution in space as a function of time. We wish to calculate the non-dimensional loss, which is proportional to the entropy generation rate integrated over time through one cycle and over the gas space. We therefore derive an expression for the local entropy generation rate as a function of the entropy distribution in space. The heat conduction is given by,

$$q = -kA \frac{\partial T}{\partial x}$$

By using continuity (Eq. E.20), and the perfect gas relation (Eq. E.26), we can express this in terms of the entropy gradient,

$$q = -kA\left(\frac{pA}{RT} \frac{\partial T}{\partial m} \right)$$

$$= -kA\left(\frac{pA}{c_p R} \frac{c_p}{T} \frac{\partial T}{\partial m} \right) \qquad (E.36)$$

$$= - \frac{kA^2}{c_p R} \, p \, \frac{\partial s}{\partial m} \tag{E.36}$$

Then the entropy generation rate is given by,

$$s_{gen} = \frac{\partial}{\partial m} \left(\frac{q}{T} \right)$$

$$= \frac{1}{T} \frac{\partial q}{\partial m} - \frac{q}{T^2} \frac{\partial T}{\partial m}$$

$$= \frac{1}{T} \frac{\partial q}{\partial m} - \frac{q}{T^2} \frac{T}{c_p} \frac{\partial s}{\partial m} \tag{E.37}$$

$$= - \frac{1}{T} \frac{kA^2}{c_p R} \, p \, \frac{\partial^2 s}{\partial m} + \frac{1}{T} \frac{1}{c_p} \frac{\partial s}{\partial m} \frac{kA^2}{c_p R} \, p \, \frac{\partial s}{\partial m}$$

$$= - \frac{kA^2}{c_p R} \frac{p}{T} \left[\frac{\partial^2 s}{\partial m^2} - \frac{1}{c_p} \left(\frac{\partial s}{\partial m} \right)^2 \right]$$

This model is now applied in two Reynolds number regimes. In the higher Reynolds number regime the gas is assumed to be isentropic far from the wall. The model is then concerned with the entropy variation in time and space between the wall and this interior space. In the lower Reynolds number regime, the entropy gradient is assumed to extend all the way across the one-dimensional cylinder space, so the gas is nowhere isentropic. The total mass remains constant under varying pressure, so the distance between the walls must vary. These walls may then be thought of as the piston and cylinder head.

The same wall boundary condition is used for both regimes, but in the lower Reynolds number regime there are walls at both ends of the gas space.

To maintain the analogy with heat conduction, we specify a sinusoidal

entropy variation at the wall instead of a sinusoidal pressure variation,

$$s\bigg|_{m=0} = s_0 + \frac{R}{2} \ln r_p \sin \omega u \qquad \text{(E.38)}$$

This boundary condition implies a pressure versus time variation which is

close to the polytropic pressure variation for the same geometry and

pressure ratio and hence is roughly realistic.

E.4.1 Higher Reynolds Number Regime

The solution of the differential equation is given in Ref. [6]

for the case of periodic temperature changes on the surface of an infinite-

ly thick plate. The general solution in the nomenclature of this model

is,

$$s = C_1 + C_2 m + C_3 \exp(\alpha m + \frac{\alpha^2}{C_{de}} u) \qquad \text{(E.39)}$$

where

$$C_{de} = \frac{c_p R T_0}{k A^2 p_0}$$

and C_1, C_2, and C_3 are arbitrary constants. By applying the boundary

conditions and using a convenient phase angle we obtain,

$$s - s_0 = \frac{R}{2} \ln r_p e^{-am} \sin(\omega u - am) \qquad \text{(E.40)}$$

where

$$a = \sqrt{\frac{\omega\, C_{de}}{2}} = \sqrt{\frac{\omega\, c_p\, R\, T_0}{2k\, A^2\, p_0}}$$

We are now ready to calculate the entropy generation. The entropy generation over a cycle of one point m is given by

$$s_{gen/cycle} = \oint \dot{s}_{gen}\, dt = \oint \dot{s}_{gen} \left(\frac{p_0}{p}\right)^{\frac{1}{\gamma}} du \qquad (E.41)$$

By substituting Eqs. (E.40) and (E.37) into Eq. (E.41), and using a series approximation for the integral, we obtain,

$$s_{gen/cycle} = \frac{\pi\, R^2 (\ln r_p)^2}{4\, c_p}\, e^{-2am} + \frac{\pi\, R^4 (\ln r_p)^4}{64\, c_p^3}\, e^{-4am} + \ldots\ldots \qquad (E.42)$$

We then integrate over the gas space,

$$S_{gen} = \int_0^\infty s_{gen/cycle}\, dm$$

$$= \pi\, A \sqrt{\frac{k\, p_0}{\omega\, T_0}} \left[\left(\frac{\gamma-1}{\gamma}\right)^{\frac{3}{2}} \frac{(\ln r_p)^2}{2^2} \right.$$

$$\left. + \left(\frac{\gamma-1}{\gamma}\right)^{\frac{7}{2}} \frac{(\ln r_p)^4}{2^7} + \ldots\ldots \right] \qquad (E.43)$$

Here we define the non-dimensional loss differently from that of Chapter 3 because we do not know the compression work,

$$L = \frac{\text{energy loss per cycle}}{\text{(reference pressure)(cross sectional area)(stroke)}}$$

(E.44)

$$= \frac{T_0 \, S_{gen}}{P_0 \, A \, s}$$

This value of the non-dimensional loss should be of the same order as L, the non-dimensional loss of Chapter 3. Substituting Eq. (E.43) into Eq. (E.44) and expressing the results in terms of the Prandtl number and average Reynolds number of Chapter 3, we have,

$$L = \sqrt{\frac{\pi b}{Re \; Pr \; s}} \; [\frac{\gamma - 1}{\gamma} \; \frac{(\ln r_p)^2}{2^2} + \frac{\gamma - 1}{\gamma} \; \frac{(\ln r_p)^4}{2^7} + \ldots \ldots] \quad (E.45)$$

The most important aspect of this result is that the non-dimensional loss is predicted to be inversely proportional to the square root of the Reynolds number for a given pressure ratio. This conclusion is in rough agreement with the experimental results. This formula is not a true prediction formula since the pressure ratio must be known to obtain the loss.

The data for ten preliminary experiments with helium was used in the formula and the results are shown in Fig. E.8. The results can be compared with the experimental results of Fig. D.3. Neglecting the effect of the individual pressure ratios we can compare the results with the experimental results of Fig. 3.3. In the higher half of the Reynolds number range the model results are about an order of magnitude lower and have a slightly steeper slope.
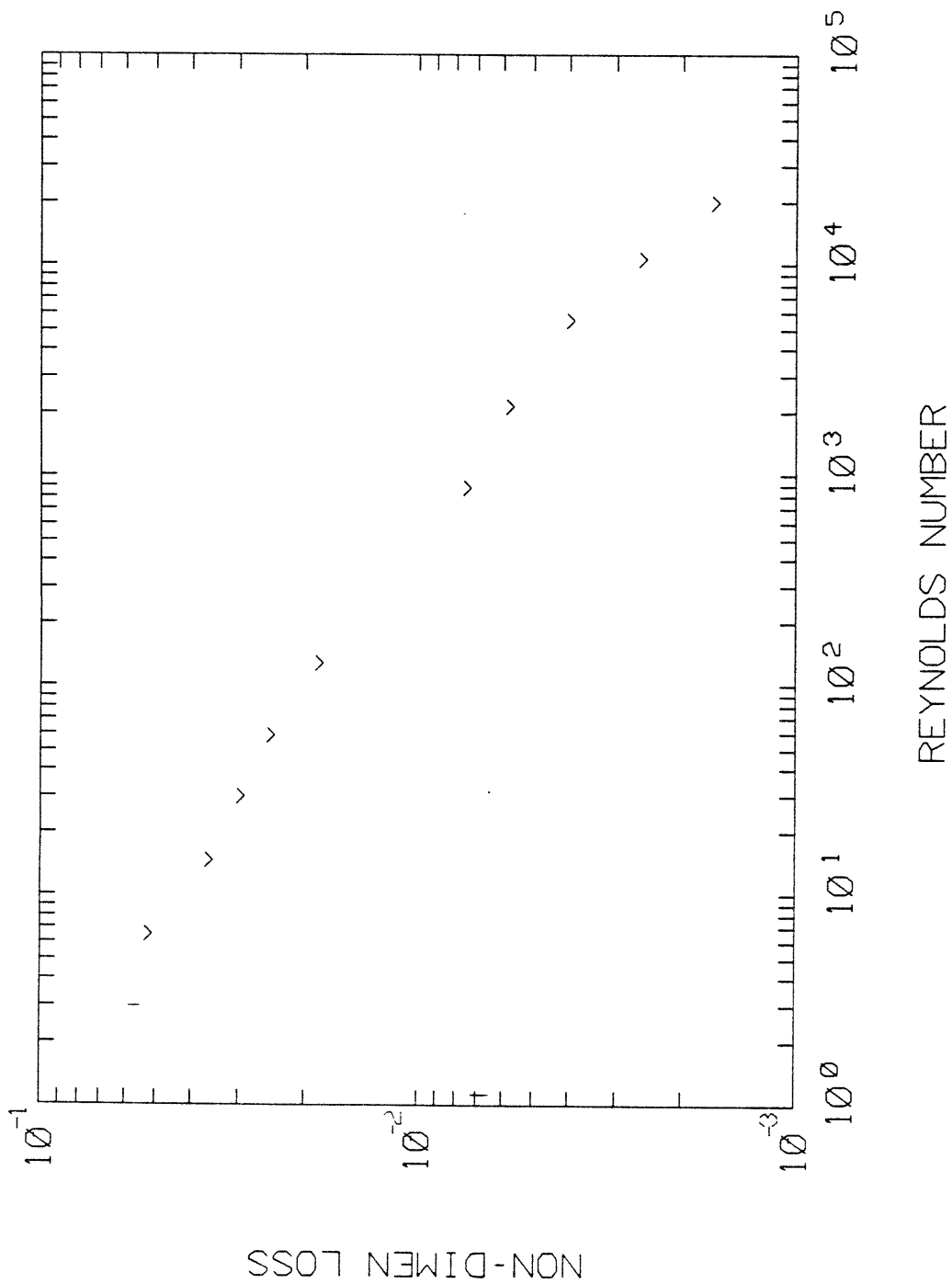
Fig. E-8. Loss vs. Reynolds Number for Entropy Generation Model, Higher Reynolds Number Regime, Helium.

E.4.2 Lower Reynolds Number Regime

The solution of the differential equation (E.35) is also given in Ref. [6] for the case of periodic temperature changes on both surfaces of a plate of finite thickness. If we apply the boundary conditions and use the nomenclature of this model, the solution becomes,

$$s - s_0 = \frac{R}{2} \ln r_p \; \zeta \; \cos(\omega u + \phi) \qquad \text{(E.46)}$$

where,

$$\zeta = \sqrt{\frac{f_c^2(\xi\sigma) + f_s^2(\xi\sigma)}{f_c^2(\sigma) + f_s^2(\sigma)}}$$

$$\phi = \tan^{-1}\left[\frac{f_c(\sigma) \, f_s(\xi\sigma) - f_s(\sigma) \, f_c(\xi\sigma)}{f_c(\sigma) \, f_c(\xi\sigma) + f_s(\sigma) \, f_s(\xi\sigma)} \right]$$

$$f_c(z) = \cos z \cosh z$$

$$f_s(z) = \sin z \sinh z$$

and where,

$$\xi = \frac{2m}{m_{total}} \; , \; \text{a non-dimensional position variable}$$

$$\sigma = a \, \frac{m_{total}}{2} \; , \; \text{a non-dimensional measure of the attenuation of the entropy wave with distance from the wall.}$$

Now we substitute Eqs. (E.46) and (E.37) into Eq. (E.41), retaining only the first four terms of the series approximation to the exponential. In addition, since $\frac{R}{2cp} \ln r_p$ is less than 1, we neglect higher order terms in this quantity. The result is,

$$s_{gen/cycle} = \frac{\pi R^2 (\ln r_p)^2}{8 \sigma^2 c_p} [(\frac{d\zeta}{d\xi})^2 + \zeta \frac{d^2\zeta}{d\xi^2}] \tag{E.47}$$

In this version of the model we are interested in the lower end of the Reynolds number range, and σ is proportional to $\sqrt{Re}$. Therefore we neglect higher order terms in σ in evaluating the derivatives. Then,

$$s_{gen/cycle} = \frac{\pi R^2 (\ln r_p)^2}{2 c_p} \sigma^2 \xi^2 \tag{E.48}$$

Now we integrate over the space,

$$S_{gen} = \int_0^{m_{total}} s_{gen/cycle} \, dm \tag{E.49}$$

$$= \frac{\pi R^2 (\ln r_p)^2}{6 c_p} \sigma^2 m_{total}$$

Finally we find the non-dimensional loss by substituting this into Eq. (E.44),

$$\bar{L} = \frac{\pi^2}{48} \frac{\ell_a^3}{bs^2} \frac{\gamma-1}{\gamma} (\ln r_p)^2 \, Pr \, Re \tag{E.50}$$

where

ℓ_a = the average length from the piston to the cylinder head

This result indicates that at low Reynolds number the non-dimensional loss should be proportional to the Reynolds number for a given pressure ratio. This conclusion is roughly in agreement with the experimental results, as was the case for the higher Reynolds number regime. The magnitude of the losses given by this formula is too high by about a factor of ten.

In conclusion, the entropy generation model seems to correctly predict the approximate slope of the loss versus Reynolds number curve in both the higher and lower Reynolds number regimes. Unfortunately the pressure ratio must be known in order to calculate the loss. The approximate loss values predicted by the formulas derived from the model are off by about a factor of ten in both cases, too high in the lower Reynolds number regime and too low in the higher Reynolds number regime.

BIOGRAPHICAL NOTE

The author was born in Brookline, Massachusetts, on October 15, 1941. He grew up there and then attended Phillips Exeter Academy. He attended Harvard College, receiving a B.A. in Engineering and Applied Physics in 1963. He went to work for the Convair Division of General Dynamics in San Diego, California, as an aircraft structures engineer. Later he entered graduate school at M.I.T., receiving an M.S. in Aeronautics and Astronautics in 1970. His master's thesis concerned a linear programming model for airline fleet planning with financial constraints. He then worked as a member of the research staff of the Flight Transportation Laboratory at M.I.T. Most of his work was concerned with the problems of short haul air transportation, particularly noise versus operating cost tradeoffs for rotary wing aircraft. Most recently he re-entered graduate school at M.I.T., where he hopes to receive a Ph.D. in Mechanical Engineering in May, 1983.

Publications:

"Short Haul Aircraft - The Technology is Nearly Ready", H.B. Faulkner, Technology Review, May 1972.

"The Cost of Noise Reduction in Intercity Commercial Helicopters", H.B. Faulkner, Journal of Aircraft, Vol. II, No. 2, February 1974.

"The Cost of Noise Reduction for Departure and Arrival Operations of Commercial Tilt Rotor Aircraft", H.B. Faulkner and W.M. Swan, NASA CR-137803, June 1976.

"Performance Loss due to Heat Transfer in the Cylinders of Stirling Engines", K.P. Lee, J.L. Smith, Jr. and H.B. Faulkner, 15th Intersociety Energy Conversion Conference, Seattle, Washington, August 1980.